Feary, D.A., Hine, A.C., Malone, M.J., et al., 2000
Proceedings of the Ocean Drilling Program, Initial Reports Volume 182

7. SITE 1129[1]

Shipboard Scientific Party[2]

BACKGROUND AND OBJECTIVES

Site 1129 is located on the uppermost slope/shelf edge adjacent to the Eucla Shelf in 202.5 m of water (Fig. F1). It was the shallowest, most proximal site of a depth transect of three sites (including intermediate-depth Site 1131 and deepest Site 1127). Site 1129 was designed to sample an impressive set of prograding sigmoidal clinoforms constituting seismic Sequence 2 as defined by Feary and James (1998, reprinted as Chap. 2) and projected to be Pliocene–Pleistocene in age (Fig. F2). Sequence 2 forms a thin succession over the outer shelf (70–90 m), reaches peak thickness at the present shelf edge (350–550 m), and thins as a wedge farther seaward beneath the modern slope (see "Seismic Stratigraphy," p. 26, in the "Site 1127" chapter). The sequence spans the entire width of the Eucla Basin (~350 km) and offers the opportunity to develop an in-depth understanding of shelf edge and upper slope depositional and progradational processes. Complex reflection onlap and erosional truncation patterns within the clinoform package reflect hiatus or erosional episodes. Site 1129 was located to intersect an expanded record of the oldest part of this clinoform sequence, as compared to Sites 1127 (younger part) and 1131 (middle part).

In addition, seismic data show the presence of mounded seismic facies that have been interpreted as possible deep-water biogenic features (Feary and James, 1995, 1998 [reprinted as Chap. 2]). Site 1129 was designed to intersect a thick interval of possible mounds at the top of the clinoform sequence, to determine the extent of biogenic contribution and to determine the factors controlling mound development. Seismic data show that the zone containing possible mounds extends deeper in the section beneath the outer shelf (see "Seismic Stratigraphy," p. 26, in the "Site 1127" chapter), indicating that such mounds have been a characteristic feature of the shelf edge and uppermost slope throughout the interval represented by Sequence 2.

F1. Map showing Site 1129 in relation to other Leg 182 sites and the AGSO160 seismic lines, p. 30.

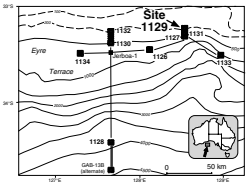

F2. Portion of seismic Line AGSO169/05a showing interpreted seismic stratigraphic sequences intersected at Site 1129, p. 31.

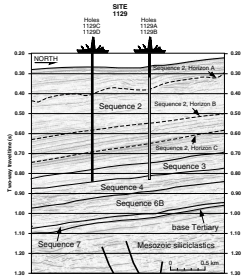

[1]Examples of how to reference the whole or part of this volume.
[2]Shipboard Scientific Party addresses.

Ms 182IR-107

The principal objective at these sites was to collect a transect of detailed high-resolution profiles through an upper Neogene shelf edge (high energy) to upper slope (low energy) succession deposited within a cool-water carbonate environment, to determine the response of such a depositional system to Pliocene–Pleistocene sea-level fluctuations.

Additional objectives were to:

1. Obtain a high-resolution record of upper Neogene paleoceanographic history within an uppermost slope/shelf edge setting as a component of the shelf-to-basin paleoceanographic transect;
2. Evaluate the diagenetic history of calcitic sediments that have accumulated in an environment that may have been near, at, or above wave base; and
3. Characterize fluid circulation and the heat-flow regime within uppermost slope/shelf edge sediments.

In addition to providing a detailed understanding of seismic Sequence 2 depositional dynamics at Site 1129, we also sought to recover an incomplete Sequence 3 record before drilling to the target depth within Sequence 4.

OPERATIONS

Transit to Site 1129

The 80-nmi transit to Site 1129 required 8.5 hr at an average speed of 9.4 kt. A beacon was launched at 1030 hr on 11 November, initiating Site 1129. A second beacon was deployed a few minutes later. Although the sea state was marginal for shallow-water rotary operations, the weather forecast was favorable, and an attempt was made to run the advanced hydraulic piston corer (APC).

Hole 1129A

The ship was stabilized on position, and Hole 1129A was spudded at 1330 hr on 11 November. The bit was positioned at 209 meters below rig floor (mbrf), and Core 1H recovered 4.35 m, indicating a water depth of 202.9 meters below sea level (mbsl). Core 1H recovered coarse-grained, unlithified bryozoan grainstones. Attempts to deepen the hole resulted in the drill string standing up in the elevators on the coarse-grained bottom. With these conditions, attempts to make a pipe connection were difficult. Thus, the hole was drilled down from 4.3 to 13.8 meters below seafloor (mbsf) in an attempt to deepen the hole below the unstable section. Core 2H was taken from 13.8 to 23.3 mbsf (Table T1); however, the pipe continued to stand up in the elevators and the heave caused the bit to pound on bottom. Hence, drilling was terminated because of shallow-water operational limitations. The pipe was pulled, both beacons were recovered, and the rig was secured for transit to Site 1130 at 1700 hr on 11 November.

T1. Site 1129 coring summary, p. 65.

Transit to Site 1129 (Hole 1129B)

Hole 1129A was terminated because of the combination of coarse-grained sediments and the marginal sea conditions for shallow-water drilling. With an improving weather forecast, the vessel returned to Site

1129 to attempt another hole. The ship was moved in dynamic positioning mode from Site 1131 back to Site 1129, and the 2-nmi transit required 0.6 hr at 3.3 kt. A beacon was dropped at 1820 hr on 19 November, followed by a second beacon, and the ship was positioned ~20 m east of Hole 1129A.

Hole 1129B

We thought it was possible to establish a stable hole by drilling in approximately two to three joints and cleaning out the coarse-grained material with frequent mud sweeps. Hole 1129B was spudded at 2030 hr on 19 November and drilled from 0 to 22.0 mbsf with two 20-bbl mud sweeps circulated on each connection. However, the bit required 40 kilopounds (kips) overpull to pull up on the second connection, and 5 m of fill was noted immediately after running back to bottom. The procedure was repeated with 5 m of fill noted again. Advanced hydraulic piston coring deepened the hole from 22.0 to 41.0 mbsf (Table T1), recovering unlithified bryozoan grainstones and rudstones. Despite pumping three more 20-bbl mud sweeps, the hole conditions remained unstable. Thus, Hole 1129B was abandoned, the drill string retrieved, and one beacon was recovered. The second beacon released but was never sighted. The rig was secured for transit back to Site 1131 at 0230 hr on 20 November.

Transit to Site 1129 (Hole 1129C)

The second attempt to core at Site 1129 suggested that the unlithified coarse-grained deposits at the top of the section were too unstable for successful coring while maintaining hole integrity. A re-examination of the seismic data indicated that a finer grained surficial succession might exist only 0.43 nmi south of Hole 1129B at the intersection of seismic Lines 169/05a and 169/05m. Approval was requested and received to spud Hole 1129C in these presumably finer grained sediments. The 44-nmi sea voyage from Site 1132 back to Site 1129 required 4.75 hr at 9.3 kt. A beacon was dropped at 2324 hr on 24 November, initiating operations.

Hole 1129C

The bit was positioned at 212.0 m, and Hole 1129C was spudded successfully at 0200 hr on 24 November. Core 1H recovered 7.29 m, indicating a water depth of 202.4 mbsl. Advanced hydraulic piston coring advanced to 216.3 mbsf with 96.2% recovery. Cores 3H–23H were oriented and Adara tool heat-flow measurements were made on Cores 4H, 8H, 10H, and 20H. The nonmagnetic APC cutting shoe was run with a standard steel flapper and 10-finger core catcher on Cores 3H, 5H, 7H, 9H, 11H, and 13H. A 20-bbl mud sweep was circulated after every fifth core. Hydrogen sulfide (H_2S) gas was detected in the core barrel on the rig floor on Core 6H, and H_2S alert procedures were implemented. The last two APC cores were partial strokes, and the last three cores had shattered liners, prompting the switch to the extended core barrel (XCB) system. Extended core barrel coring deepened the hole from 216.3 to 451.6 mbsf with 48.7% recovery (Table T1). Coring had to be terminated because of deteriorating weather conditions, which caused heave to exceed shallow-water limitations. The hole was abandoned

with 150 bbl of mud. The drill string was retrieved, and the rig floor was secured for transit at 1830 hr on 26 November.

Transit to Site 1129 (Hole 1129D)

Improving weather conditions provided the opportunity to complete operations near Hole 1129C with a rotary core barrel (RCB) hole and logging. The 26-nmi transit from Site 1133 to Site 1129 required 2.5 hr at an average speed of 10.4 kt. A beacon was deployed at 1642 hr on 28 November, and the ship was positioned on location.

Hole 1129D

A standard RCB bottom-hole assembly (BHA) was run to the seafloor, and Hole 1129D was spudded at 1915 hr on 28 November. The hole was drilled with a center bit from 0 to 280.0 mbsf in 7 hr. Rotary core barrel spot cores were taken from 280.0 to 299.6 mbsf with 16.1% recovery. After H_2S was detected in Core 1R, H_2S alert procedures were implemented. The hole was drilled again with a center bit from 299.6 to 373.2 mbsf in 2.75 hr, and RCB coring resumed from 373.2 to 604.2 mbsf (Table **T1**) with overall recovery of 30.6%. A wiper trip was performed in preparation for logging, noting 1 m of fill on bottom, and the bit was released with the mechanical bit release. The hole was filled with mud, and the end of pipe was positioned at 100 mbsf. The following logging tool strings were run from 604 mbsf: (1) triple combination logging tool (triple combo), (2) Formation MicroScanner (FMS)/sonic, and (3) well seismic tool (WST) in a 10-station check-shot survey. The pipe was run in to 150 mbsf, and the hole was abandoned with 50 bbl of mud. Both beacons were recovered, and the rig floor was secured for transit at 2215 hr on 29 November, ending operations at Site 1129.

LITHOSTRATIGRAPHY

Introduction

Site 1129 is located at a water depth of 202.4 m at the present-day shelf edge of the eastern Eucla Shelf and is the shallowest site drilled during Leg 182. The site is situated at the most landward position on a transect that include Sites 1127 and 1131.

Seismic data indicate that the seafloor on the present-day shelf edge is underlain by a thick Pleistocene succession composed of a mounded facies in the upper part and a prograding clinoform package in the lower part (Feary and James, 1998, reprinted as **Chap. 2;** see **"Seismic Stratigraphy,"** p. 26, in the "Site 1127" chapter). The near-surface, moundlike seismic feature is inferred to represent an extensive bryozoan mound complex.

The 604.2-m-thick succession of carbonate sediments recovered at Site 1129 consists of a thick Pleistocene bryozoan floatstone-dominated package, a massive upper Pliocene–Pleistocene bioclastic packstone-dominated package, and a thin middle Miocene package composed of packstone and grainstone with chert. The boundary between the Pliocene–Pleistocene and middle Miocene strata is sharp and represents a major hiatus.

The succession is divided into three units on the basis of major sediment type and compositional changes (Fig. **F3**). The sediments found at

F3. Summary of Site 1129 lithostratigraphy, **p. 32.**

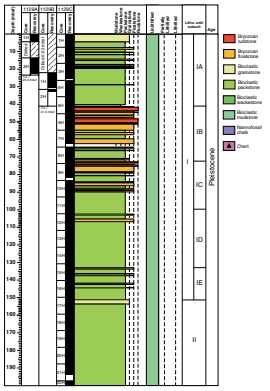

Site 1129 resemble those found at Site 1131, although some differences exist. Most of the units identified at Site 1129 can be correlated with those of Site 1131.

One of the highlights at this site is the presence of a major bryozoan mound complex in the upper 150 m of the Pleistocene succession. The temporal and spatial variability within the complex provides much important sedimentological and ecological information about cool-water carbonate biogenic accumulations.

Lithostratigraphic Units

Unit I

Intervals: Cores 182-1129A-1H through 2H; Cores 182-1129B-1H through 2H; Cores 182-1129C-1H through Section 17H-1
Depth: 0–23.30 mbsf (Hole 1129A); 22.00–41.00 mbsf (Hole 1129B); 0–151.30 mbsf (Hole 1129C)
Age: Pleistocene

Unit I consists mainly of bryozoan floatstone to rudstone and bioclastic packstone to grainstone, with abundant bryozoan fragments. The floatstone and rudstone are pale yellow to light gray and have a very fine to medium sand-sized, poorly sorted bioclastic packstone matrix. The floatstone and rudstone contain abundant granule- to pebble-sized bryozoan fragments showing highly diverse growth forms (e.g., Bone and James, 1993). The bioclastic packstone to grainstone is pale yellow, light gray, and light olive gray, and it consists of very fine to fine sand-sized bioclasts with some coarse sand- to granule-sized bryozoan fragments.

The sediments are mainly unlithified, but some poorly consolidated lumps are present in the lower part. The unit is divided into five subunits, each forming a package grading upward from bioclastic packstone at the base to bryozoan floatstone and rudstone at the top.

Subunit IA

Intervals: Cores 182-1129A-1H through 2H; Cores 182-1129B-1H through 2H; Core 182-1129C-1H through Section 5H-4, 110 cm
Depth: 0–23.30 mbsf (Hole 1129A); 22.00–41.00 mbsf (Hole 1129B); 0–41.00 mbsf (Hole 1129C)
Age: Pleistocene

Subunit IA consists of bioclastic packstone and grainstone with some thin floatstone intervals (<1 m thick) in the middle part. The boundary between different lithologies is generally gradational. The color is light gray to light olive gray. The sediment is unlithified and intensely burrowed throughout. Some of the burrows are recognized as white patches.

The packstone consists of very fine to medium sand-sized bioclasts with abundant sand- to pebble-sized bryozoan fragments floating in the packstone matrix. The granule- and pebble-sized bryozoan fragments include delicate branching, flat robust branching, arborescent/nodular, and fenestrate growth forms (Fig. F4). Granule-sized serpulid tubes are also present. The very fine to medium sand-sized fraction contains bioclasts, articulated zooidal bryozoan fragments, benthic foraminifers, sponge spicules, planktonic foraminifers, echinoid test fragments and spines, gastropods, tunicate spicules, blackened grains, and quartz grains. The bioclastic grainstone at the top of Subunit IA contains the

F4. Stratigraphic distribution of bryozoan growth forms, Unit I, p. 35.

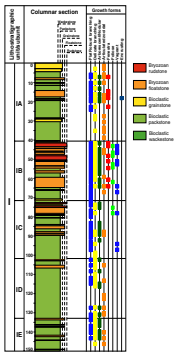

same sand-sized components as that of the packstone, together with rare glauconite grains.

The intercalated bryozoan floatstone beds contain granule- to pebble-sized bryozoan fragments, including delicate branching, flat robust branching, nodular/arborescent, and fenestrate growth forms. The matrix between the bryozoans shows a packstone texture and contains very fine to fine sand-sized bioclasts with benthic and planktonic foraminifers, delicate branching and articulated zooidal bryozoan fragments, sponge spicules, and blackened grains.

Subunit IB

Interval: Sections 182-1129C-5H-4, 110 cm, through 8H-6, 50 cm
Depth: 41.40–72.30 mbsf
Age: Pleistocene

Subunit IB consists of thick bryozoan floatstone to rudstone beds and thin bioclastic packstone beds. Floatstone and rudstone are dominant in the upper part of the subunit. The color varies between pale olive gray, light gray, and olive, and the sediment is strongly bioturbated. The upper boundary is placed where bryozoan floatstone is overlain by bioclastic packstone without the bryozoan fragments of Subunit IA.

Subunit IB has the thickest bryozoan floatstone and rudstone intervals and the most highly diverse bryozoan faunas in Unit I (Fig. **F4**). The bryozoan floatstone to rudstone contain abundant bryozoan fragments with a bioclastic packstone matrix. The bryozoan fauna has a high diversity and includes delicate branching, flat robust branching, foliose, fenestrate, vagrant, articulated zooidal, and arborescent/nodular growth forms. Granule-sized serpulid tubes also are present. The packstone matrix between the large bryozoan fragments is composed of fine sand-sized bioclasts, bryozoan fragments, benthic and planktonic foraminifers, pellets, sponge spicules, ostracodes, echinoid spines, and blackened grains.

The bioclastic packstone and grainstone contain granule- to pebble-sized nodular, flat robust branching, and articulated branching bryozoan fragments. The very fine to medium sand-sized fraction contains dominant bioclasts, common benthic foraminifers, articulated zooidal and articulated branching bryozoan fragments, present planktonic foraminifers, and rare sponge spicules, ostracodes, and echinoid spines. Blackened grains are present throughout. The finer matrix contains dominant nannofossils, abundant bioclasts, rare benthic foraminifers, sponge and tunicate spicules, and traces of pyrite (see **"Site 1129 Smear Slides,"** p. 77).

Subunit IC

Interval: Sections 182-1129C-8H-6, 50 cm, through 11H-5, 80 cm
Depth: 72.30–99.60 mbsf
Age: Pleistocene

Subunit IC consists of bryozoan floatstone and rudstone and bioclastic packstone with bryozoan fragments. The color is white, pale yellow, light gray, and light olive gray. The sediment is unlithified and strongly bioturbated. The upper boundary of Subunit IC is placed where bioclastic packstone is overlain by a graded packstone bed of Subunit IB.

The bryozoan floatstone and rudstone contain dominant bryozoan fragments, including delicate branching, flat robust branching, arborescent/nodular, foliose, and vagrant growth forms. The matrix between

the large bryozoans consists of bioclastic packstone. The medium to coarse sand-sized fraction contains pellets, benthic foraminifers, and serpulid tubes. The very fine to fine sand-sized fraction contains bioclasts with common benthic foraminifers, present planktonic foraminifers and sponge spicules, rare echinoid spines, and traces of ostracodes and blackened grains.

The bioclastic packstone consists of very fine to fine sand-sized bioclasts, with common benthic foraminifers, and present tunicate and sponge spicules, bryozoan fragments, ostracodes, pteropods, and blackened grains. Coarse sand- to granule-sized bryozoan and bivalve fragments are also present. The dominant forms of bryozoans are flat robust branching, articulated branching, foliose, and vagrant. Within the packstone, two subfacies are distinguished: one characterized by as much as 10% blackened grains and another characterized by abundant bryozoan fragments. The bioclastic packstone with blackened grains is dominant in the lower part.

Subunit ID

Interval: Sections 182-1129C-11H-5, 80 cm, through 15H-2, 65 cm
Depth: 99.60–132.95 mbsf
Age: Pleistocene

Subunit ID consists mainly of bioclastic packstone with two bryozoan floatstone beds in the upper part. The color is pale yellow, light gray, and gray. The sediments are mainly unlithified, but partially lithified lumps are present in some intervals (i.e., Section 14H-2). The sediment is strongly bioturbated. The upper boundary is placed where bioclastic packstone with abundant delicate branching bryozoan fragments is overlain by bioclastic packstone with rare bryozoans of Subunit IC.

The two bryozoan floatstone beds at the top of Subunit ID contain dominant granule-sized, blackened, delicate branching bryozoan fragments and minor amounts of flat robust branching bryozoans. The matrix consists of fine sand-sized bioclastic wackestone to packstone composed of benthic foraminifers, bioclasts, planktonic foraminifers, sponge spicules, and echinoid spines.

The packstone is dominated by bioclasts with various amounts of sand- to granule-sized bryozoan fragments. The bryozoan fauna is dominated by delicate and robust flat branching, arborescent/nodular, and articulated zooidal growth forms. In addition to the bioclasts, the very fine to fine sand-sized fraction includes common benthic foraminifers, serpulid tubes, present planktonic foraminifers, rare ostracodes, echinoid spines, and some blackened grains. Some bioclastic grains have a coating of calcite cement.

Subunit IE

Interval: Section 182-1129C-15H-2, 65 cm, through Section 17H-1
Depth: 132.95–151.30 mbsf
Age: Pleistocene

Subunit IE consists of bioclastic packstone with five bryozoan floatstone beds, each less than 80 cm thick. The color is pale yellow to light gray. The sediment is mainly unlithified, but some partially lithified lumps are scattered throughout, and the sediment is intensely bioturbated. The upper boundary is placed where bryozoan floatstone with abundant arborescent bryozoan fragments is overlain by the fine sand-sized, well-sorted bioclastic packstone of Subunit ID.

The bioclastic packstone is poorly sorted and contains dominant very fine to fine sand-sized bioclasts with scattered granule-sized bryozoan fragments. The bryozoans are usually abraded, and arborescent, delicate branching, and flat robust branching growth forms are represented. In addition to bioclasts, major components include benthic and planktonic foraminifers, articulated zooidal and delicate branching bryozoan fragments, sponge spicules, echinoid debris, ostracodes, brown organic filaments, quartz grains, and blackened grains. The bioclasts commonly have a coating of calcite cement. The texture and composition is relatively uniform throughout. The bryozoan floatstone beds are dominated by granule and larger sized particles of arborescent, robust branching and delicate branching bryozoan growth forms.

Unit II

Intervals: Section 182-1129C-17H-1 through Core 48X; Core 182-1129D-1R through Section 22R-1, 60 cm
Depth: 151.30–451.60 mbsf (Hole 1129C); 280.00–556.70 mbsf (Hole 1129D)
Age: Pliocene–Pleistocene

Unit II consists of thick light gray, light olive-gray, and gray bioturbated bioclastic packstone and minor grainstone and wackestone beds, with four nannofossil chalk intervals. The sediments are unlithified in the upper part of Unit II in interval 182-1129C-17H through 25X, whereas the sediments are partially lithified and well lithified in the middle and lower part of the unit. The sediments are slightly neomorphosed and dolomitized in the lower part of Unit II, with dolomite grains constituting ~10% (see **"Inorganic Geochemistry,"** p. 20). Body fossils commonly occur as molds. Some shells, molds, and vugs are filled with celestite. A remarkable diagenetic feature of Unit II is the presence of 3- and 6-cm oval concretions of pale yellow to yellow native sulfur in Cores 182-1129C-20H through 22H.

The sediment is bioturbated throughout and is uniform in appearance in the upper part of the unit; however, burrows are observed as diffuse green mottles in the middle to lower part. The lower part especially is dominated by abundant, well-defined burrows, including *Palaeophycus heberti, Planolites, Chondrites,* and *Zoophycos*. These burrows are filled with a variety of material, including planktonic foraminifers and unidentified green material, and commonly have a dark wall lining.

Bioclastic packstone, the dominant lithology of Unit II, is very fine to fine grained, generally well sorted, and uniform due to bioturbation. The packstone consists mainly of skeletal components with rare coarse sand- to granule-sized bryozoan fragments, represented by delicate branching and flat robust branching growth forms. The size, abundance, and diversity of bryozoan fragments are much lower than in Unit I. The other millimeter-sized fraction contains well-preserved benthic foraminifers and shell fragments. The very fine to fine sand-sized fraction contains abundant bioclasts with common benthic and planktonic foraminifers, articulated zooidal bryozoan fragments, and rare ostracodes, sponge spicules, and echinoid spines. Blackened grains are present throughout. Most of the skeletal components have calcite overgrowths.

Some grainstone beds are present in the upper and middle part of Unit II. The bioclastic grainstone beds are well sorted and have the

same composition as the packstone, with very fine to medium sand-sized grains.

The lower part of Unit II is dominated by bioclastic wackestone with subordinate bioclastic mudstone and packstone. The color is light olive gray, light gray, light brownish gray, and gray, and the grain size is silt to very fine sand sized. The coarse fraction contains planktonic and benthic foraminifers, with rare sponge spicules, glauconite grains, blackened grains, and pyrite grains. Planktonic foraminifers are abundant in some levels, and the lithology is close to chalk. The sediment is intensely bioturbated, and abundant, well-defined burrows of *P. heberti, Planolites, Zoophycos,* and *Chondrites* are present. A dense assemblage of *P. heberti* is observed in Section 182-1129D-13R-5 (Fig. F5).

Four nannofossil chalk intervals with subordinate bioclastic mudstone, wackestone, and packstone occur in Sections 182-1129C-25X, 28X, and 47X and in Sections 182-1129D-8R through 9R and 16R. The color is light olive gray and light gray, and the grain size is silt to very fine sand sized. The chalks have mudstone and wackestone textures and consist dominantly of nannofossils with abundant bioclasts. Planktonic foraminifers are also present, as well as rare sponge spicules and traces of radiolarians and tunicate spicules. The sediment is pervasively burrowed, and burrows of *Chondrites* and *Zoophycos* are observed. Intervals with a compacted, high-density *Chondrites* fabric occur at several levels (Fig. F6).

The base of Unit II consists of a clean bryozoan grainstone to rudstone bed in interval 182-1129D-22R-1, 57–60 cm. It has a sharp base that forms the boundary between Units II and III (Fig. F7). The bed is slightly graded. The coarse fraction is dominated by bryozoan fragments with delicate branching, articulated branching, flat robust branching, and vagrant growth forms. The other components are blackened grains, bioclasts, benthic foraminifers, and lithoclasts of very fine grained packstone.

Five cycles are recognized in Unit II, each grading upward from a nannofossil chalk at the base to bioclastic packstone and grainstone. The upper three cycles are dominated by very fine to fine sand-sized, generally well-sorted massive bioclastic packstone, with subordinate grainstone and wackestone. The lower two cycles are characterized by muddy bioclastic mudstone, wackestone, and packstone with abundant, well-defined burrows.

F5. *Palaeophycus heberti* within packstone from the lower part of Unit II, p. 36.

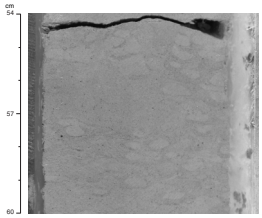

F6. *Chondrites* burrows within a bioclastic packstone, Unit II, p. 37.

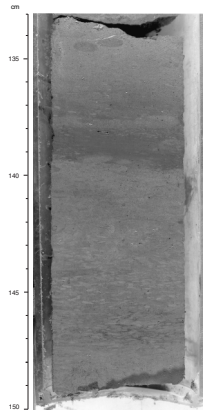

F7. The sharp boundary between Units II and III, p. 38.

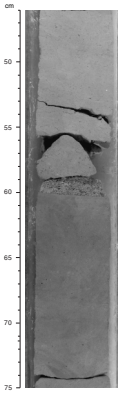

Unit III

Interval: Section 182-1129D-22R-1, 60 cm, through Core 26R
Depth: 556.70–604.20 mbsf
Age: early–middle Miocene

Unit III is characterized by very poor core recovery. The available material shows, however, that it is lithologically distinct from the overlying deposits, and this is supported by micropaleontological study (see "Biostratigraphy," p. 12). Unit III consists of bioclastic packstone to grainstone with dark gray to black chert. The upper boundary is placed at the sharp base of the thin, graded bryozoan grainstone to rudstone bed of Unit II.

The light gray, partially dolomitized, bioclastic packstone to grainstone is well lithified. The main constituents are dolomite, bioclasts, bryozoan fragments, ostracodes, planktonic and benthic foraminifers, echinoid spines, glauconite, and quartz (see "Site 1129 Thin Sections,"

p. 78). The dolomite content reaches ~40%, and the dolomite crystals are clear and silt to fine sand sized, with rhombohedral facies.

The chert is dark gray to almost black and crushed or brecciated by drilling. Chert pebbles often show ghosts after millimeter-thick burrows, probably *Chondrites,* and contain larger, poorly silicified, light gray to white burrow fills. Some pebbles have a 1- to 2-mm white rim of poorly silicified carbonate.

Discussion

The succession recovered at Site 1129 provides a sedimentologic and paleoceanographic record of a shelf edge to upper slope setting of middle Miocene to Pleistocene age.

Lower–Middle Miocene Packstone to Grainstone with Chert: Unit III

It is difficult to interpret Unit III because of its poor recovery. The limited material suggests that the succession consists of bioclastic packstone to grainstone with horizons that have been preferentially silicified. The age is interpreted as early–middle Miocene (see **"Biostratigraphy,"** p. 12). The lithology is similar to that of Unit IV at Site 1132 in the same upper slope setting on the western transect (see **"Lithostratigraphy,"** p. 3, in the "Site 1132" chapter). This indicates that both sites were situated in a similar depositional environment in the lower–middle Miocene.

It is remarkable that the top part of Unit III (interval 182-1129D-22R-1, 105–109 cm) contains as much as 20% bryozoan fragments in the coarse fraction. A tentative interpretation based on thin-section observations suggests that the sediment was deposited in a deep-slope environment. This indicates that the bryozoan fragments were brought into the deep-slope setting from the shelf edge near the site by downslope transportation and that bryozoan faunas may thus have already colonized shallower water environments by early–middle Miocene time.

Major Hiatus between Units II and III

The sharp boundary between Units II and III corresponds to the sequence boundary between seismic Sequences 2 and 3, and it represents a major hiatus between the middle Miocene and the upper Pliocene. The unit boundary can be traced to Sites 1127 and 1131, where the late Miocene–early Pliocene age interval is also absent (see **"Lithostratigraphy,"** p. 3, in the "Site 1127" chapter and **"Lithostratigraphy,"** p. 3, in the "Site 1131" chapter). Upper Miocene sediments, however, are recovered from Sites 1130 and 1132 in the western transect (see **"Lithostratigraphy,"** p. 3, in the "Site 1130" chapter and **"Lithostratigraphy,"** p. 3, in the "Site 1132" chapter).

The seismic record indicates that the sequence boundary between seismic Sequences 2 and 3, correlated with the hiatus, truncates the top of both seismic Sequences 3 and 4, implying marine erosion controlled by current flow (Feary and James, 1998, reprinted as **Chap. 2**). Further, the distribution of seismic Sequence 3 extends westward, and it is the thinnest on the transect through Site 1129 (see Fig. **F16,** p. 17, in Feary and James, Chap. 2, this volume).

Pliocene–Pleistocene Prograding Clinoform Package on a Shelf Edge Setting: Unit II

Unit II corresponds to the thick prograding clinoform package of seismic Sequence 2 (see "Seismic Stratigraphy," p. 26, in the "Site 1127" chapter), and Site 1129 intersects the proximal portion of the prograding wedge. The base of Unit II consists of a graded bryozoan grainstone to rudstone bed, with several growth forms. This indicates that bryozoan colonization of the upper slope and shelf edge had already occurred in the upper Pliocene. The thick bioclastic packstone-dominated package of Unit II, including neritic faunal elements, is interpreted as representing offshelf transport of shallow-water material (James and von der Borch, 1991).

The upper three cycles of Unit II are dominated by uniform bioclastic packstone, whereas the lower two cycles are characterized by muddy bioclastic sediments with abundant burrows. Sediment accumulation rates of the upper and lower part of this unit are calculated to be ~50 cm/k.y. and 20 cm/k.y., respectively (see "Biostratigraphy," p. 12; and "Paleomagnetism," p. 16). The differences in lithology and sedimentation rates between the upper and lower parts of Unit II seem to indicate a different depositional environment, corresponding to the change from a distal to proximal position on the prograding slope. This interpretation is supported by the transition into the bryozoan floatstone-dominated deposits of Unit I overlying this unit, which accumulated in the upper slope to shelf edge setting. Unit II is thus interpreted as being part of this overall shallowing-upward succession. Unit II contains a smaller scale cyclicity, as indicated by textural change from wackestone to grainstone and by varying abundance of blackened grains. These cycles may be related to Milankovitch-driven rhythmicity, which controls sea-level change, climate, and oceanographic dynamics. These factors are considered to significantly influence the offshelf transport and productivity of the cool-water shelf carbonates. Detailed postcruise analyses should clarify the mechanisms involved in the development of this thick prograding wedge.

One of the most remarkable aspects of Unit II is the occurrence of four nannofossil chalk intervals. Similar chalk intervals are present in Unit II at Site 1127 but are absent at Site 1131, which is located between both sites (see "Lithostratigraphy," p. 3, in the "Site 1127" chapter and "Lithostratigraphy," p. 3, in the "Site 1131" chapters). The reason for the absence of chalk at Site 1131 is unknown at present.

Pleistocene Bryozoan Mound Complex: Unit I

Unit I consists of five subunits, each representing development of a bryozoan mound. The bryozoan mound development reached a climax in Subunit IB, with the thickest floatstone to rudstone interval containing highly diverse bryozoan growth forms. Furthermore, different orders of cyclicity within the coarsening-upward succession are recognized, as is the case at Site 1132 (see "Lithostratigraphy," p. 3, in the "Site 1132" chapter). The larger cycles represent development of major mound systems, including establishment, aggradation, and lateral migration stages of the mounds. The smaller cycles may reflect Milankovitch-driven rhythmicity in either productivity or current velocity.

Subunit IA resembles the lower parts of other subunits, with a dominance of packstone and grainstone with rare floatstone. Seismic evi-

dence shows that the mound complexes are overlapping and laterally migrating with time. This subunit probably represents an intermittent stage or initial stage in mound development.

The main subunit boundaries within the bryozoan mound complex appear to correlate with seismic reflectors seen in dip sections across the shelf-slope break. Therefore, a synthesis of internal structure of the mound succession and geometric distribution of seismic reflectors will give important information on the dynamic architecture and temporal evolution of the bryozoan mound complex as a whole.

BIOSTRATIGRAPHY

Introduction

Site 1129, the shallowest (202.4 m water depth) site of an upper slope/shelf edge transect that includes Site 1131 (333.6 m water depth) and Site 1127 (479.3 m water depth), is situated at the present-day shelf edge. This site includes two biostratigraphic units: (1) an expanded Quaternary section more than 540 m thick that is underlain by a thin (16 m thick) and conformable Pliocene section (see **"Paleomagnetism,"** p. 16); and (2) a middle–lower Miocene section (Fig. **F8**). These units are separated at 556 mbsf by an unconformity of ~12 m.y. The unconformity is marked by a bryozoan turbidite overlying indurated sediments and chert layers (see **"Lithostratigraphy,"** p. 4). Calcareous nannofossils are generally abundant and moderately well preserved in the upper parts of the succession and poorly preserved below 371 mbsf. Preservation and abundance of planktonic foraminifers become increasingly degraded in the upper part of the section. Below ~68 mbsf, most characteristic features of foraminifers are obscured by carbonate cement and recrystallization.

Benthic foraminifers are generally abundant and well preserved in the upper part of Hole 1129C, and both preservation and abundance deteriorate markedly at ~140 mbsf. Three main assemblages are recognized at Site 1129: a distinctive well-preserved Pleistocene assemblage found in bryozoan-rich accumulations (down to ~140 mbsf); a Pleistocene–Pliocene assemblage (140 mbsf–565 mbsf), which includes a variable redeposited neritic component; and a sparse Miocene assemblage in Core 182-1129D-24R. The two Pleistocene assemblages indicate upper bathyal paleodepths, whereas the Miocene assemblage indicates an upper to middle bathyal paleodepth.

Sedimentation rates for most of the Pleistocene were relatively high, reaching a maximum of 542 m/m.y. (Fig. **F9**). However, in the upper Pliocene and lower Pleistocene to the bottom of the Jaramillo, the sedimentation rate was considerably lower (142 m/m.y.). A sedimentation rate was not calculated for the sediments below the unconformity because of the lack of datum levels.

Calcareous Nannofossils

Site 1129 contains an expanded Pleistocene sequence (~554.70 m), overlying a short middle–lower Miocene sequence (~40 m), a succession similar to those at Sites 1127 and 1131. Hole 1129C is rich in nannofossils that are moderately well preserved in the upper 360 mbsf, but degraded to poorly preserved in the bottom 80 m of the hole. Although

F8. Calcareous nannofossil and planktonic foraminiferal zones and benthic foraminiferal assemblages, **p. 39.**

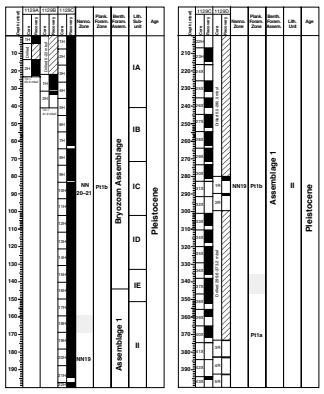

F9. Sedimentation rate curve from Site 1129 datum levels, **p. 41.**

sediments from Hole 1129D are also rich in nannofossils, they are generally poorly preserved.

The upper 160 mbsf at Site 1129 is characterized by common to abundant *Gephyrocapsa caribbeanica,* common small *Gephyrocapsa* spp., and common occurrences of *Calcidiscus leptoporus*. The lack of *Pseudoemiliania lacunosa* indicates that this section should be assigned to the combined Zones NN21–NN20. Also present in this section are *Coccolithus pelagicus, Dictyococcites antarcticus, Dictyococcites productus, Helicosphaera carteri, Oolithotus fragilis, Rhabdosphaera clavigera,* and *Umbilicosphaera sibogae*.

Sample 182-1129C-18H-CC, 8–11 cm (168.85 mbsf), contains the highest stratigraphic occurrence of *P. lacunosa,* indicating that sediments below this horizon in Hole 1129C (to 444.88 mbsf) and from Samples 182-1129D-1R-CC, 6–9 cm (282.33 mbsf), to 21R-CC, 31–34 cm (554.70 mbsf), belong to Zone NN19. Proceeding downhole, abundances of small *Gephyrocapsa* spp. increase, *G. caribbeanica* decrease, and *C. leptoporus* varies from rare to common. The highest stratigraphic occurrence of *Calcidiscus macintyrei* is found in Sample 182-1129C-37X-CC, 24–27 cm (347.47 mbsf). This occurrence may be caused by reworking because it does not occur again until Sample 182-1129C-45X-CC, 20–23 cm (414.00 mbsf).

Samples 182-1129D-22R-CC, 16–19 cm (557.68 mbsf), to 26R-CC, 30–33 cm (594.90 mbsf), contain *Sphenolithus heteromorphus,* together with *Cyclicargolithus floridanus, Sphenolithus moriformis,* and *Braarudosphaera bigelowii*. This association indicates a zonal assignment to the combined Zones NN5–NN4. This section lies directly below a bryozoan turbidite marking an unconformity that spans 12 m.y. (see **"Lithostratigraphy,"** p. 4).

Planktonic Foraminifers

The section at Site 1129 is comprised of two biostratigraphic units: (1) a Pleistocene interval that exceeds 540 m in thickness, underlain conformably by an ~17-m-thick upper Pliocene unit; and (2) a middle Miocene unit. The biostratigraphic units are separated by an unconformity that coincides with the boundary between lithostratigraphic Units II and III at 556.7 mbsf (see **"Lithostratigraphy,"** p. 4), and appears to correspond to the base of seismic Sequence 2 (see **"Seismic Stratigraphy,"** p. 26, in the "Site 1127" chapter). The succession of biostratigraphic units is similar to those at Sites 1127 and 1131.

Preservation and Abundance

Planktonic foraminifers are comparatively rare, although beautifully preserved, among abundant bryozoans, gastropods, ostracodes, and benthic foraminifers in the sand-sized fraction above 36.28 mbsf. However, preservation and abundance decline rapidly, from moderate below 36.28 mbsf to poor below ~68 mbsf, and carbonate cement and recrystallized overgrowths obscure test features throughout the remainder of the section. Some intervals are so degraded that they contain no recognizable taxa. In general, the inferior condition of the tests makes us uncertain whether we accurately recognized the first and last occurrences of species used to mark zonal boundaries. This is borne out by magnetostratigraphic results and is discussed in **"Paleomagnetism,"** p. 16.

Quaternary

The two most abundant species of the well-preserved, temperate assemblage above ~68 mbsf are *Globigerinoides ruber* and *Globorotalia inflata*. Eleven other species are rare to common and include *Globigerina bulloides, Globigerina falconensis, Globigerina quinqueloba, Globigerinita glutinata, Globorotalia hirsuta, Globorotalia truncatulinoides, Orbulina universa, Neogloboquadrina pachyderma* (dextral), and *Zeaglobigerina rubescens*. Only a few robust and distinctive species, however, are consistently recognized in the poorly preserved section below ~68 mbsf. They are *Globorotalia inflata, G. ruber, N. pachyderma,* and *G. truncatulinoides*.

Samples above ~414 mbsf are placed in Pleistocene Zones Pt1 (Berggren et al., 1995) and SN14 of Jenkins (1985, 1993), based on the presence of *G. truncatulinoides*. The last occurrence of *Globorotalia tosaensis* between 335.83 and 347.47 mbsf (Sample 182-1129C-37X-CC, 24–27 cm) is used to divide the zone into Subzones Pt1b and Pt1a. Poor preservation, however, may have deepened the last appearance of *G. tosaensis,* which occurs between 335.83 and 347.47 mbsf. This is only slightly above the Brunhes/Matuyama boundary, which lies between 338.8 and 347.2 mbsf in Hole 1129C (see **"Paleomagnetism,"** p. 16). The last occurrence of *G. tosaensis* occurred at 0.65 Ma in subtropical latitudes and locally at 0.71 Ma. Based on data from Site 1127, this datum should lie 71 to 38 m above the Brunhes/Matuyama boundary, based on estimates from the sedimentation rate for this interval (Fig. **F9**).

Placement of the base of Zone Pt 1 also may be affected by poor preservation. The poor preservation may have caused the first appearance of *G. truncatulinoides* to be recognized at a depth that is too shallow. This horizon occurs 42 m below the onset of the Jaramillo Subchron, and its age is estimated to be 1.04 Ma on the basis of the sedimentation rate. The estimate is much younger than the age of the first appearance of *G. truncatulinoides* in subtropical regions (excluding the southwest Pacific Ocean according to Berggren et al., 1995). The estimate is also younger than the age estimated at 1.23 Ma at nearby Site 1127 in which preservation is superior.

Globorotalia crassaformis Interval

Samples from 413.86–432.93 mbsf to 554.7–554.70 mbsf contain most of the species found in the Pleistocene Zone Pt1 described above, although without *G. truncatulinoides* and with more common *G. crassaformis*. Therefore, the unit is placed in the *G. crassaformis* interval, which at this site includes a lengthy portion of the lower Pleistocene and a portion of the upper Pliocene (Fig. **F8**) on the basis of magnetostratigraphy (see **"Paleomagnetism,"** p. 16) (Berggren et al., 1995).

Miocene

The middle Miocene section below the disconformity at 556.7 mbsf (see **"Lithostratigraphy,"** p. 4) contains two samples (Samples 182-1129D-22R-CC, 16–19 cm, and 24R-1, 20–25 cm, from 557.68 and 575.60 mbsf, respectively) containing sparse and poorly preserved planktonic foraminifers. Both samples contain *Globigerinoides trilobus* and *Globoconella conoidea,* an association consistent with a late–middle Miocene age. The latter sample also contains *Globigerinella obesa, Zeaglobigerina woodi, Globigerinita glutinata, O. universa, Globoconella*

miozea, Globoquadrina dehiscens, Globigerinita juvenilis, and *Neogloboquadrina continuosa*. The association of the last five species is consistent with a middle Miocene age.

Benthic Foraminifers

Benthic foraminifers were studied from the only two core-catcher samples recovered at Hole 1129B and from every fourth core-catcher sample from Holes 1129C and 1129D. Additional samples were examined from intervals in which marked lithologic change occurred. Benthic foraminifers are generally abundant and well preserved at Hole 1129B and in the upper part of Hole 1129C (Cores 1H–15H). Abundance decreases significantly and preservation deteriorates markedly below Core 182-1129C-15H. Between 100 and 300 benthic foraminifers were picked from the >63-µm fraction, except in samples in which abundance was low. The benthic foraminiferal assemblages at Site 1129 contain mainly cosmopolitan taxa, although they also include species with a more geographically restricted distribution. Postcruise studies will be necessary to fully document benthic foraminifer distribution at Site 1129 during the Pleistocene and to investigate faunal changes in relation to climate, sea-level, and/or circulation fluctuations within a sequence stratigraphic framework. A shallowing-upward trend from middle bathyal paleodepths in the Miocene to upper bathyal paleodepths in the Pleistocene is exhibited by the following assemblages at Site 1129.

Bryozoan Assemblage (Pleistocene)

Cores 182-1129B-1H through 2H and 182-1129C-1H through 15H

This relatively diverse, well-preserved assemblage is found in core-catcher samples together with abundant, well-preserved bryozoan fragments. It includes some large specimens (>1 mm) of *Sigmoilina obesa, Heterolepa dutemplei, Textularia* spp., *Spirillina* spp., and miliolids. Also present as rare to few constituents of the assemblage are *Sphaeroidina bulloides, Martinottiella communis, Sphaeroidina variabilis, Hoeglundia elegans, Bigenerina nodosaria, Uvigerina hispidocostata, Bulimina marginata, Bolivina* spp., *Loxostomum* spp., *Loxostomoides* spp., *Rosalina* spp., *Cibicidoides* spp., *Anomalinoides* spp., and various nodosariids. The presence of *S. bulloides, Hoeglundia elegans, B. nodosaria,* and *Bulimina marginata* indicates upper bathyal paleodepths. Similar benthic foraminiferal assemblages were found at Sites 1131 and 1132. They appear to have been associated with the establishment of diversified bryozoan communities at the seafloor at various times during the Pleistocene. Variations in the composition of the assemblage may reflect changes in circulation or sea level in the Great Australian Bight, which may have also influenced the development of bryozoan buildups during the Pleistocene. Further sedimentological and micropaleontological work will clarify the evolution of these bryozoan buildups and the paleoceanographic setting of the Great Australian Bight.

Assemblage 1 (Pleistocene)

Cores 182-1129C-16H through 48X and 182-1129D-1R through 22R

This impoverished assemblage is characterized by fluctuating numbers of *Hoeglundia elegans, M. communis, H. dutemplei, S. bulloides, Plan-*

ulina wuellerstorfi, U. hispidocostata, Loxostomum spp., *Loxostomoides* spp., *Elphidium* spp., *Rosalina* spp, *Cibicidoides* spp., *Anomalinoides* spp., *Palliolatella* spp., miliolids, and various nodosariids. Upper bathyal paleodepths are suggested by the presence of the depth-indicative species *Hoeglundia elegans, S. bulloides, M. communis, H. dutemplei,* and *U. hispidocostata*. Variable abundance of small miliolids and *Elphidium* spp. suggests that part of the assemblage was redeposited from shallower depths. However, poor preservation in many of the samples and generally low abundance overall prevent detailed analysis of faunal changes within this interval.

Assemblage 2 (Miocene)

Sample 182-1129D-24R-1, 20–25 cm

A sparse assemblage was found in Sample 182-1129D-24R-1, 20–25 cm, within an interval of poor recovery in which mostly chert fragments were recovered. This assemblage is characterized by *Vulvulina spinosa, Plectofrondicularia vaughni, Rectuvigerina striata, Siphonina tenuicarinata, Bolivina* spp., and various nodosariids. Middle bathyal paleodepths are suggested by the presence of *V. spinosa, P. vaughni,* and *R. striata*.

Sedimentation Rates

Sediment accumulation rates were calculated from preliminary biostratigraphic and paleomagnetic data from Site 1129. The results are presented in Figure **F9.** The biostratigraphic datum levels, together with the paleomagnetic data used, are listed in Table **T2.**

T2. Datum levels used in the graph of sedimentation rate, **p. 68.**

An exceptionally high sedimentation rate, averaging 364 m/m.y., is calculated for the Pleistocene section. During the Jaramillo polarity reversal, the sedimentation rate reached its peak of 542 m/m.y. In contrast, the underlying lower part of the Pleistocene registered 142 m/m.y., the slowest rate for the entire Pliocene section. A major disconformity below the Pliocene section is indicated by the simultaneous downhole disappearance of two planktonic foraminifers, *G. crassaformis* and *G. puncticulata,* that originate in the lower Pliocene, with the downhole appearance of the middle–lower Miocene nannofossil *S. heteromorphus*. Biostratigraphic data suggest that the entire lower Pliocene and the greater part of the Miocene (nannofossil Zones NN18–NN6) are missing. The duration of this hiatus is >11 m.y.

PALEOMAGNETISM

Shipboard paleomagnetic measurements for Holes 1129C and 1129D consisted of long-core measurements at 5- to 10-cm intervals of the natural remanent magnetization (NRM) and the remanence after alternating field (AF) demagnetization at 20 mT, as described in **"Paleomagnetism,"** p. 12, in the "Explanatory Notes" chapter. Measurements were performed on archive halves of all APC and XCB cores, except for intervals affected by core disturbance. Long-core measurements established a magnetostratigraphy to a depth of ~550 mbsf, which includes the Brunhes and upper Matuyama epochs. In partially lithified materials below 250 mbsf, measurements on discrete samples were used to confirm polarity determinations obtained from long-core measurements. Discrete samples were also collected from representative

core material and subjected to progressive AF demagnetization up to 30 mT. These samples were also used for anhysteretic remanent magnetization (ARM) and isothermal remanent magnetization (IRM) acquisition and demagnetization experiments.

Long-Core Measurements

The intensity of initial remanence is very low, with a median of ~2 × 10^{-4} A/m. High values occur in the uppermost 10 mbsf, as well as anomalous spikes observed at the top of several cores. The NRM is of shallow negative to moderate positive inclination (Fig. **F10**). After partial demagnetization (20 mT), magnetizations above ~340 mbsf are of moderately to steeply negative inclination, except for isolated outliers. This indicates that "blanket" demagnetization preferentially removes a magnetization of positive inclination. Inclinations are scattered, and the mean (I = –35°) is more shallow than expected for the present latitude of the site. The scatter is larger than expected for the natural variation of the geomagnetic field and larger than observed at other sites on the eastern shelf-slope transect (Sites 1127 and 1131).

We attribute most of the scatter observed in inclination values to instrument noise and partial contamination, reflecting the fact that intensity of the magnetization is significantly lower than at Sites 1127 and 1131. Differences in intensity between this and other sites are more significant in the upper 250 mbsf, with intensities at Site 1129 one order of magnitude lower than at Site 1127. Intensities at Site 1131 are only slightly higher than at 1129. Similarly, the lowest scatter around the mean inclination and the best estimate of expected value for the present latitude of the site is observed at Site 1127, with considerable scatter around the mean at Site 1129. Interestingly, below ~275 mbsf all three sites are characterized by similar intensities. This observation may suggest that diagenetic reactions that partially consume ferromagnetic phases within the sedimentary package are more active in the shallower sites of the transect.

Below depths of ~350 mbsf in Hole 1129C, long-core measurements are affected by persistent core disturbance (biscuits). Discrete samples obtained from disturbed sediments carry a magnetically hard remanence of high intensity, and thus polarity determinations are based on independent measurements on discrete samples and biscuits chosen to exclude disturbed sediment. Measurements of discrete samples reveal a characteristic magnetization that is isolated after removing a spurious overprint, which we interpreted as a drilling-induced remanence. Median destructive fields range between ~15 and 30 mT. In a biscuit from the interval 182-1129C-30X-1, 100–103 cm (Fig. **F11A**), a soft component with a steep downward inclination is removed first, isolating a characteristic magnetization of normal polarity and moderately high coercivity. In a biscuit from the interval 182-1129C-30X-3, 78–81 cm (Fig. **F11B**), a similar magnetization is isolated only after demagnetization with inductions of 20 mT. For samples obtained from Hole 1129D, the overprinting magnetization is of negative inclination. In the interval 182-1129D-3R-1, 24–28 cm (Fig. **F11C**), a prominent "soft" steep magnetization is removed with inductions of 10 mT, isolating a characteristic magnetization of reverse polarity. The different sign of the overprinting magnetization in XCB and APC cores and in RCB cores suggests that this is indeed associated with the BHA.

The magnetic Tensor tool was used in APC Cores 182-1129C-3H through 19H, although reorientation of declination data was unsuc-

F10. Downhole inclination, with interpreted magnetostratigraphy, **p. 42.**

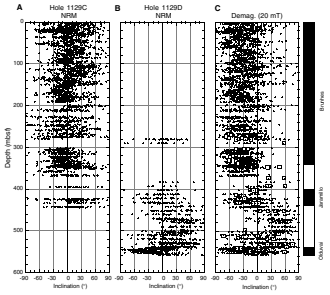

F11. Normalized intensity decay and demagnetization diagrams of representative samples, **p. 43.**

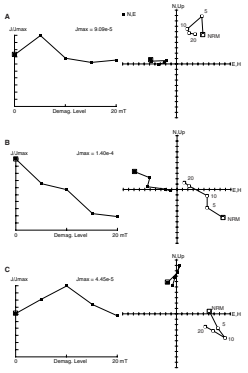

cessful. Uncorrected declinations of the NRM long-core measurements of APC cores from Hole 1129C are consistently biased in the direction of the fiducial orientation line (0° declination in sample coordinates). After partial demagnetization, declinations are more scattered, although the bias toward 0° declination persists. Furthermore, when declinations are corrected using Tensor tool data, between-core declinations are more scattered. For XCB cores where azimuthal orientation is not available, declinations are preferentially at 90° from the core fiducial line.

Normal polarity magnetizations are persistent in Cores 182-1129C-1H through 37X (0 to ~340 mbsf) (Fig. F10). Within this normal polarity, we observed intensity fluctuations in NRM after 20-mT demagnetization. These are particularly well developed at depths above 200 mbsf. Because these oscillations probably reflect secular variation of the geomagnetic field, they may provide an independent tool for between-hole stratigraphic correlation after normalizing to account for the effects of variations in concentration of ferromagnetic minerals.

Rock Magnetism

Rock magnetism analysis consisted of measurements of weak-field susceptibility, IRM acquisition, and AF demagnetization of ARM. Rock magnetic properties are rather uniform within the cored interval, although there is an overall trend suggesting that coercivity of the NRM decreases downhole, an observation generally attributed to dissolution of fine-grained particles (Karlin and Levi, 1983). Decay of the NRM upon AF demagnetization is typical of a cubic phase, either magnetite or greigite. Representative samples were given a 400-mT IRM and subsequently demagnetized (Fig. F12). Inductions of 400 mT are not sufficient to reach saturation, suggesting that magnetic sulfides are present and may be important remanence carriers. AF decay of the IRM suggests that in some of the cored intervals, contributions from single-domain-size particles is less important than from multidomain particles (Cisowski, 1981). This is also manifest in the lower ARM:IRM ratios observed at this site. Magnetic susceptibility is of low negative values and is therefore dominated by the contributions of the diamagnetic carbonate matrix.

F12. Acquisition of IRM and its AF demagnetization, p. 44.

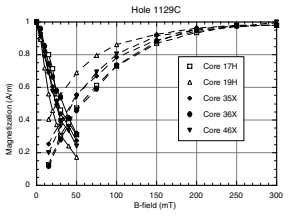

Magnetostratigraphy

Moderately to steeply positive inclinations in discrete samples from Core 182-1129C-37X (at ~340 mbsf) are interpreted as reverse magnetizations, placing the Brunhes/Matuyama boundary between 338.8 and 347.2 mbsf. Long-core and discrete sample measurements in Hole 1129D define a long interval of predominantly reverse polarity magnetizations to a depth of ~540 mbsf, which is interpreted as the upper part of the Matuyama (C1r). The top of the Jaramillo Subchron (C1r1n) is recorded in both holes at depths of ~400–440 mbsf. Discrete samples place the upper boundary between 392.9 and 402.6 mbsf. Long-core measurements place the lower boundary of this subchron between Sections 182-1129D-9R-2 and 10R-1, at 440.8 mbsf. Normal polarities are recorded again in Hole 1129D at depths of 540–550 mbsf, possibly representing Chron C2n (Olduvai). This correlation to the Pliocene–Pleistocene geomagnetic polarity timescale implies a variable sedimentation rate, with an upper Pleistocene sedimentation rate nearly triple that of the lower Pleistocene. Correlation with the geomagnetic polarity time

scale is nonunique, but is supported by the available biostratigraphic data.

ORGANIC GEOCHEMISTRY

At Site 1129, in addition to routine monitoring of hydrocarbon and H_2S gases for safety, analyses were conducted for inorganic carbon, total carbon, nitrogen, sulfur, and organic matter characterization. The analytical procedures are described in "Organic Geochemistry," p. 16, in the "Explanatory Notes" chapter.

Volatile Hydrocarbons and Hydrogen Sulfide

Concentrations of volatile hydrocarbons and H_2S were routinely determined in samples from Holes 1129C and 1129D using standard ODP headspace or vacutainer sampling procedures. The striking results from Site 1129, as at Sites 1127 and 1131, are the high concentrations of methane (C_1) and H_2S in much of the section (Tables T3, T4). Eight gas pockets occurred in Hole 1129C from 62.3 to 366.3 mbsf, with seven of the eight between 313.9 and 366.3 mbsf. These were sampled directly through the core liner using a gas-tight syringe (vacutainer). Concentrations of C_1 in these gas pockets ranged from a low of 313 ppm in the shallow pocket to between 19,344 and 244,598 ppm in the deeper pockets (Table T3). By comparison, gas pockets at Site 1129 were twice as abundant as at Site 1131; however, gas pockets at Site 1127 were much more abundant than at Sites 1129 and 1131. Methane concentrations in the gas pockets at Site 1129 fall between the levels found at Site 1127, which had a high of 585,000 ppm, and Site 1131, which had a high of 81,267 ppm (see "Organic Geochemistry," p. 19, in the "Site 1127" chapter and "Organic Geochemistry," p. 17, in the "Site 1131" chapter).

T3. Vacutainer gas compositions, Hole 1129C, p. 69.

T4. Headspace gas compositions, p. 70.

Methane occurs at lower concentrations in the headspace samples from Holes 1129C and 1129D than in vacutainer samples. The lowest values are at the tops and bottoms of the cored interval and reach a maximum at 258.9 mbsf (Table T4; Fig. F13). From 4.5 to 40.3 mbsf, C_1 values are <10 ppm. From 49.8 to 258.9 mbsf, C_1 increases to 12,043 ppm, the highest value, and then decreases with some scatter to 235 ppm at the bottom of Hole 1129D. The C_1 profile at Site 1129 is similar to the profile at Site 1131, except that the maximum in C_1 concentration occurs at a deeper level at Site 1129 (see "Organic Geochemistry," p. 17, in the "Site 1131" chapter).

F13. Headspace gas compositions for Holes 1129C and 1129D, p. 45.

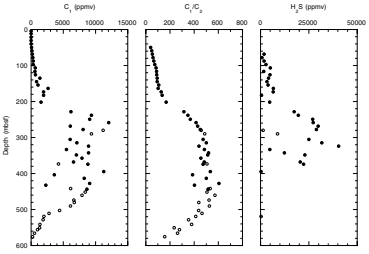

Ethane (C_2) occurs from 49.8 mbsf to the base of Hole 1129D at concentrations as high as 28.9 ppm in headspace samples (Table T4). C_1/C_2 values in headspace samples from the same depth interval first increase from 40 to 605 and then decrease to a low of 157 at the bottom of Hole 1129D (Table T4; Fig. F13). The same pattern of increasing and decreasing C_1/C_2 values with depth is present at Site 1131 (see "Organic Geochemistry," p. 17, in the "Site 1131" chapter). The change in ratio with depth tracks the increase and decrease in C_1 concentration, as C_2 concentrations do not vary significantly from 135.3 mbsf to the base of Hole 1129C. Heavier hydrocarbon gases (C_{3+}) were detected in a few headspace samples, primarily from 324.3 to 528.6 mbsf in Holes 1129C and 1129D, as well as in the seven deepest gas pockets.

The concentrations of H_2S in the eight gas pockets in Hole 1129C range from 313 ppm, in the shallowest pocket, to a high of 136,577 ppm, which is intermediate between values measured from Sites 1127 and 1131 (Table T3). The H_2S in headspace samples from Hole 1129C reaches concentrations as high as 40,445 ppm at 324.3 mbsf. The headspace concentrations are lower than those found in gas pockets, although as with the gas pockets, the H_2S values are intermediate between those at Sites 1127 and 1131 (Table T4; see "Organic Geochemistry," p. 17, in the "Site 1127" chapter and "Organic Geochemistry," p. 17, in the "Site 1131" chapter).

Inorganic and Organic Carbon, Sulfur, and Nitrogen

Throughout Hole 1129C, carbonate values are uniform and range primarily from 88 to 94 wt% (Table T5; Fig. F14). Organic carbon (C_{org}) ranges primarily from 0.3 to 0.7 wt%, with little variation throughout the section, except for one value of 1.46 wt% at 433.0 mbsf (Table T5; Fig. F14).

Nitrogen concentrations are <0.1 wt%, and many samples have no detectable nitrogen. One exception is the sample with highest C_{org} at 433.0 mbsf, which has a nitrogen content of 0.12 wt%. Sulfur was not detected in any sample (Table T5).

Characterization of Organic Matter at Sites 1127, 1129, 1131, and 1132

Rock-Eval pyrolysis data for selected samples with higher concentrations of organic carbon from Sites 1127, 1129, 1131, and 1132 indicate that the organic matter is immature type I (Table T6; Fig. F15). T_{max} values are generally between 410° and 425°C, and hydrogen indices (HI) range as high as 470. Samples from Site 1127 have higher T_{max} and HI values than samples from Sites 1129, 1131, and 1132.

INORGANIC GEOCHEMISTRY

Interstitial Waters

One 5-cm whole-round core was taken from Hole 1129A for interstitial water analysis. Similar whole-round samples were taken from Hole 1129C at a rate of one sample per section from the upper 15 cores and every other core thereafter, recovery permitting. Samples were analyzed according to the procedures outlined in "Inorganic Geochemistry," p. 18, in the "Explanatory Notes" chapter. These data are presented in Table T7 and Figures F16, F17, and F18.

Salinity, Chlorinity, Potassium, and Sodium

Salinity exhibits no change over the upper five cores, to a depth of 40.3 mbsf. This same trend of invariant change is exhibited in all conservative and nonconservative tracers, and is considered to be equivalent to the flushed zone discovered during Leg 166 on the margin of Great Bahama Bank (Eberli, Swart, Malone, et al., 1997) (see "Discussion," p. 21). Below the flushed zone, the concentrations of Na^+, Cl^-, and K^+ all increase steadily to the base of the cored interval. The Na^+/Cl^-

T5. C, C_{org}, N, and S data, Holes 1129C and 1129D, p. 71.

F14. $CaCO_3$ and C_{org} contents for Holes 1129C and 1129D, p. 46.

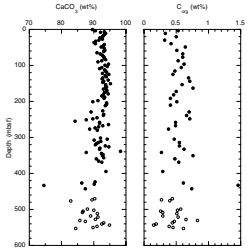

T6. Rock-Eval data, Sites 1127, 1129, 1131, and 1132, p. 73.

F15. T_{max} vs. HI for Sites 1127, 1129, 1131, and 1132, p. 47.

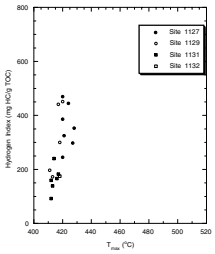

T7. Interstitial water geochemistry, p. 74.

ratio exhibits a midprofile maximum of 1.05 at a depth of 135.2 mbsf (Fig. F16).

Calcium, Magnesium, Lithium, Silica, and Strontium

As mentioned previously, the upper 40.3 mbsf is characterized by essentially constant concentrations of the nonconservative elements, including Mg^{2+}, Ca^{2+}, Sr^{2+}, Li^{+}, and $H_4SiO_4^0$. Below this depth, the concentrations of Mg^{2+} and Ca^{2+} exhibit significant decreases in the upper 300 mbsf, with Mg^{2+} falling to 14.6 mM and Ca^{2+} to 3.9 mM at 201.7 mbsf (Fig. F17). With increasing depth, the concentrations steadily rise to the base of the cored interval, although ratios relative to Cl^- remain lower than in normal seawater (Fig. F18). The concentration of Sr^{2+} shows two principal increases below the flushed zone, the first between 40.3 and 87.7 mbsf, and the second between 201.7 and 305.4 mbsf (Fig. F17). The first increase in Sr^{2+} is associated with a decrease in the concentration of high-Mg calcite (HMC) and the appearance of dolomite, whereas the second is associated with increasing amounts of cementation (see "Lithostratigraphy," p. 4) and a decreasing amount of aragonite. Note that in the flushed zone, there is no measurable concentration of dolomite.

Sulfate, Alkalinity, Ammonia, Iron, and pH

Although there is no net deficit of SO_4^{2-} in the upper 116.2 mbsf, alkalinity increases downward substantially and H_2S is abundant over the same interval (see "Organic Geochemistry," p. 19). This suggests that H_2S is diffusing upward from underlying sediments and is being oxidized to SO_4^{2-} (Fig. F18). Below 116.2 mbsf, the normalized concentration of SO_4^{2-} decreases to a minimum at 268.3 mbsf. Over the same interval, the concentrations of NH_4^+ reach 26.7 mM (Table T7).

Alkalinity shows a maximum value of 97.28 mM at a depth of 28.6 mbsf. Toward the bottom of the hole, alkalinity decreases to a value of 29.51 mM. Values for pH and pH determined using the push-in electrode (ppH) are relatively consistent, decreasing to 5.9 at a depth of 427.3 mbsf (Fig. F18).

X-Ray Mineralogy

The sediments at Site 1129 are composed of low-Mg calcite, HMC, quartz, aragonite, and dolomite (Fig. F19; Table T8, also in ASCII format). High-Mg calcite is the dominant mineralogy at the top of the cored interval, but it decreases rapidly to zero coincident with the boundary between lithostratigraphic Units I and II (see "Lithostratigraphy," p. 4). This boundary marks the transition between bryozoan mounds and the underlying bioclastic packstones. The decrease in HMC is concurrent with the increase in dolomite, which reaches sustained concentrations of ~20% and has a maximum concentration of 30%. At the base of Unit II, the concentration of aragonite decreases to ~5%.

Discussion

Sites 1129, 1131, and 1127 form a depth transect from shallow water (200 m) to deeper water (480 m) and present an ideal opportunity to ex-

F16. Concentration depth profiles of salinity, Cl^-, Na^+, K^+, and Na^+/Cl^-, p. 48.

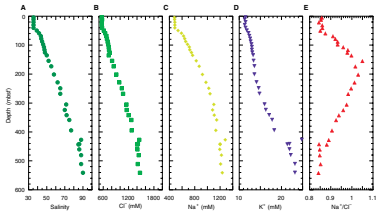

F17. Concentration depth profiles of Mg^{2+}, Ca^{2+}, Sr^{2+}, Li^+, and $H_4SiO_4^0$, p. 49.

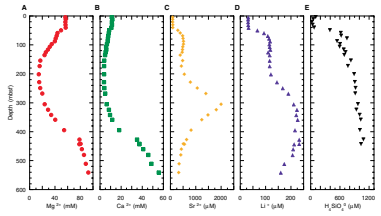

F18. Variations in pH and interstitial water compositions, p. 50.

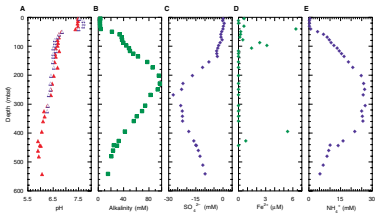

F19. Variations in mineral concentrations, p. 51.

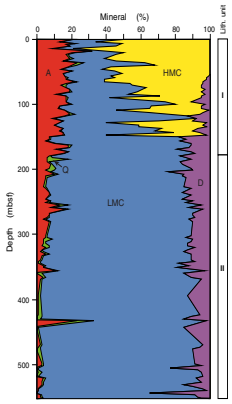

T8. XRD data, p. 75.

amine pore-water geochemistry in a transect from the platform margin toward deeper water and to understand the origins of the saline fluids, high alkalinities, and sulfate reduction observed at these three sites.

Salinity

All three sites are influenced by the presence of high-salinity fluids within and beneath the cored intervals. A contour plot of the Cl^- (Fig. F20) data reveals that contours of equal Cl^- concentration crosscut sequence boundaries (i.e., they are subhorizontal). This observation is consistent with emplacement of the brine during previous sea-level lowstands, under the influence of a hydraulic head from the adjacent continent. The present concentrations in the pore waters are derived from the diffusion of cations and anions from a region of high concentration (the brine) to a region of low concentration (overlying seawater and underlying sediments). The Na^+/Cl^- ratio also changes between the proximal and the distal sites (Fig. F21). At Sites 1129 and 1131, there is a pronounced maximum in the ratio, although at Site 1127, this ratio has decreased (Fig. F21). The presence of fluids with a high Na^+/Cl^- ratio suggest that the sediments were also influenced by a brine that had either dissolved Na^+/Cl^- or had been involved in the precipitation of evaporite minerals. The higher Na^+/Cl^- in the proximal sites is consistent with origination of this brine on the continent. The location of the fluids with high Na^+/Cl^- within the Pleistocene constrains the timing of the brine emplacement.

F20. Contour plot showing Cl^- variation; Sites 1127, 1129, and 1131, p. 52.

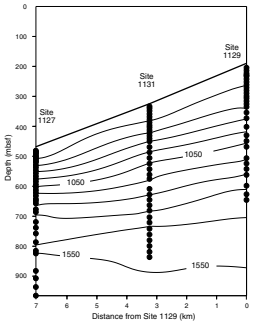

F21. Na^+/Cl^- vs. depth; Sites 1127, 1131, and 1129, p. 53.

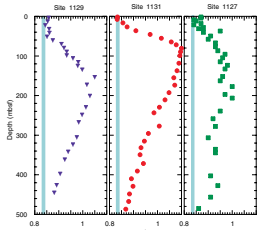

Alkalinity and Sulfate

Although the maximum amount of sulfate reduction occurs in the sediments from Site 1129 (Fig. F22), Site 1131 shows the maximum increase in alkalinity (Fig. F23) and exhibits the highest concentrations of H_2S and CH_4 (see "Organic Geochemistry," p. 19; "Organic Geochemistry," p. 17, in the "Site 1127" chapter, and "Organic Geochemistry," p. 17, in the "Site 1131" chapter). Although the connection between the degree of sulfate reduction and alkalinity remains to be precisely defined at these sites, the high alkalinity at Site 1131 is a combination of SO_4^{2-} supply, the amount and nature of organic material, and the amount of mud in the sediment. At Site 1127 for example, the sediment appears to be somewhat finer grained than at the two more proximal sites (see "Lithostratigraphy," p. 3, in the "Site 1127" chapter). This allows the pore fluids at Site 1127 to act as a closed system and to become more depleted in SO_4^{2-} near the sediment/seawater interface. In contrast, SO_4^{2-} is never completely depleted at the other sites and the zone of lowest SO_4^{2-} concentration is much deeper at Sites 1129 and 1131 than at Site 1127 (Fig. F22). At all three sites, the relatively steep SO_4^{2-} concentration gradient in the lower portion of the cored intervals allows the higher than normal rates of diffusion of SO_4^{2-} to the zone of organic material oxidation. At both proximal sites (Sites 1129 and 1131), the upper profile of SO_4^{2-} in the sediments is modified by oxidation of H_2S in the upper portion of the profile.

F22. Excess SO_4^{2-}; Sites 1127, 1131, and 1129, p. 54.

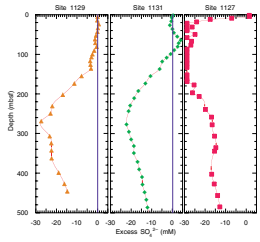

F23. Contour map of alkalinity; Sites 1127, 1131, and 1129, p. 55.

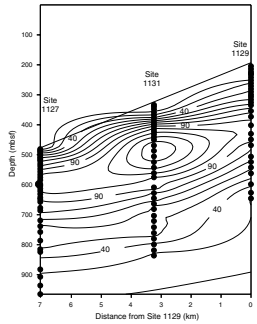

Carbonate Diagenesis

Of the three sites in this transect, Site 1127 exhibits the lowest amount of carbonate recrystallization. This conclusion is supported by

observations of the degree of cementation (see "Lithostratigraphy," p. 4, and "Biostratigraphy," p. 12; "Lithostratigraphy," p. 3, and "Biostratigraphy," p. 9, in the "Site 1127" chapter; and "Lithostratigraphy," p. 3, and "Biostratigraphy," p. 9, in the "Site 1131" chapter) and the nature of the Sr^{2+} profile in the pore waters. At Site 1127, the concentration of Sr^{2+} exhibits a very small increase over the upper 180 mbsf, before rising rapidly to 600 µM between ~180 and 220 mbsf. Preservation of carbonate microfossils is good at this site, with minimal amounts of overgrowth and dissolution. At Site 1131, an initial rapid rise in Sr^{2+} not seen at Site 1127 indicates shallow carbonate recrystallization. At Site 1129, the presence of a flushed zone in the upper 43 mbsf eliminates any gradients in the concentration of Sr^{2+}. Below this depth, the Sr^{2+} concentration increases to between 400 and 500 µM. In this interval, the concentration of dolomite increases and HMC decreases (Table T8). A second rapid increase occurs between 201.7 and 305.4 mbsf, with Sr^{2+} values exceeding 2000 µM. The gradual decrease in aragonite toward the base of the Pleistocene can be interpreted as being the result of the increasing recrystallization of carbonate with depth. The loss of HMC at both Sites 1131 and 1129 appears to be mainly a facies-dependent signal (see "Lithostratigraphy," p. 4, and "Lithostratigraphy," p. 3, in the "Site 1131" chapter). However, the absence of HMC in the lower portion of the cored interval at both Sites 1131 and 1129 probably reflects the recrystallization of fine amounts of HMC, which is more soluble than aragonite (Morse and Mackenzie, 1990). In contrast, the persistence of HMC to deeper intervals at Site 1127 is a result of the complete removal of sulfate, which produces a pore-water environment supersaturated with respect to aragonite and HMC (Ben-Yaakov, 1973).

PHYSICAL PROPERTIES

Introduction

Measurements of physical properties at Site 1129 followed the procedures outlined in "Physical Properties," p. 19, in the "Explanatory Notes" chapter. These included nondestructive measurements of *P*-wave velocity (PWL) (every 4 cm; Table T9, also in ASCII format), gamma-ray attenuation (GRA) bulk density (every 4 cm; Table T10, also in ASCII format), magnetic susceptibility (MS) (every 8 cm; Table T11, also in ASCII format), and natural gamma radiation (NGR) (every 16 cm; Table T12, also in ASCII format) using the multisensor track (MST). The *P*-wave velocity was activated only on APC cores. Thermal conductivity was measured in unconsolidated sediment at a frequency of one determination per core (Table T13, also in ASCII format), with two additional samples analyzed after deployments of the Adara temperature tool and Davis-Villinger temperature probe (DVTP) (Table T14, also in ASCII format). For this site, thermal conductivity measurements were also made on lithified sediments using the half-space needle-probe method on split cores (see "Thermal Conductivity," p. 20, in the "Explanatory Notes" chapter). Four in situ measurements of formation temperature were made (Table T15, also in ASCII format). A minimum of two discrete *P*-wave velocity measurements per section were made on the working half of the split cores (Table T15), and measurement frequency was increased to five per section after the *P*-wave velocity was turned off. Standard index properties (Table T16, also in

T9. *P*-wave velocity measurements, p. 77.

T10. GRA densiometry measurements, p. 78.

T11. Magnetic susceptibility measurements, p. 79.

T12. Natural gamma-ray measurements, p. 80.

T13. Thermal conductivity measurements, p. 81.

T14. In situ formation temperature estimates, p. 82.

T15. Discrete *P*-wave velocity measurements, p. 83.

T16. Index properties measurements, p. 84.

ASCII format) and undrained shear strength (only in unconsolidated and semilithified sediments) were measured at a frequency of one per section (Table T17, also in ASCII format).

The following sections describe the quality of the data obtained, downhole variations in sediment physical properties, and their relationships to lithology and downhole logging data (see "Lithostratigraphy," p. 4, and "Downhole Measurements," p. 26). Variations in MS data are described within "Paleomagnetism," p. 16.

T17. Undrained shear strength measurements, p. 85.

Data Quality

The MST provided high-quality NGR and GRA bulk density data, although problems occurred with *P*-wave velocity and MS measurements (see "Paleomagnetism," p. 21, in the "Site 1132" chapter). Discrete *P*-wave velocity measurements were affected by the presence of voids between core and liner because of the high gas content of the recovered sediment. Magnetic susceptibility measurements were hindered by a low signal:noise ratio. Affected data were omitted from figures in this report but are included in the raw data tables. Difficulties also occurred with the pycnometer used for determination of dry volume for index properties measurements (see "Index Properties," p. 21, in the "Explanatory Notes" chapter).

Index Properties, *P*-wave Velocity, Natural Gamma Radiation, and GRA Densiometry

Physical properties measurements at Site 1129 correlate well with lithologic changes observed in the sedimentary section and provide an important data set for core-log correlation. Values of NGR from both whole-core and downhole logging measurements show an excellent correlation that supports the integrity of both data sets. Moisture-and-density and GRA data have similar patterns to the downhole logging data, although values are generally lower. This difference likely results from the fact that in situ density includes the influence of sediment overburden and hydrostatic pressure, whereas the laboratory measurements do not. In general, Site 1129 is characterized by significant variations in *P*-wave velocity, NGR, and bulk density. Variations are much less marked in porosity and MS (Fig. F24). A well-defined cyclicity is seen in the NGR record (Fig. F24) that can be correlated to downhole gamma-ray data and NGR records of Sites 1127 and 1131. Three physical properties units (PP units) can be recognized at Site 1129 on the basis of trends in measured parameters (Fig. F24).

F24. *P*-wave velocity, bulk density, porosity, MS, and NGR measurements, p. 56.

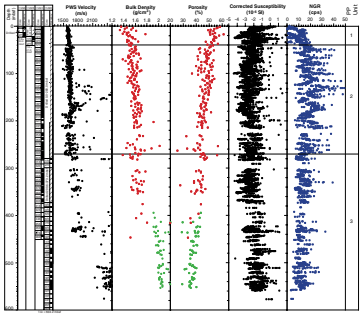

Physical properties Unit 1 (0–40 mbsf) is characterized by an increase in NGR (from 0 to 20 cps), as seen at many other Leg 182 sites (Fig. F24). The base of PP Unit 1 coincides with the top of three bryozoan mound sequences, which form the lower part of lithostratigraphic Unit I (see "Lithostratigraphy," p. 4). Bulk density and *P*-wave velocity also increase toward the base of the unit (from 1.57 to 1.66 km/s and from 1.27 to 1.62 g/cm^3, respectively), whereas porosity decreases from ~60% to 50% (Fig. F24).

Physical properties Unit 2 (40–270 mbsf) is characterized by high NGR values (12–52 cps) with cyclic variations. These cyclic variations correlate with coarsening-upward bryozoan floatstone-rudstone sequences (Fig. F24; see "Lithostratigraphy," p. 4). Within Unit 2, a significant *P*-wave velocity peak can be seen at 90 mbsf (2.02 km/s) that

may correlate with a strong seismic reflector designated as Horizon 2A (see "Seismic Stratigraphy," p. 26, in the "Site 1127" chapter). Between 123 mbsf and the base of Unit 2, discrete *P*-wave velocity data are relatively variable (Fig. F24), corresponding to alternations between unlithified and partially lithified sediments. This variability is also seen in the shear strength data (see below) (Fig. F25). A peak in *P*-wave velocity (2.5 km/s; Fig. F24) can be seen near 150 m, which correlates with the boundary between lithostratigraphic Units I and II (see "Lithostratigraphy," p. 4) and also with the disappearance of HMC (see "Inorganic Geochemistry," p. 20). Within PP Unit 2, bulk density has low variability averaging 1.5 g/cm³ for moisture and density (MAD) and 1.7 for GRA data (Fig. F24). Some density excursions are seen that correlate with more indurated sediments (Fig. F24). Porosity decreases throughout PP Unit 2 from ~58% to 40% at the base of the unit.

Physical properties Unit 3 (270–604 mbsf) is defined by lower and generally decreasing NGR (18–12 cps) with increasing depth (Fig. F24). In contrast, *P*-wave velocity (1.8–2.5 km/s) and MAD bulk density (1.6–2.0 g/cm³) within Unit 3 increase with a significant shift to higher values near 390 m (Fig. F24). This change does not correlate with any noted lithologic change (see "Lithostratigraphy," p. 4) but does roughly correlate with seismic Horizon 2C (see "Seismic Stratigraphy," p. 26, in the "Site 1127" chapter). Porosity decreases (42%–34%) throughout Unit 3.

Shear Strength

Undrained peak and residual shear strength were measured on unconsolidated sediments from 0 to 227 mbsf (Fig. F25). Shear strength at Site 1129 shows an overall downhole increase (2–30 kPa), resulting from sediment compaction, with high variability below 50 mbsf resulting from alternations between partially lithified to lithified sediment (Fig. F25). In some intervals, variability may also result from drilling disturbance or cracking of the sediment before sediment failure, resulting in lower values for peak strength.

Thermal Conductivity

Thermal conductivity values at Site 1129 range from 0.71 to 1.75 W/(m·K) (Fig. F26; Table T13). From the seafloor to 440 mbsf, thermal conductivity data define a regular increase with depth that correlates well with variations in bulk density (Fig. F26). Below 440 mbsf, thermal conductivity values increase and become more variable.

In Situ Temperature Measurements

Four in situ temperature measurements were made at Site 1129, three using the Adara tool and one using the DVTP. There was relatively little variation in estimates of mudline temperature (16.24–16.97°C; average = 16.51° ± 0.22°C) (Fig. F27). Two additional estimates of seafloor temperatures (13.56° and 13.15°C) were obtained from Holes 1129B and 1129C using an expendable bathythermograph. Both yielded values lower than those obtained from the in situ temperature tools, possibly as a result of calibration differences. None of the in situ temperature measurements was affected by postemplacement movement of the probe, and differences between early and late data fits resulted in only minor differences in temperature (Table T14).

F25. Maximum shear strength data with PP units, p. 58.

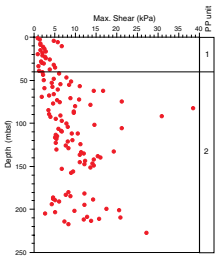

F26. Thermal conductivity data with GRA bulk density, p. 59.

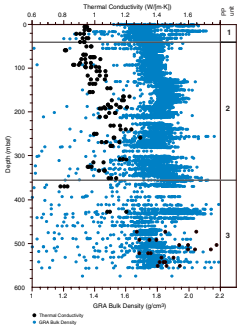

F27. Variation of formation temperature with depth, p. 60.

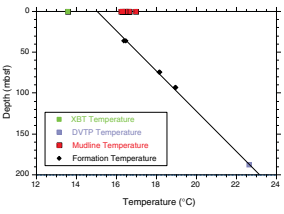

The in situ measurements define a linear temperature relationship with an intercept of 15.02° ($r^2 = 0.99$, $N = 6$) (Fig. F27). This intercept is significantly less than the average mudline temperature, suggesting that there may be circulation of seawater within the upper 30–40 mbsf (cf. evidence for a 40.3-m-thick fluid advection zone noted in geochemical data; see "Inorganic Geochemistry," p. 20). However, this interpretation depends on the higher estimates of seafloor temperature from mudline readings being correct. The geothermal gradient derived from the regression equation is 41.4° ± 0.9°C/km (all uncertainties are 1 standard deviation). The geometric mean of the thermal conductivity data between 0 and 188 mbsf (1.0 ± 0.086 W/[m·K]) and the geothermal gradient determined above were used to estimate heat flow at the site. The resultant value of 41.4 mW/m² is very similar to that determined at other sites at a similar depth on the shelf margin, although it is less than the value determined in much deeper water off the platform margin at Site 1128.

DOWNHOLE MEASUREMENTS

Logging Operations

After completion of drilling operations at Hole 1129D, the hole was prepared for logging (see "Operations," p. 2). As a precaution against H_2S damage to the wireline cable and logging tools, and also to prevent caving, the hole was loaded with a mixture of sepiolite mud and seawater. The lower end of the BHA was placed at 100 mbsf. The wireline heave compensator (WHC) was used during all logging runs and coped well with the moderate heave conditions. Three different logging strings were deployed in the following order: (1) triple combo, (2) FMS/sonic, and (3) WST (Table T18; see "Downhole Measurements," p. 25, in the "Explanatory Notes" chapter). All logging runs reached total drilled depth (604 mbsf).

T18. Tool strings, intervals logged, and logging speeds, Hole 1129D, p. 86.

Before the main run with the triple combo, a short quality-control run was made from the base of the hole at 604 mbsf to 550 mbsf. The main run was logged from 604 mbsf to the mudline. A single pass was made with the FMS/sonic from 604 mbsf to the pipe. The FMS calipers were closed at 140 mbsf, when the WHC was closed down. The WST recorded 10 stations, with individual stations located near changes in log character and at estimated depths of significant seismic reflectors (see "Seismic Stratigraphy," p. 26, in the "Site 1127" chapter).

Data Quality

The overall quality of the data from the triple combo and the FMS/sonic was good, although washouts between 360 and 460 mbsf may have degraded the quality of the porosity log and the FMS images from this interval.

Measurements of NGR from downhole logging and sediment physical properties show good agreement, although there are slight depth discrepancies caused by incomplete recovery and heave effects. Between 100 and 402 mbsf, downhole porosity and density measurements show poor agreement with discrete measurements of density and porosity of the core (MAD), whereas there is good agreement between GRA density and log density. Below 402 mbsf, correlation of the density log to GRA data becomes poor, possibly as a result of biscuiting of the

recovered core. Moisture and density data show decreased correlation to log density in this interval, which coincides with a change in the calibration of the pycnometer used in determining MAD parameters between Holes 1129C and 1129D.

Preliminary Observations

The logs acquired in Hole 1129D are remarkably similar to those acquired in Hole 1131A (located immediately seaward of Hole 1129D), although the level of gamma radiation is higher in the upper 267 mbsf of Hole 1129D, possibly reflecting greater sedimentary organic carbon content. The gamma-ray signal is dominated by uranium, which is often associated with organic matter in carbonate successions, although uranium occurring within grain coatings observed in the recovered core may be another potential source. The importance of diagenesis at Site 1129 is clearly seen by the number of gamma-ray peaks associated with lithified intervals (Fig. F28). Three major logging units have been defined at Site 1129, mainly on the basis of variations in gamma-ray and sonic logs.

Logging Unit 1: 0–267 mbsf

Logging Unit 1 was measured through pipe to 100 mbsf, and in open hole for the remainder of the interval. Other than a small peak in thorium, the gamma-ray log measured through pipe is generally featureless (Fig. F29). The open-hole portion of Unit 1 is characterized by elevated levels of gamma radiation resulting from high uranium concentrations. These data exhibit high-magnitude, high-frequency excursions throughout Unit 1 (~2–9 ppm) (Fig. F30). Once cleared of pipe effects, photoelectric effect (PEF) values are more or less constant throughout Unit 1 at values of ~4.5 barn/e$^-$, indicating an almost clean carbonate. Within this unit, density and velocity gradually increase, whereas porosity decreases downhole (Fig. F29). There is a slight separation of shallow, medium, and deep resistivity between 150 and 267 mbsf, indicating some fluid invasion into the formation. Within logging Unit 1, peaks in shallow resistivity (205, 235, and 256 mbsf) generally coincide with low porosity and high density, sonic velocity, and gamma-ray values. These intervals are interpreted as lithified horizons or firmgrounds (Fig. F29). On FMS images, these horizons are seen as thin (25–125 cm), highly resistive intervals. The firmground at 235 mbsf corresponds to an overall change from unlithified to partially lithified sediments within lithostratigraphic Unit II (see "Lithostratigraphy," p. 4). The base of Unit 1 is marked by a shift to lower and less variable levels of gamma radiation (20–50 American Petroleum Institute [API] units), resulting from decreased uranium content (Fig. F30).

Logging Unit 2: 267–559 mbsf

Logging Unit 2 (267–559 mbsf) exhibits cyclic variations in gamma-ray values that are dominated by changes in uranium concentration. The frequency of these cyclic variations decreases toward the base of the unit (Fig. F30). The NGR cyclicity within Unit 2 is similar to the cyclicity seen in logging Unit 2 in Hole 1131A, and patterns can be correlated between the two sites. The correlation with Hole 1127B, further seaward, is not as clear, but seismic reflectors can be used as guidelines for cycle to cycle correlation. Within Unit 2, bulk density and sonic ve-

F28. Summary of triple combo and sonic logs vs. depth for the open-hole logged interval, p. 61.

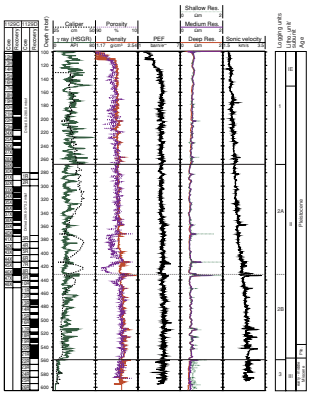

F29. Summary of spectral gamma-ray logs from the HNGS for the interval logged through pipe, p. 62.

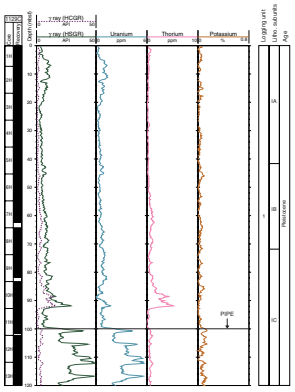

F30. Summary of spectral gamma-ray logs from the HNGS for the open-hole logged interval, p. 63.

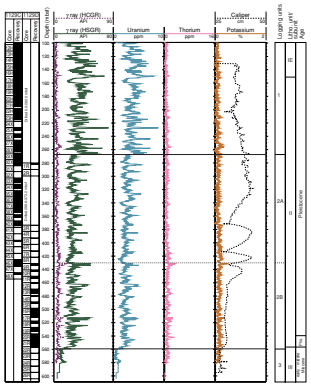

locity generally increase, whereas porosity decreases, typical of a compaction profile (Fig. F29).

Unit 2 is divided into two subunits at a significant shift (433 mbsf) to higher *P*-wave velocity, bulk density, resistivity, and NGR (Fig. F29). This shift is interpreted to be a firmground within the sedimentary section within lithostratigraphic Unit II (see "Lithostratigraphy," p. 4). Similar, but smaller excursions are seen throughout Unit 2. One of these intervals was recovered in the core (414 mbsf) and contains pyrite, thus explaining the increase in PEF values (Fig. F29). Many of the lithified layers seen in the logs were not recovered during coring. Within Subunit 2A, high-porosity excursions between 370 and 433 mbsf are likely to represent washouts of the borehole wall exhibited by increases in caliper values. As at Hole 1131A, the base of logging Unit 2 is defined by a marked decrease in gamma-ray values. The base of Unit 2 is also clearly seen in the FMS images as a distinct change in the nature of the sediment (Fig. F31).

Logging Unit 3: 559–604 mbsf

Logging Unit 3 is characterized by uniformly low gamma-ray values (~10 API units) and variable PEF, indicating an alternation of silica-rich beds with intervals rich in calcium carbonate (Fig. F29). Resistivity logs show a typical fluid-invasion profile (Fig. F29), with the separation of the shallow and deep resistivity curves indicating a permeable formation. The upper boundary of logging Unit 3 corresponds to the top of lithostratigraphic Unit III, which consists mainly of chert and lithified packstone and grainstone (see "Lithostratigraphy," p. 4). The alternation between chert horizons and carbonates is clearly seen on FMS images as a succession of thin (~20 cm), resistive chert layers alternating with thicker (~2 m), more conductive carbonate layers (Fig. F31).

F31. FMS image showing logging Unit 2/Unit 3 boundary, coinciding with lithostratigraphic Unit II/Unit III boundary, p. 64.

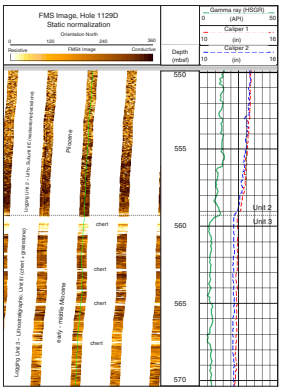

SEISMIC STRATIGRAPHY

The seismic stratigraphic results from Sites 1127, 1129, and 1131 are considered together, as these sites represent a transect of three closely spaced sample points through the same sequences that form spectacular clinoforms beneath the modern shelf edge. For a discussion of these results, see "Seismic Stratigraphy," p. 26, in the "Site 1127" chapter.

REFERENCES

Ben-Yaakov, S., 1973. pH buffering of pore water of recent anoxic marine sediments. *Limnol. Oceanogr.,* 18:86–94.

Berggren, W.A., Kent, D.V., Swisher, C.C., III, and Aubry, M.-P., 1995. A revised Cenozoic geochronology and chronostratigraphy. *In* Berggren, W.A., Kent, D.V., Aubry, M.-P., and Hardenbol, J. (Eds.), *Geochronology, Time Scales and Global Stratigraphic Correlation*. Spec. Publ.—Soc. Econ. Paleontol. Mineral. (Soc. Sediment. Geol.), 54:129–212.

Bone, Y., and James, N.P., 1993. Bryozoans as carbonate sediment producers on the cool-water Lacepede Shelf, Southern Australia. *Sediment. Geol.,* 86:247–271.

Cisowski, S., 1981. Interacting vs. non-interacting single domain behavior in natural and synthetic samples. *Phys. Earth Planet. Inter.,* 26:56–62.

Eberli, G.P., Swart, P.K., Malone, M.J., et al., 1997. *Proc. ODP, Init. Repts.,* 166: College Station, TX (Ocean Drilling Program).

Feary, D.A., and James, N.P., 1995. Cenozoic biogenic mounds and buried Miocene (?) barrier reef on a predominantly cool-water carbonate continental margin, Eucla Basin, western Great Australian Bight. *Geology,* 23:427–430.

————, 1998. Seismic stratigraphy and geological evolution of the Cenozoic, cool-water, Eucla Platform, Great Australian Bight. *AAPG Bull.,* 82:792–816.

James, N.P., and von der Borch, C.C., 1991. Carbonate shelf edge off southern Australia: a prograding open-platform margin. *Geology,* 19:1005–1008.

Jenkins, D.G., 1985. Southern mid-latitude Paleocene to Holocene planktic foraminifera. *In* Bolli, H.M., Saunders, J.B., and Perch-Nielsen, K. (Eds.), *Plankton Stratigraphy:* Cambridge (Cambridge Univ. Press), 263–282.

————, 1993. Cenozoic Southern mid- and high-latitude biostratigraphy and chronostratigraphy based on planktonic foraminifera. *In* Kennett, J.P., and Warnke, D.A. (Eds.), *The Antarctic Paleoenvironment: A Perspective on Global Change.* Antarct. Res. Ser., 60:125–144.

Karlin, R., and Levi, S., 1983. Diagenesis of magnetic minerals in recent hemipelagic sediments. *Nature,* 303:327–330.

Morse, J.W., and Mackenzie, F.T., 1990. *Geochemistry of Sedimentary Carbonates:* Amsterdam (Elsevier).

Figure F1. Map showing the location of Site 1129 (on the eastern Eyre Terrace uppermost slope/shelf edge) in relation to other Leg 182 sites and the Australian Geological Survey Organisation Survey 169 (AGSO169) seismic lines.

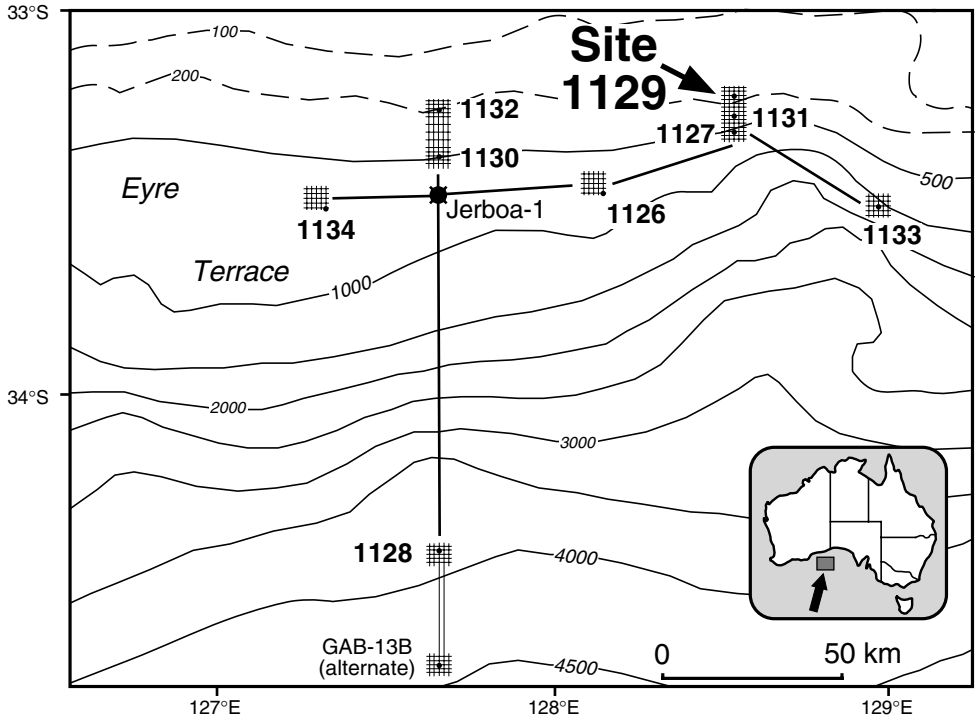

Figure F2. Portion of seismic Line AGSO169/05a showing interpreted seismic stratigraphic sequences intersected at Site 1129. Unstable hole conditions at Holes 1129A and 1129B forced abandonment in this location; however, drilling at Holes 1129C and 1129D was completed successfully and reached the target depth.

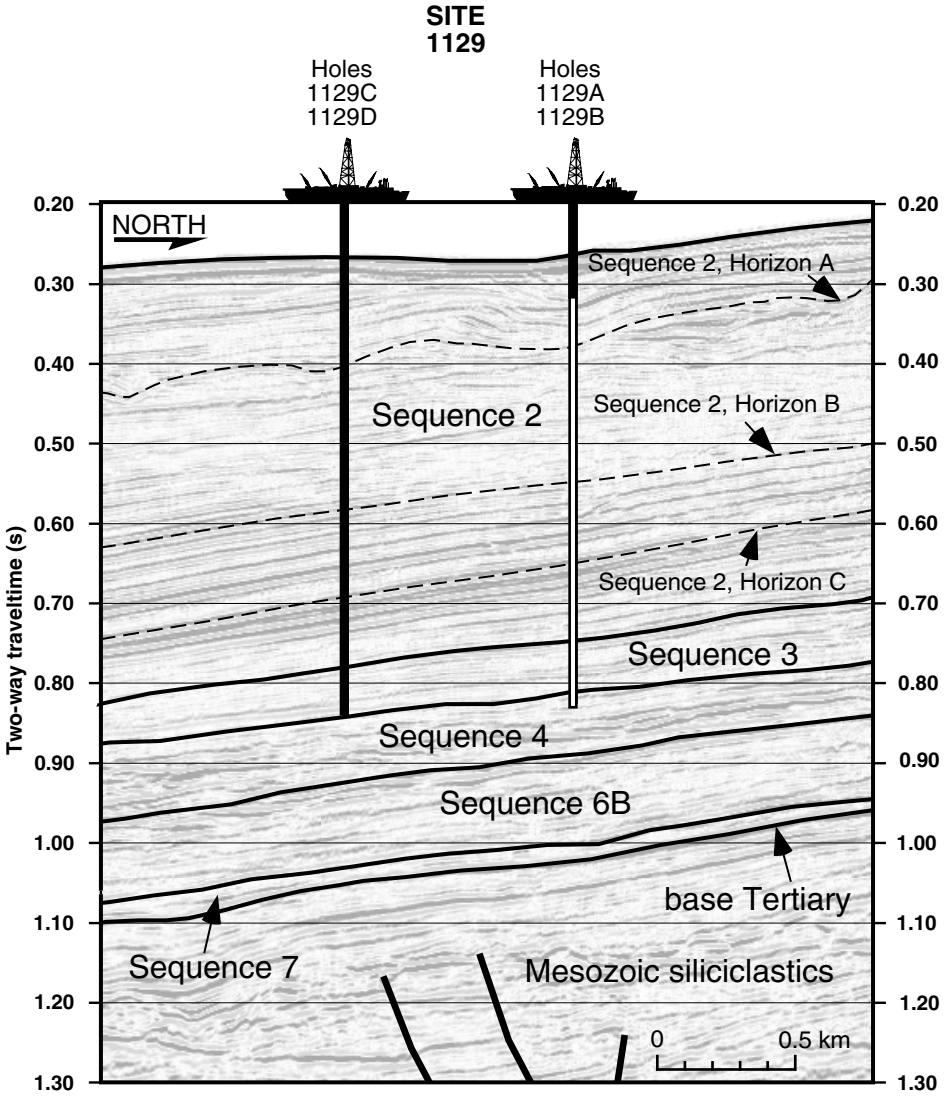

Figure F3. Summary of lithostratigraphy at Site 1129. Ages are from "Biostratigraphy," p. 12, and "Paleomagnetism," p. 16. (Continued on next two pages.)

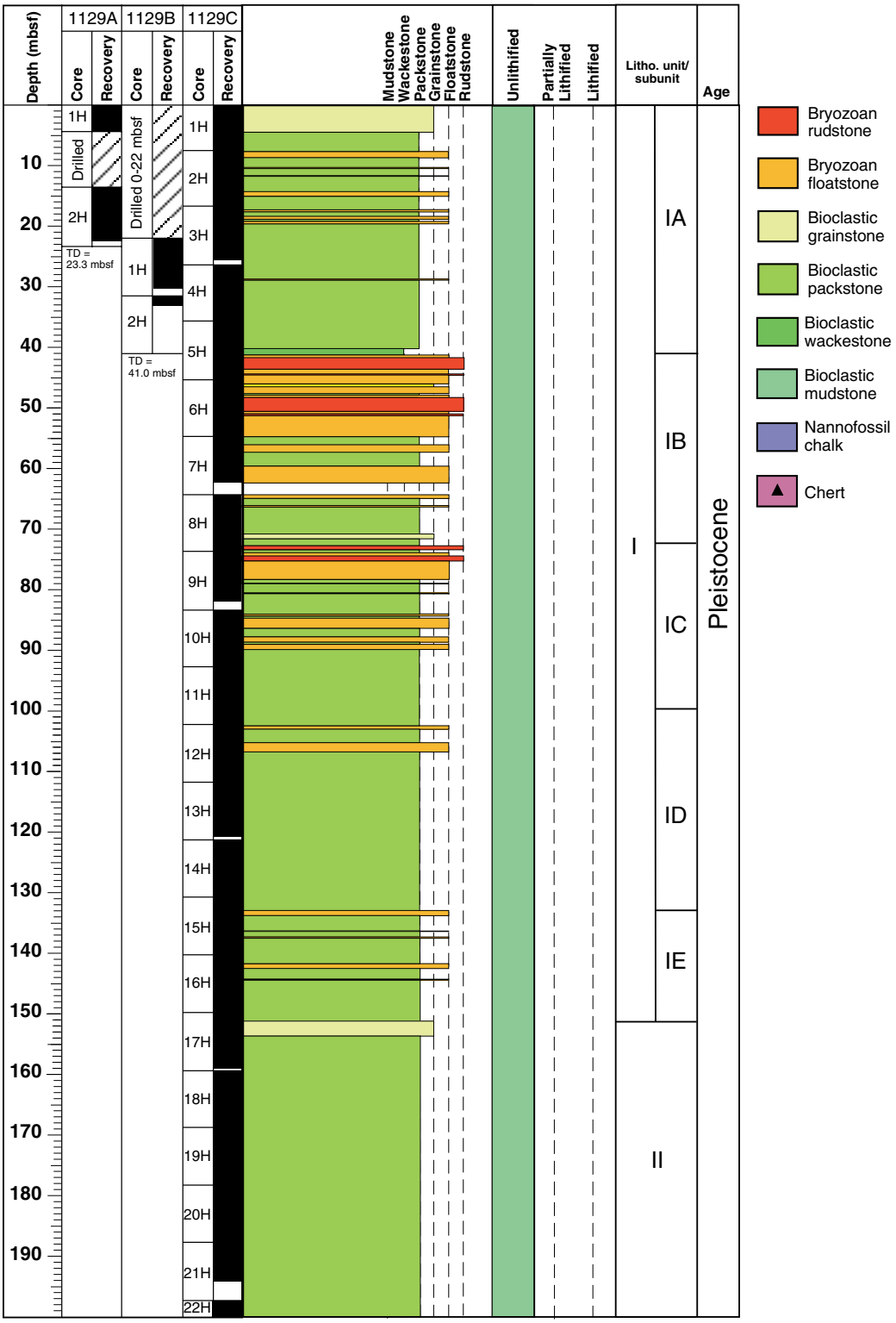

Figure F3 (continued).

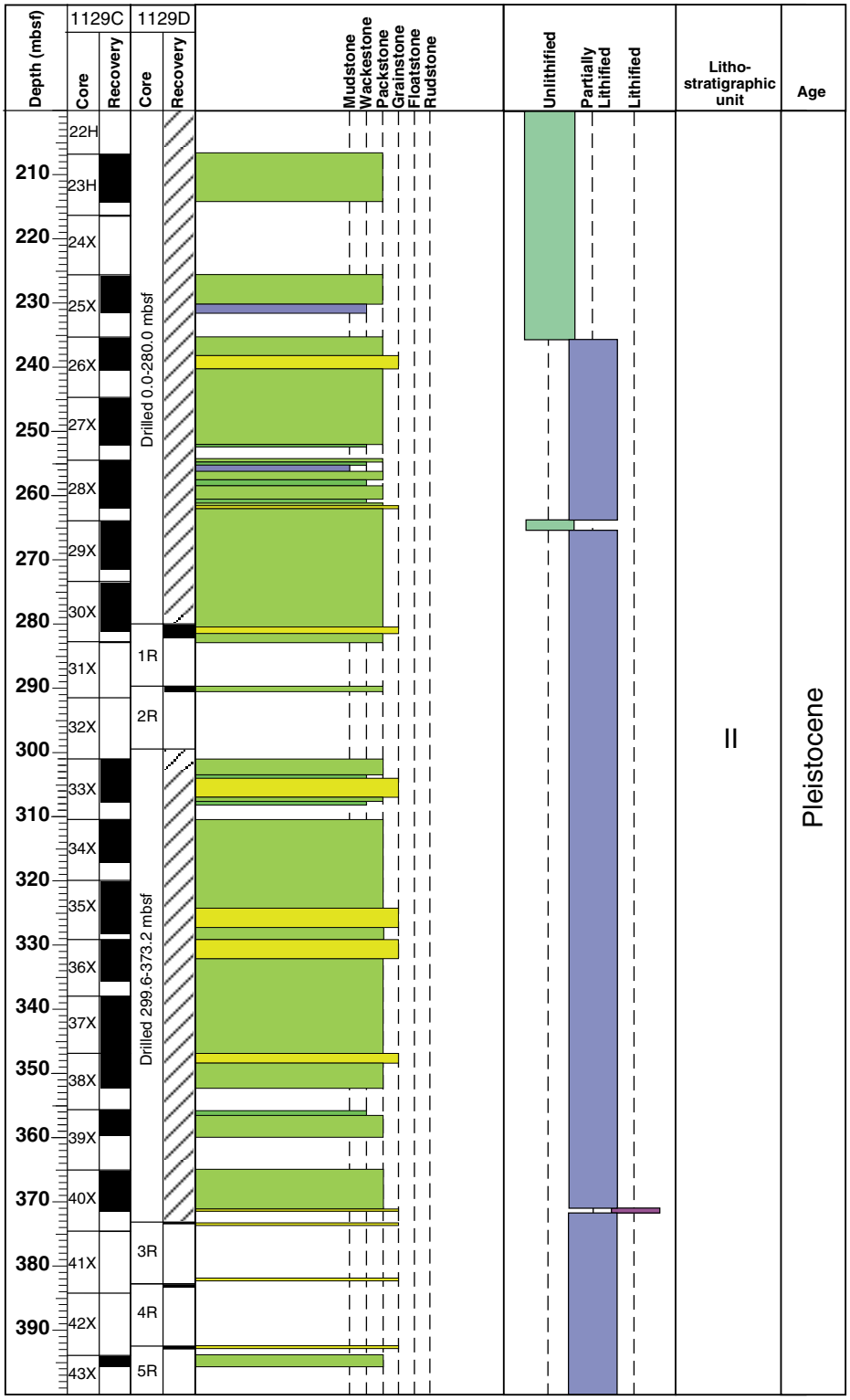

Figure F3 (continued).

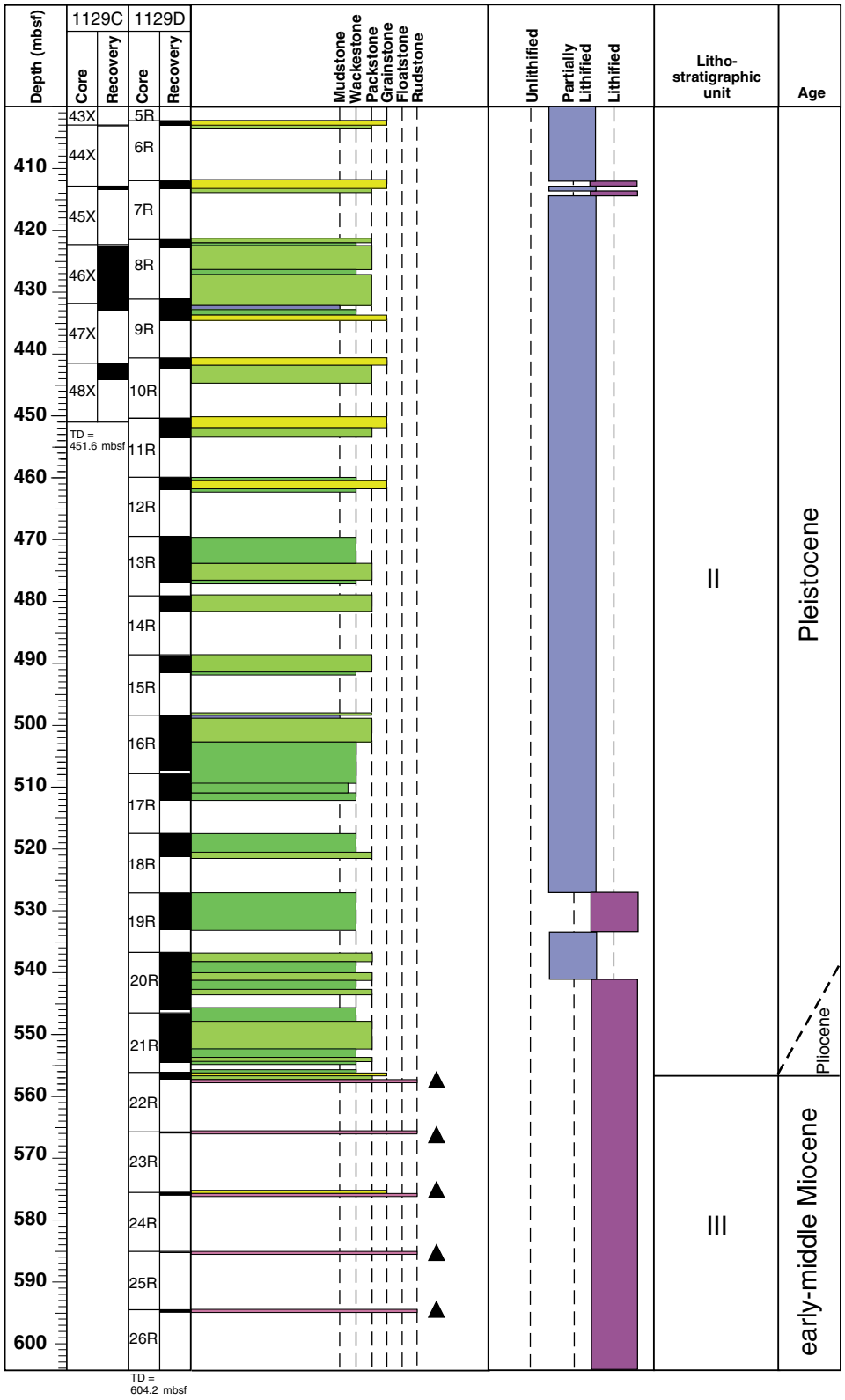

Figure F4. Summary showing stratigraphic distribution of bryozoan growth forms, Unit I. Each subunit is interpreted to form a package grading upward from bioclastic packstone at the base to bryozoan floatstone and rudstone at the top. The diversity of bryozoan growth forms is low in the lower packstone-dominated part and high in the upper floatstone-dominated part. The growth of the bryozoan mound complex reached a climax in Subunit IB, which contains a thick floatstone to rudstone interval with highly diverse bryozoan growth forms.

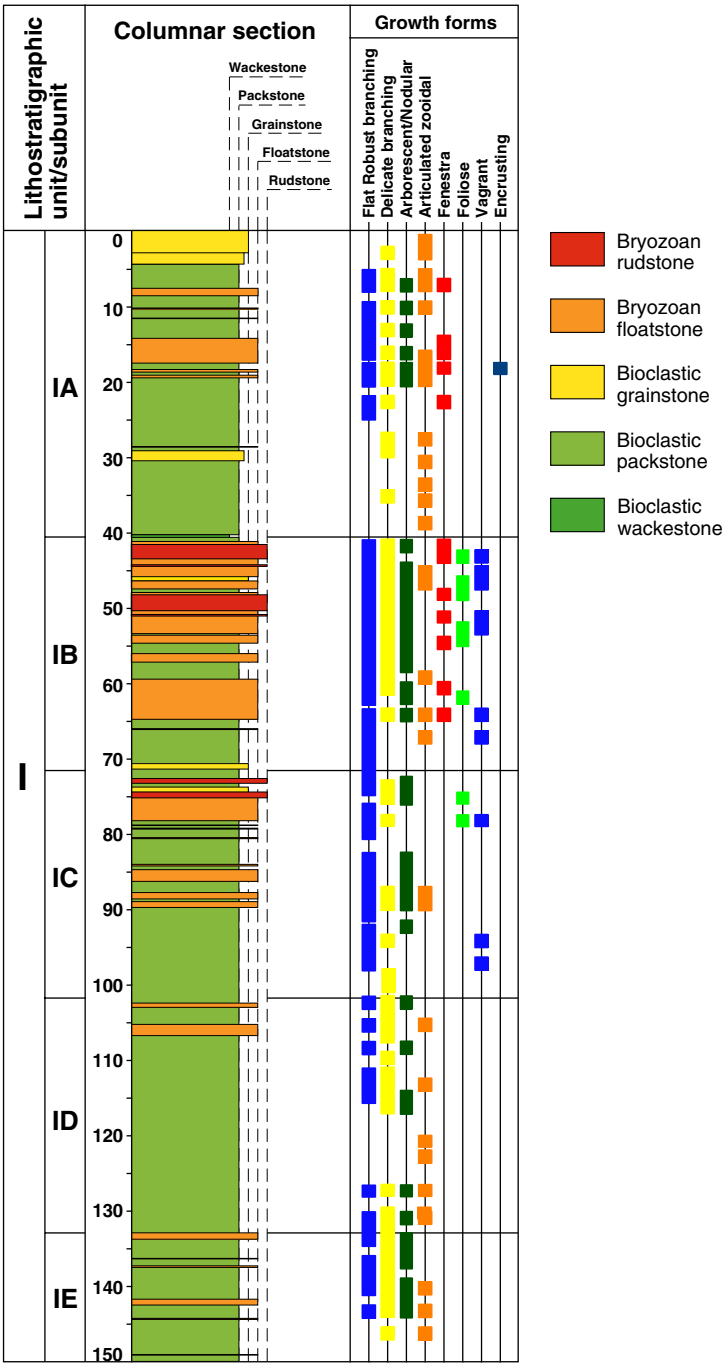

Figure F5. A dense assemblage of *Palaeophycus heberti* within partially lithified foraminiferal packstone from the lower part of Unit II (interval 182-1129D-13R-5, 54–60 cm).

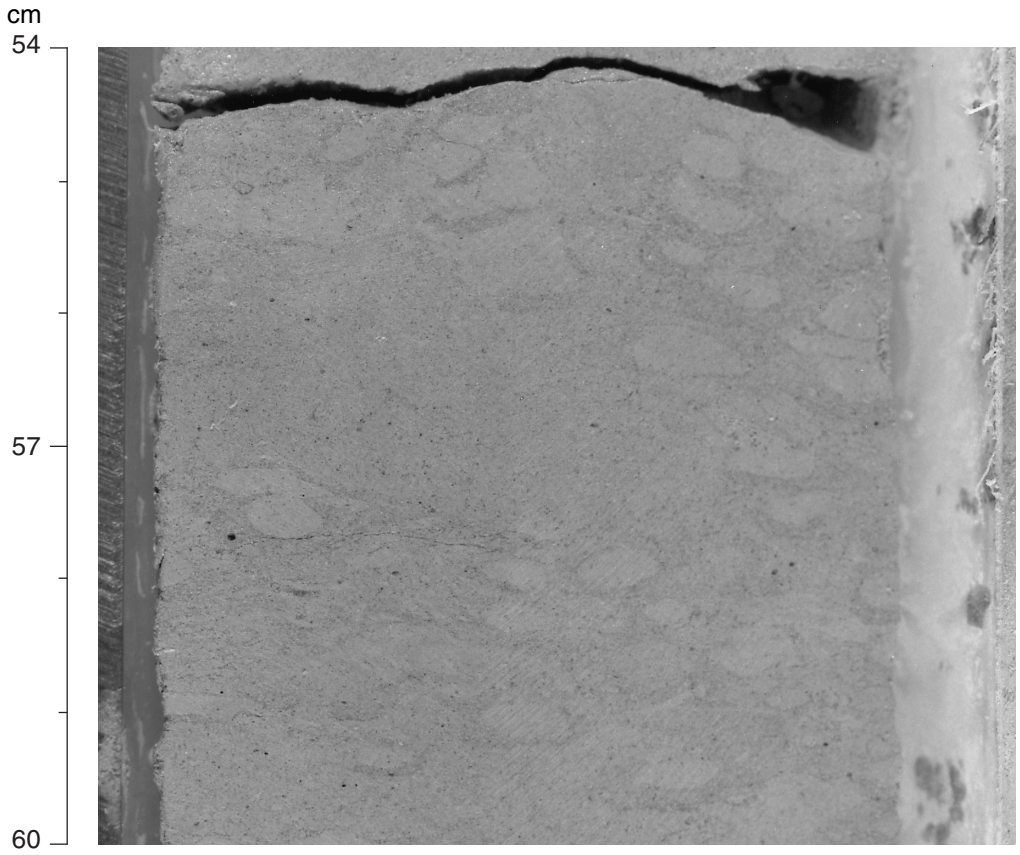

Figure F6. Condensed and flattened burrows of *Chondrites* within a bioclastic packstone from Unit II (interval 182-1129D-9R-1, 133–150 cm).

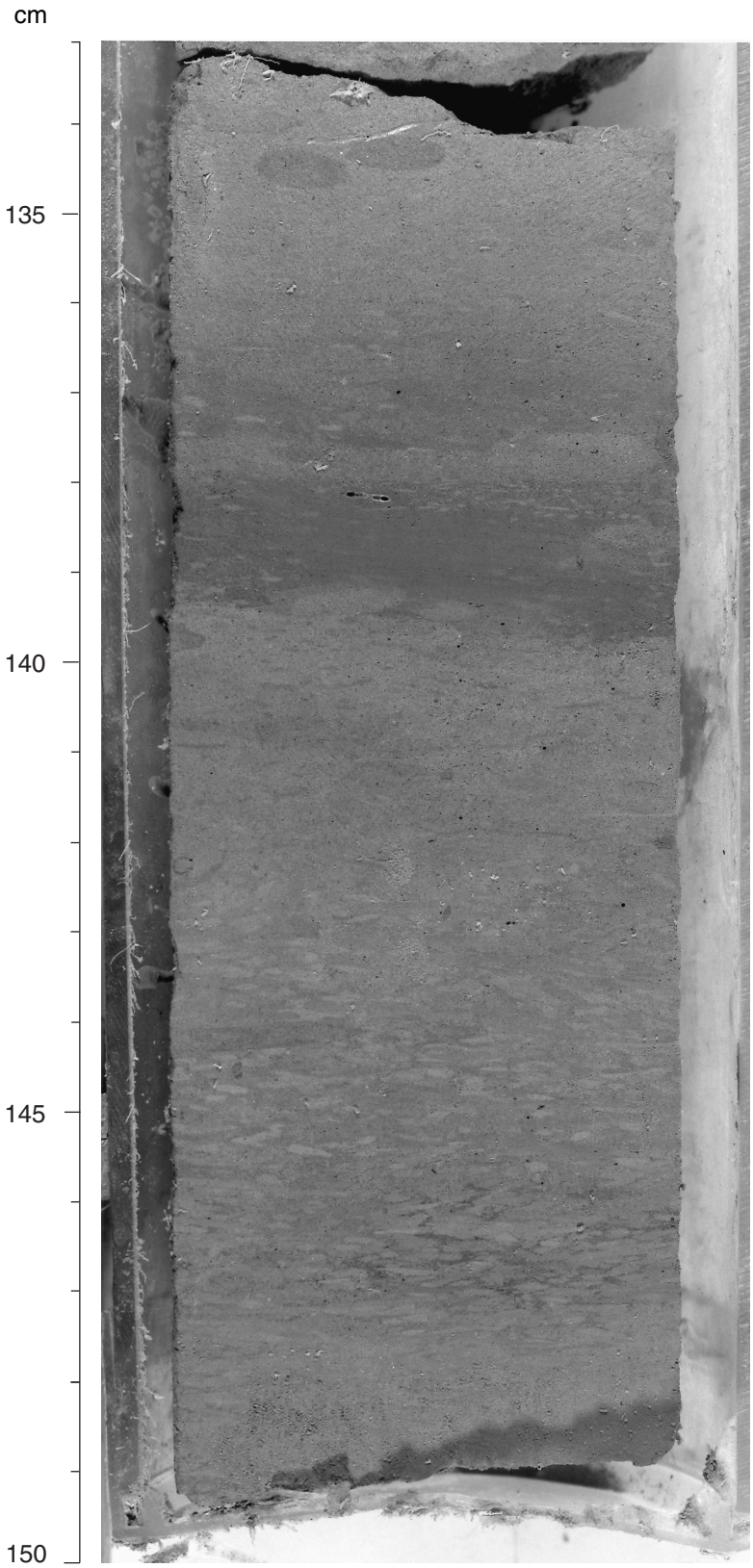

Figure F7. The sharp boundary between Units II and III (at 60 cm), which represents a major hiatus between the lower–middle Miocene and upper Pliocene (interval 182-1129D-22R-1, 46–75 cm). The over-lying bryozoan grainstone to rudstone is 3 cm thick and grades upward. The underlying partially dolomitized bioclastic packstone to grainstone is well lithified.

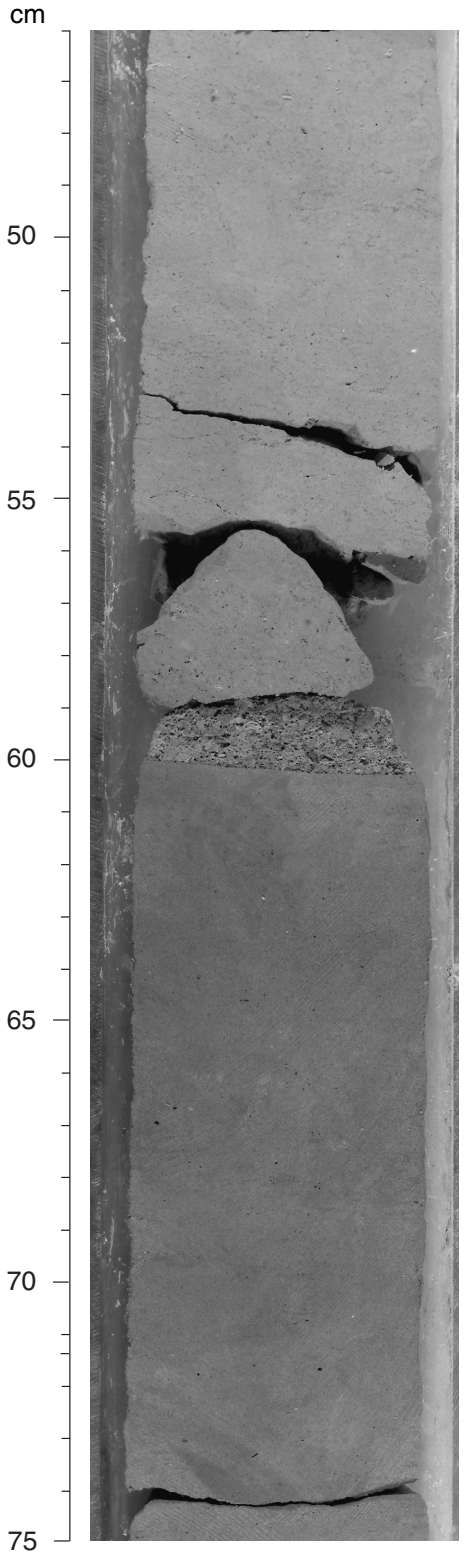

Figure F8. Stratigraphic position of calcareous nannofossil and planktonic foraminiferal zones and benthic foraminiferal assemblages at Site 1129. Dashed boundaries and gray blocks imply uncertainty. Lithostratigraphic units are taken from "Lithostratigraphy," p. 4. (Continued on next page.)

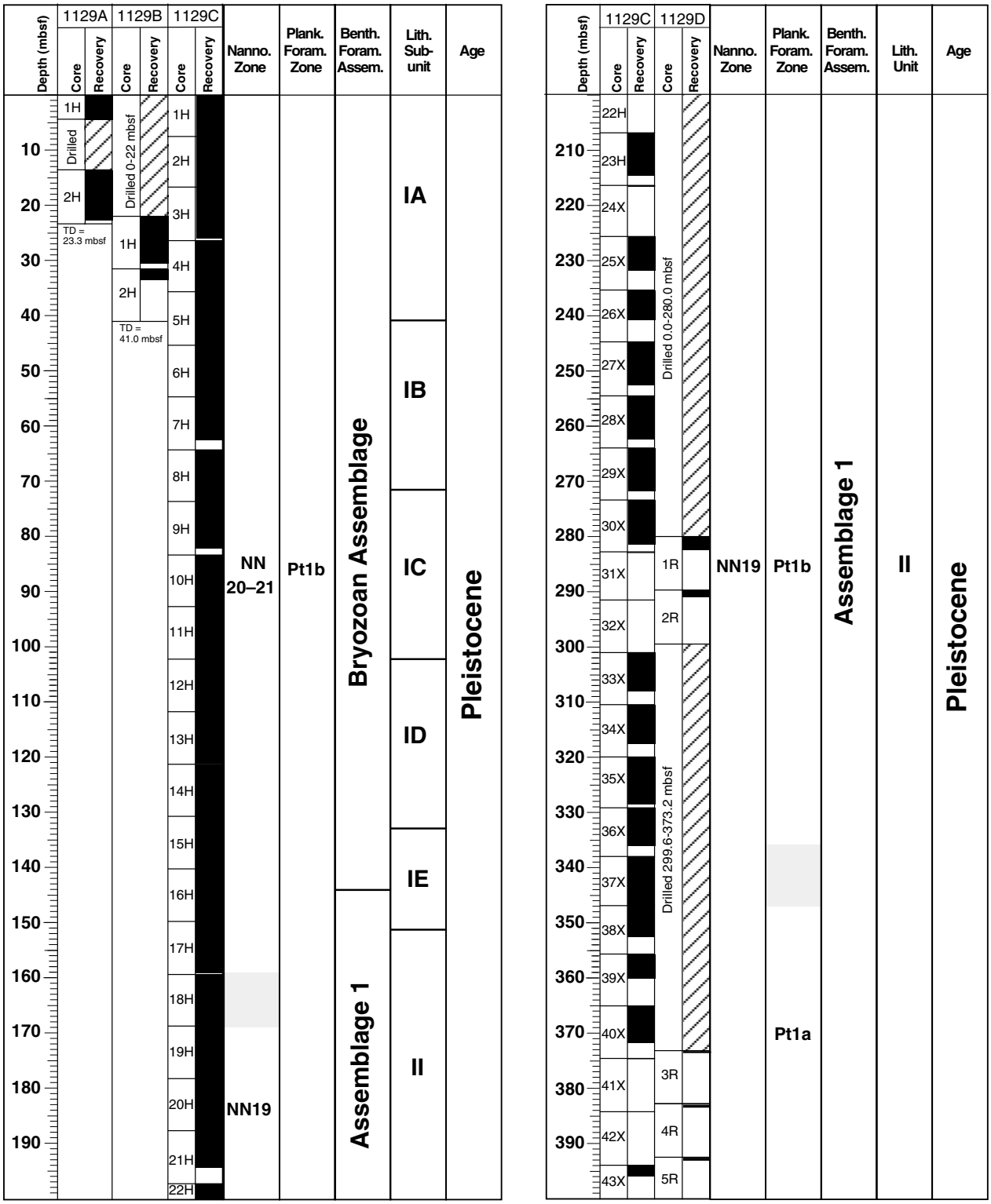

Figure F8 (continued).

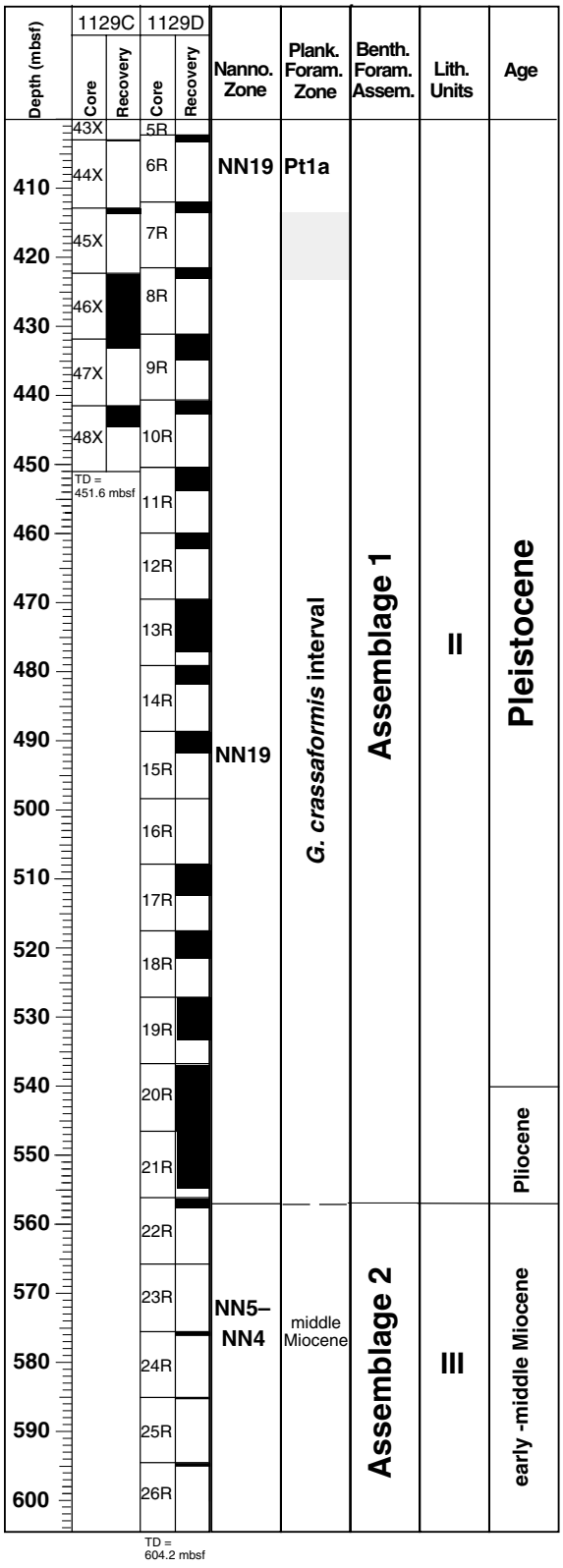

Figure F9. Sedimentation rate curve constructed from the datum levels listed in Table T2, p. 68. Stratigraphic error is indicated by the length of the error bars.

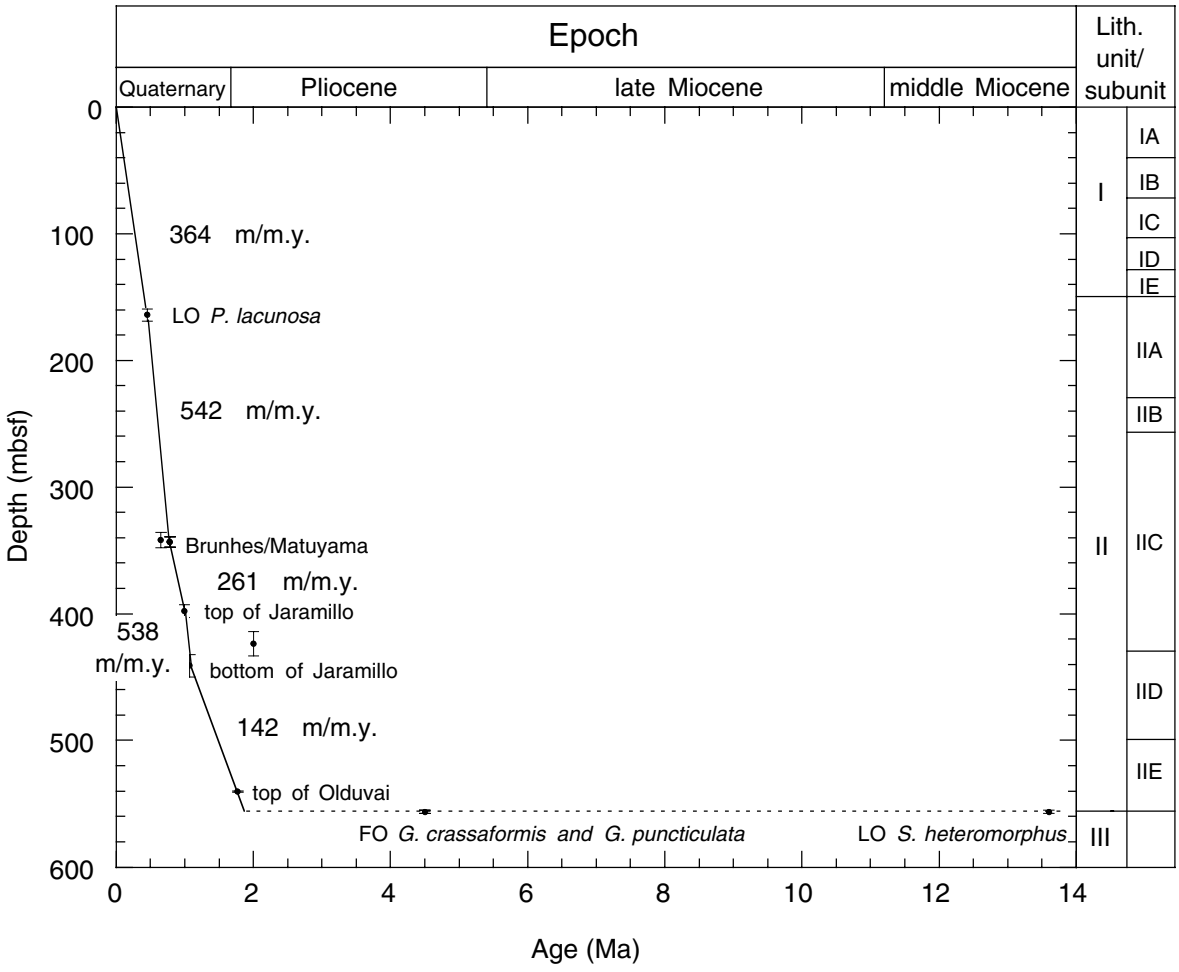

Figure F10. Downhole inclination determined (**A**, **B**) from natural remanent magnetization (NRM) long-core measurements and (**C**) after partial demagnetization, together with interpreted magnetostratigraphy. Magnetic polarity and chron are shown in the column on the right. Long-core measurements (crosses) are compared with results from discrete samples (open squares). Data from Holes 1129C and 1129D are combined in (C).

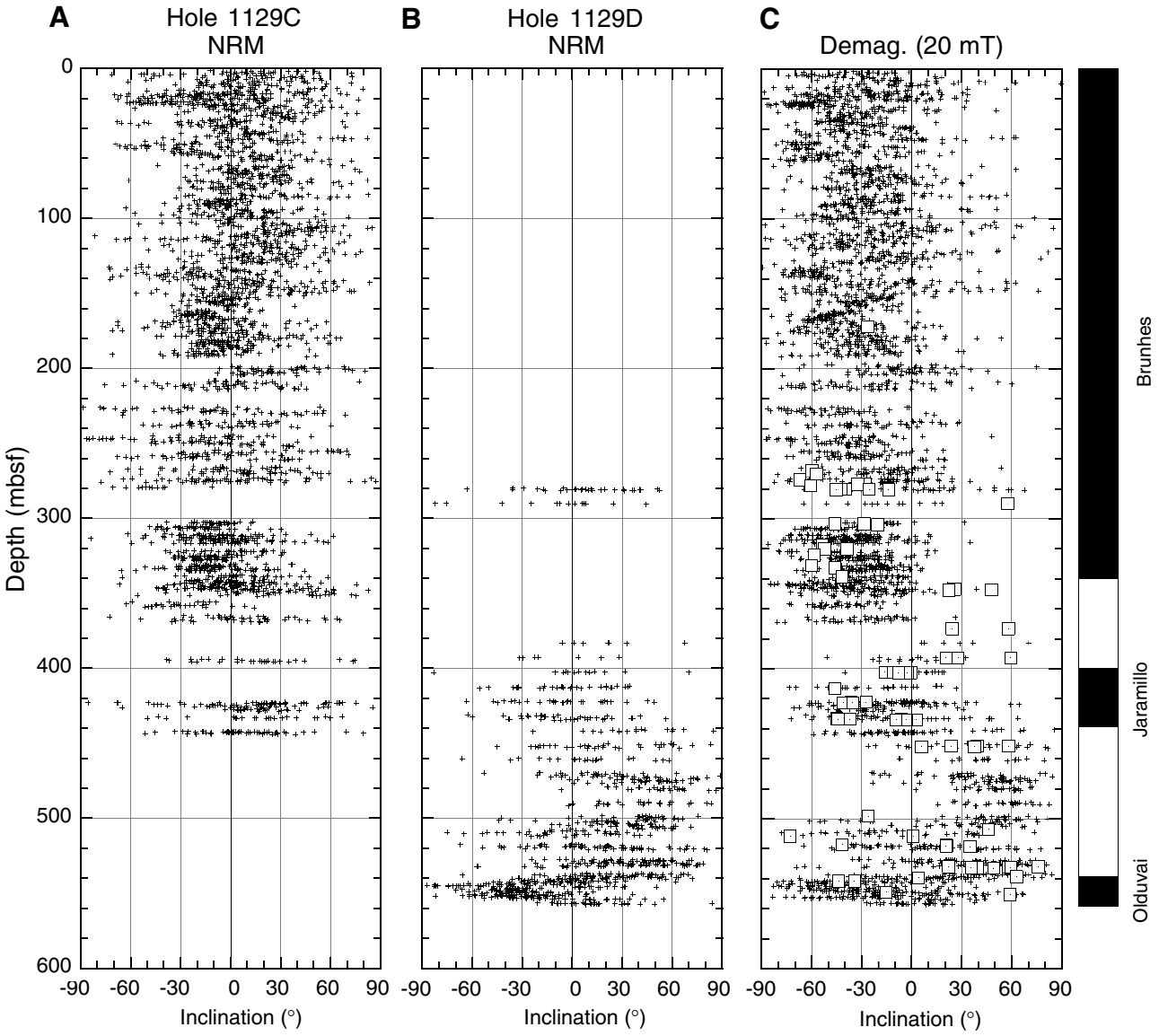

Figure F11. Normalized intensity decay (left), and demagnetization diagrams (right) of representative samples. **A.** Alternating-field demagnetization showing two-component magnetization with a characteristic magnetization of normal polarity and a soft drilling-induced overprint (Sample 182-1129C-30X-1, 100–103 cm). **B.** Normal polarity magnetization (end-point) overprinted by a prominent secondary magnetization (Sample 182-1129C-30X-3, 78–81 cm). **C.** Magnetization of reverse polarity over-printed by an upward-directed drilling-induced magnetization (Sample 182-1129D-3R-1, 24–28 cm). Demagnetization diagrams show projections of the natural remanent magnetization (NRM) vector in the vertical (open symbols) and horizontal (solid symbols) planes during progressive demagnetization.

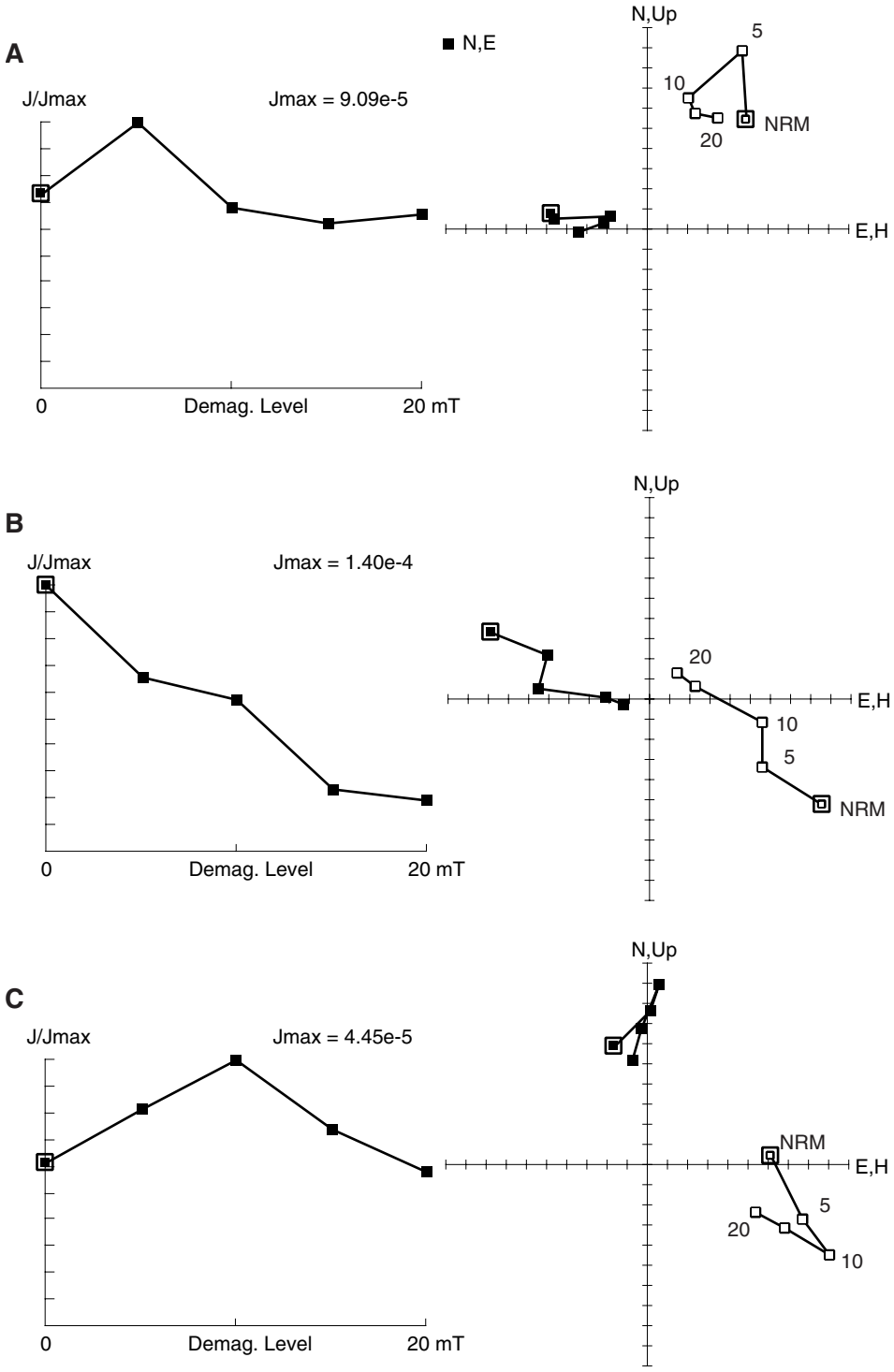

Figure F12. Acquisition of isothermal remanent magnetization and its alternating-field demagnetization for representative samples from advanced hydraulic piston and extended core barrel cores.

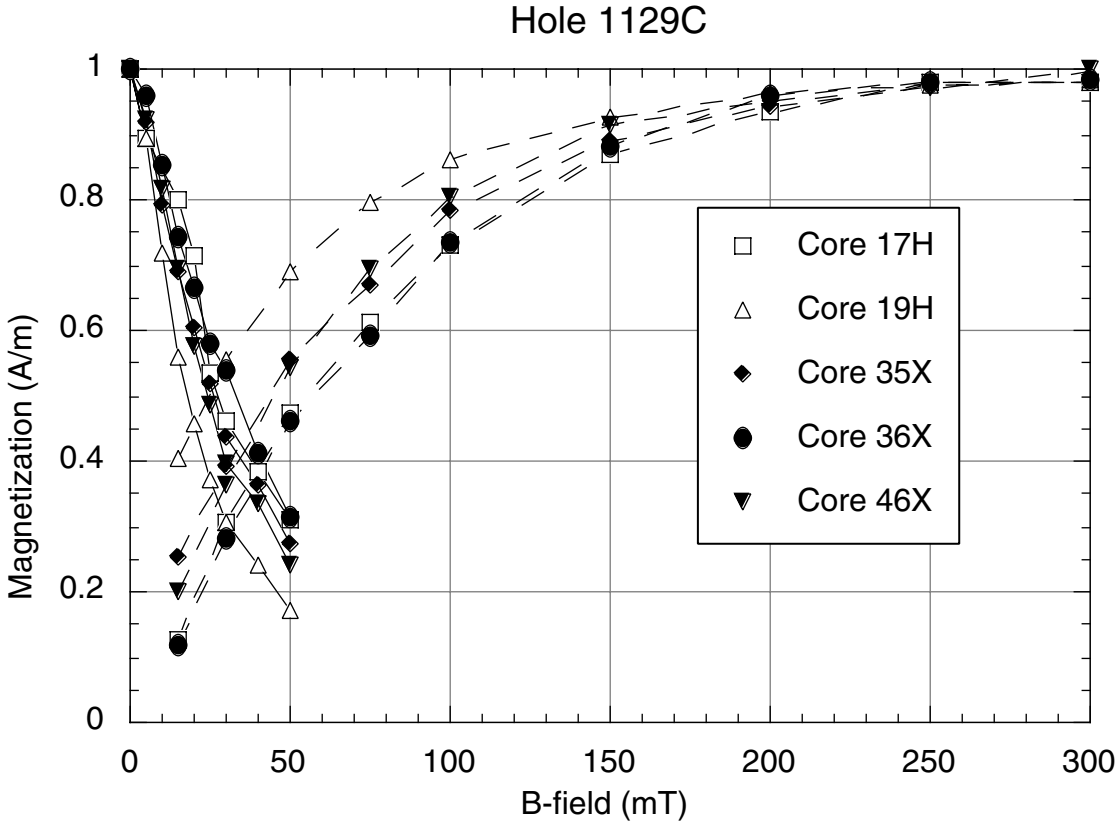

Figure F13. Methane (C_1) concentration, methane/ethane (C_1/C_2) values, and hydrogen sulfide (H_2S) concentration of headspace gases from Holes 1129C and 1129D. Solid circles = Hole 1129C; open circles = Hole 1129D; ppmv = parts per million by volume.

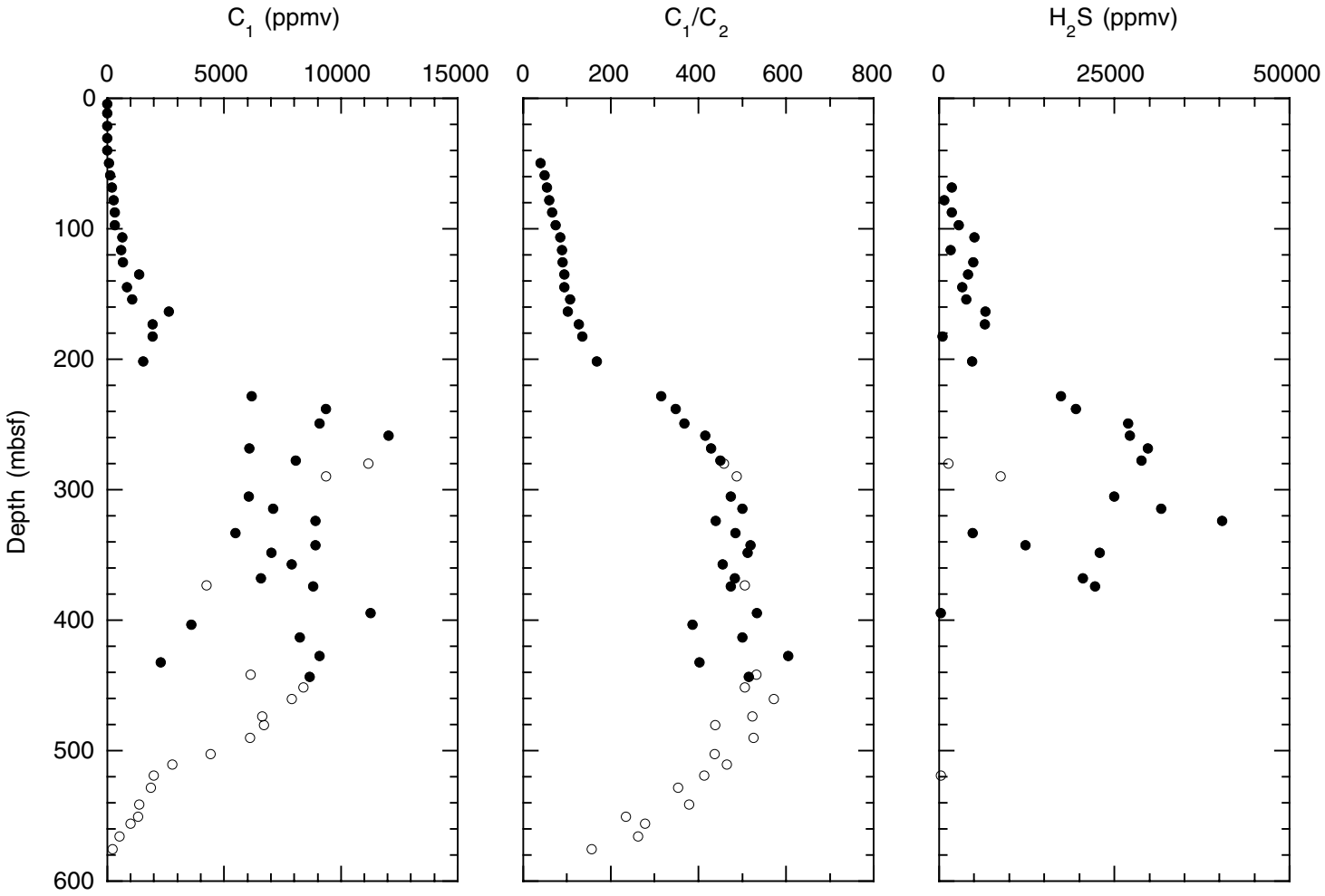

Figure F14. Calcium carbonate and organic carbon contents in samples from Holes 1129C and 1129D. Solid circles = Hole 1129C; open circles = Hole 1129D.

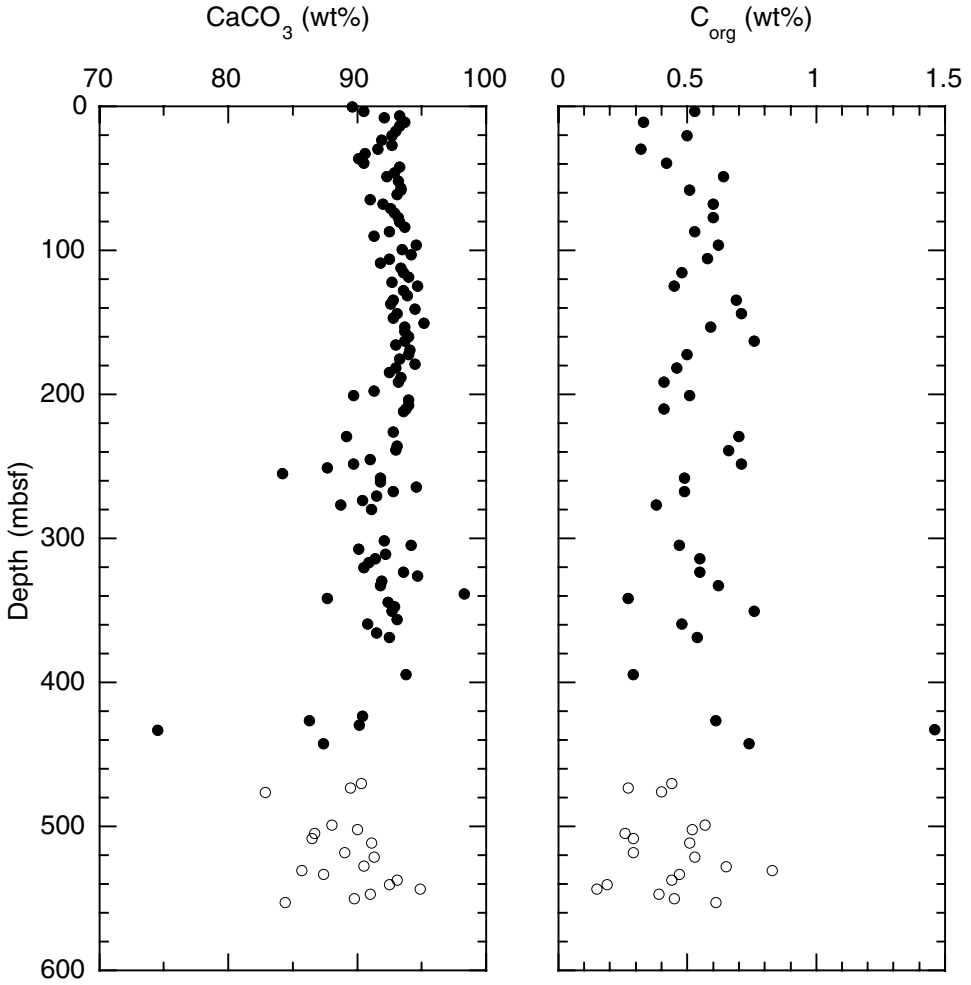

Figure F15. T_{max} vs. hydrogen index for selected samples from Sites 1127, 1129, 1131, and 1132.

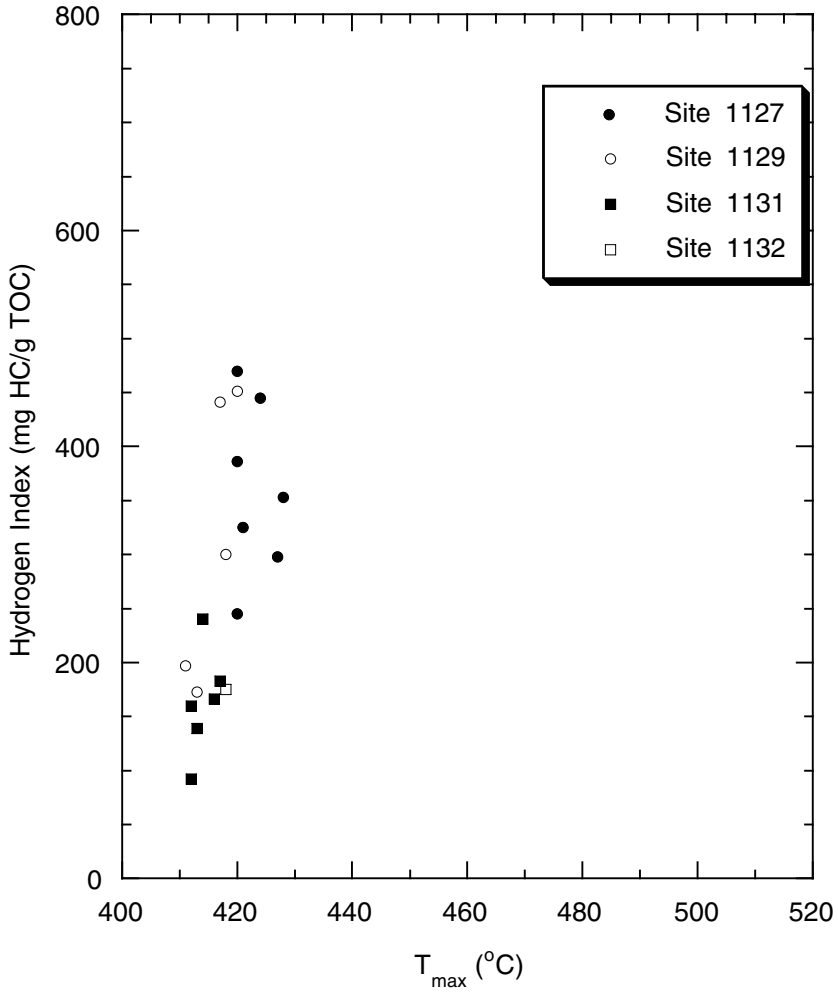

Figure F16. Summary trends at Site 1129 in (**A**) salinity, (**B**) Cl^-, (**C**) Na^+, (**D**) K^+, and (**E**) Na^+/Cl^-. Although the ion concentration trends show a diffusive profile, the Na^+/Cl^- ratio shows a maximum between 90 and 120 mbsf. Note the absence of gradients in the upper 40.3 mbsf, which indicates the advection of fluids through the sediments.

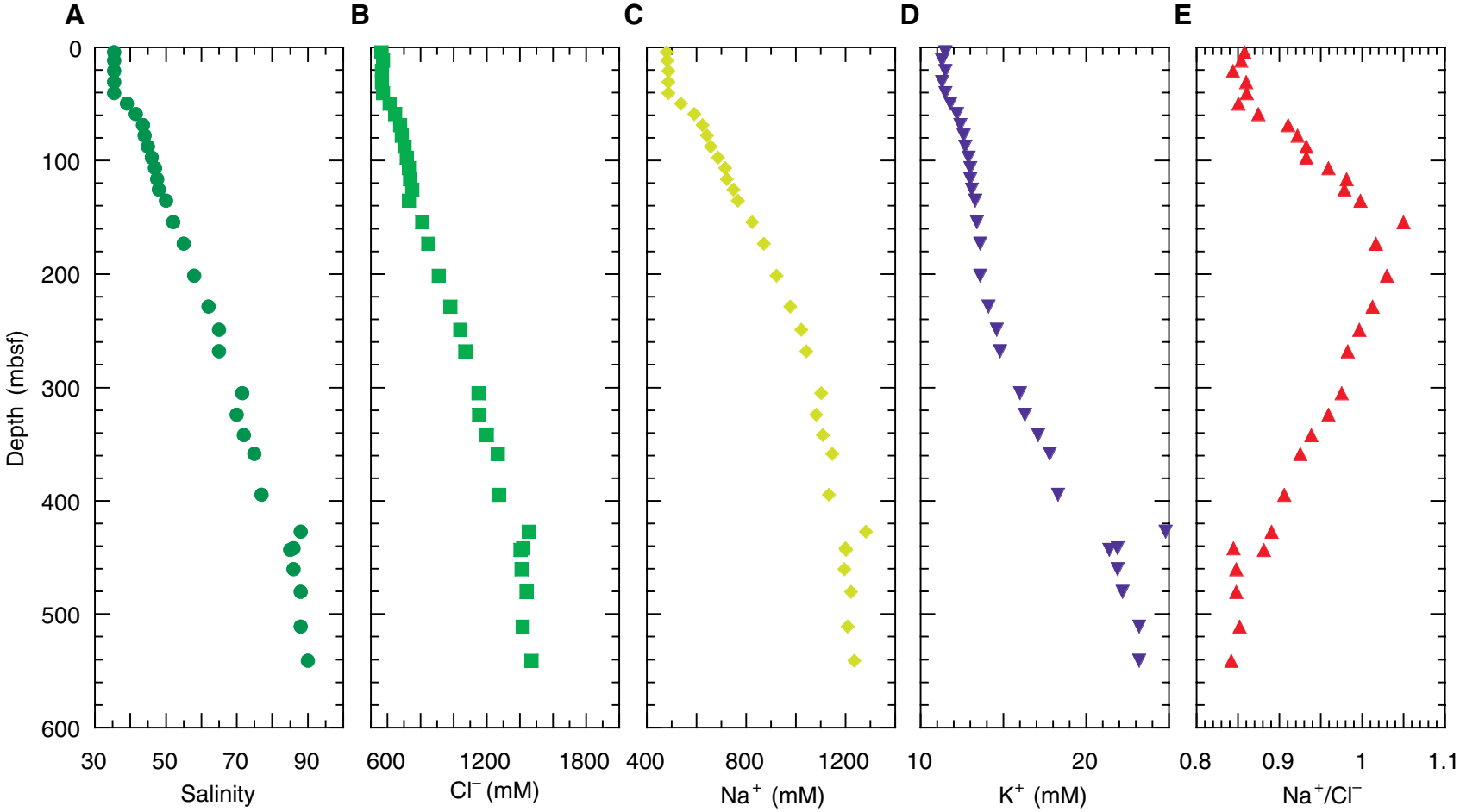

Figure F17. Concentrations of (**A**) Mg^{2+}, (**B**) Ca^{2+}, (**C**) Sr^{2+}, (**D**) Li^{+}, and (**E**) $H_4SiO_4^0$. Note the absence of gradients in the upper 40.3 mbsf, which indicates the advection of fluids through the sediments.

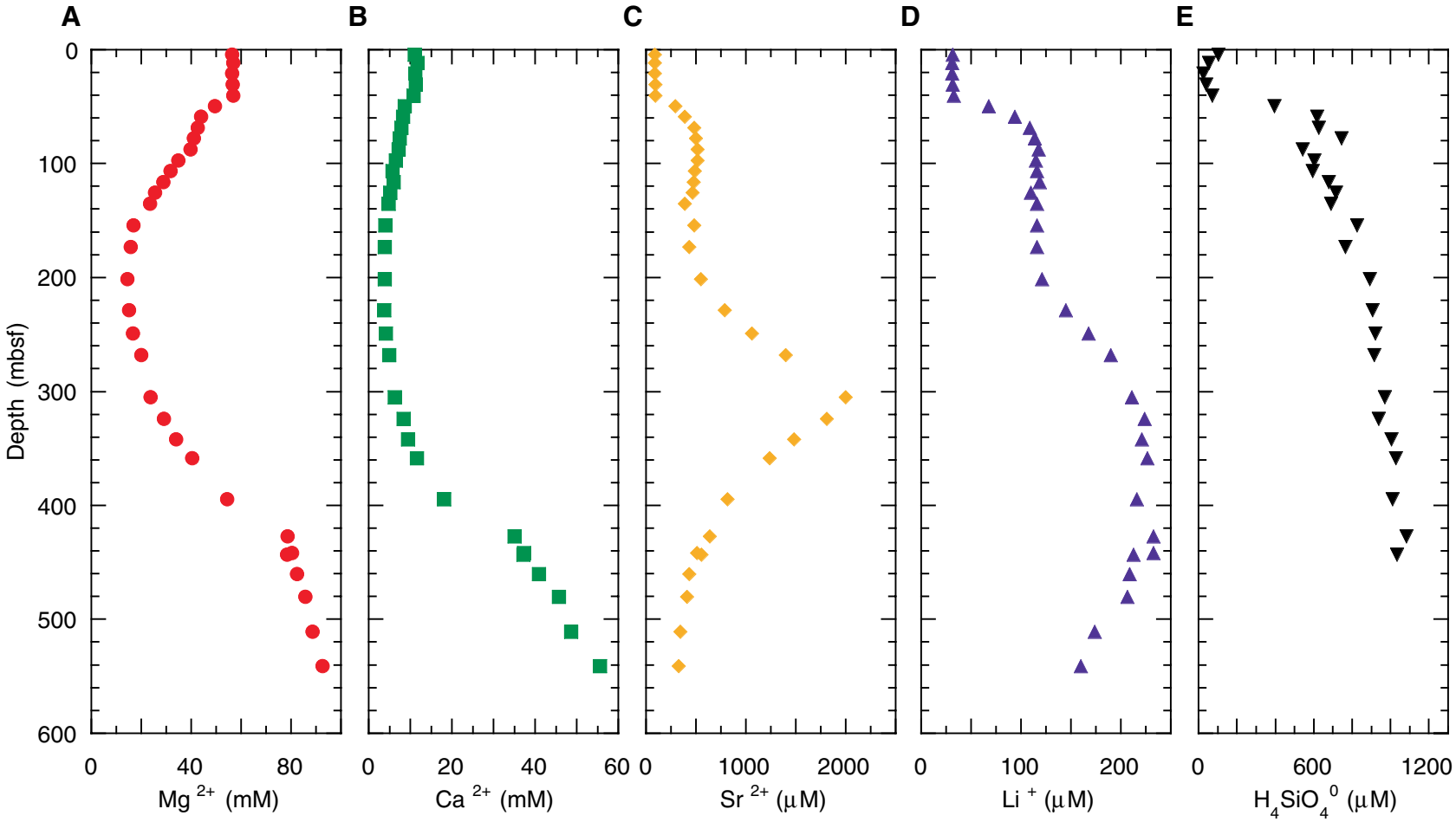

Figure F18. Variations in (**A**) pH (the punch-in pH values are shown by the open triangles), (**B**) alkalinity, (**C**) SO_4^{2-}, (**D**) Fe^{2+}, and (**E**) NH_4^+ from Site 1129. Note the absence of gradients in the upper 40.3 mbsf, which indicates the advection of fluids through the sediments.

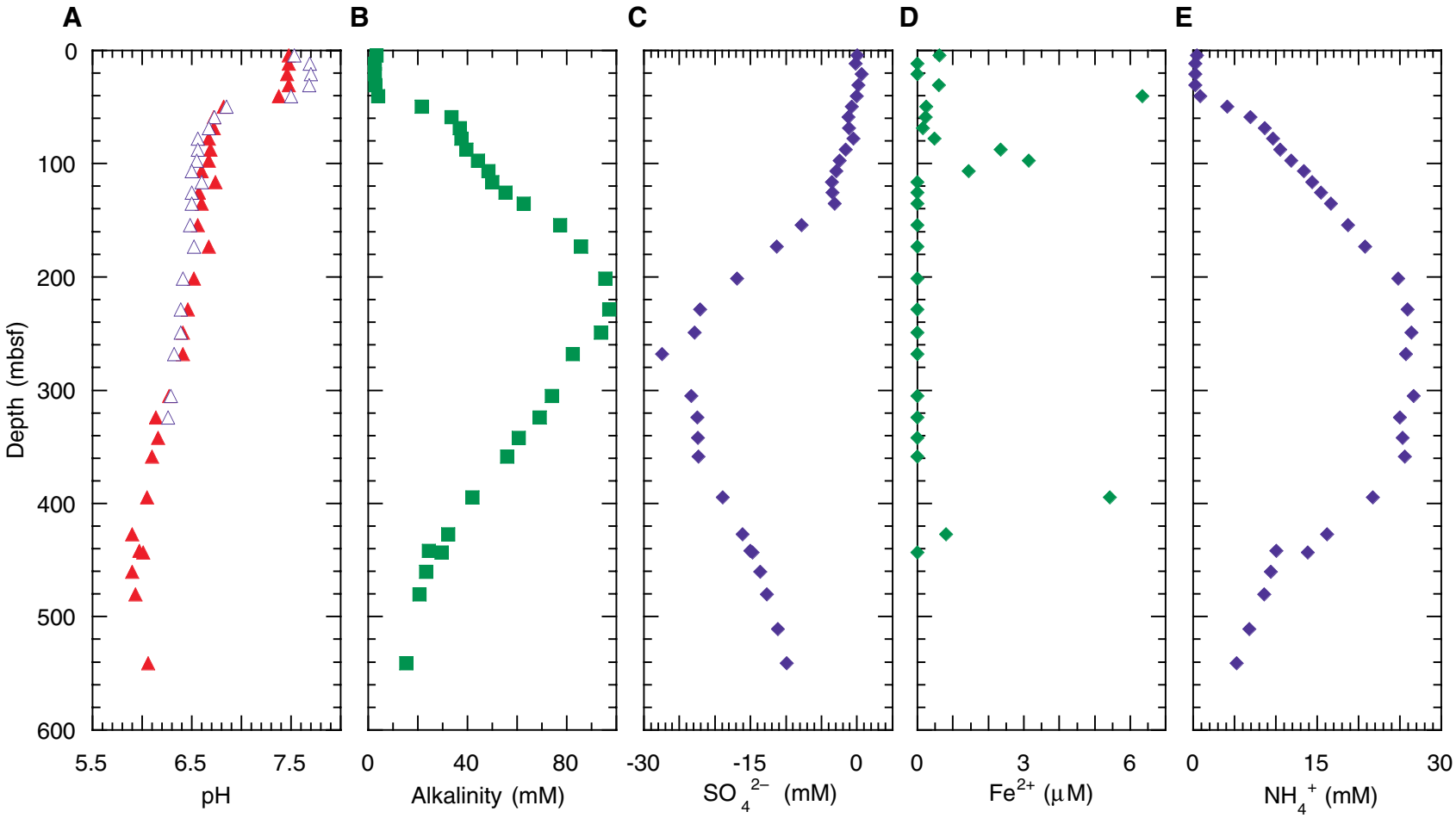

Figure F19. Variations in the concentrations of aragonite (A), high-Mg calcite (HMC), quartz (Q), low-Mg calcite (LMC), and dolomite (D) from Site 1129. Lithostratigraphic units are shown on the right.

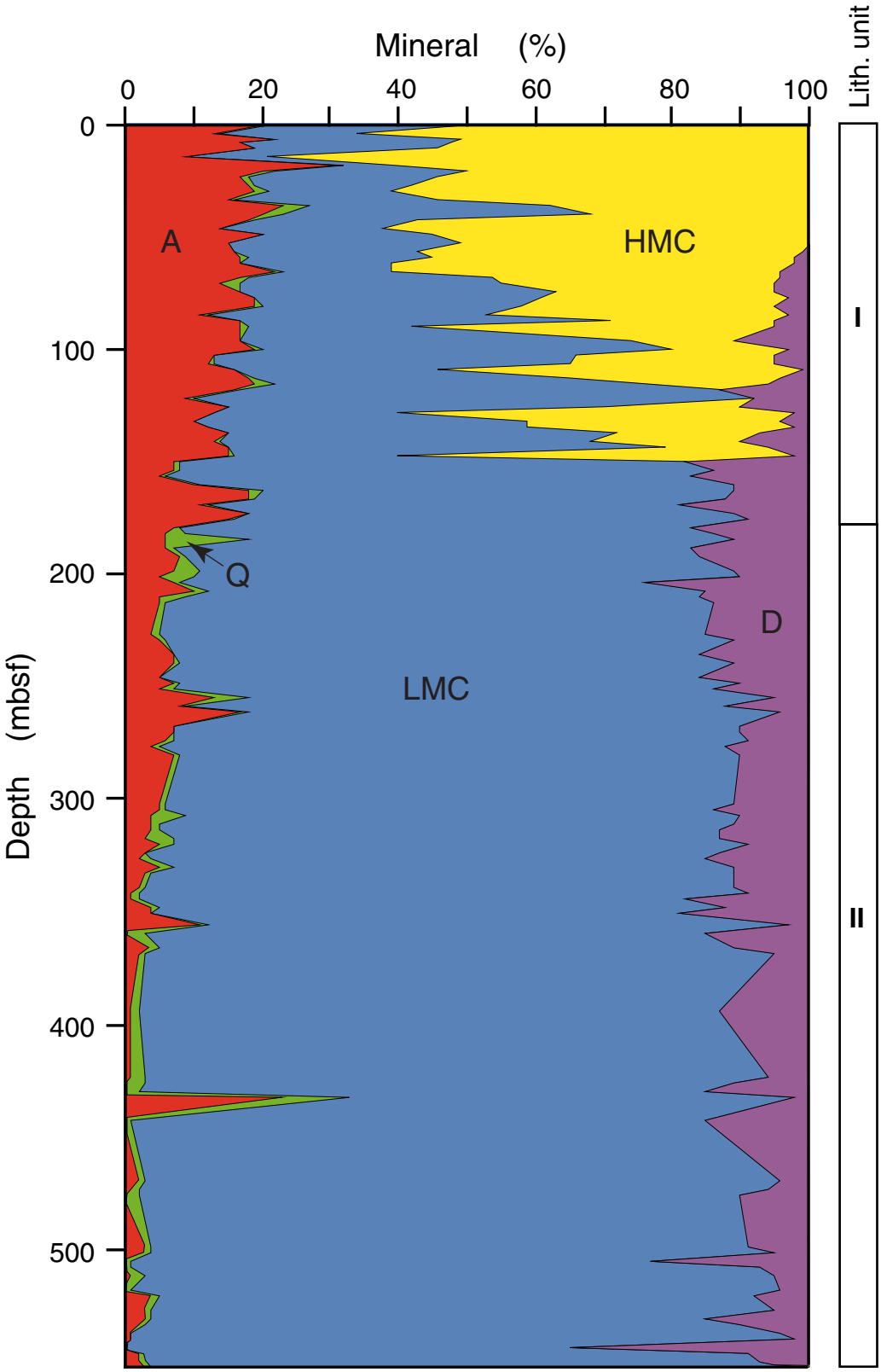

Figure F20. Contour plot showing the variation in the concentration of Cl^- from Sites 1127, 1129, and 1131. The contour interval is 100 mM. Note the inclined angle of the contour lines, which are not parallel to the sediment/seawater interface.

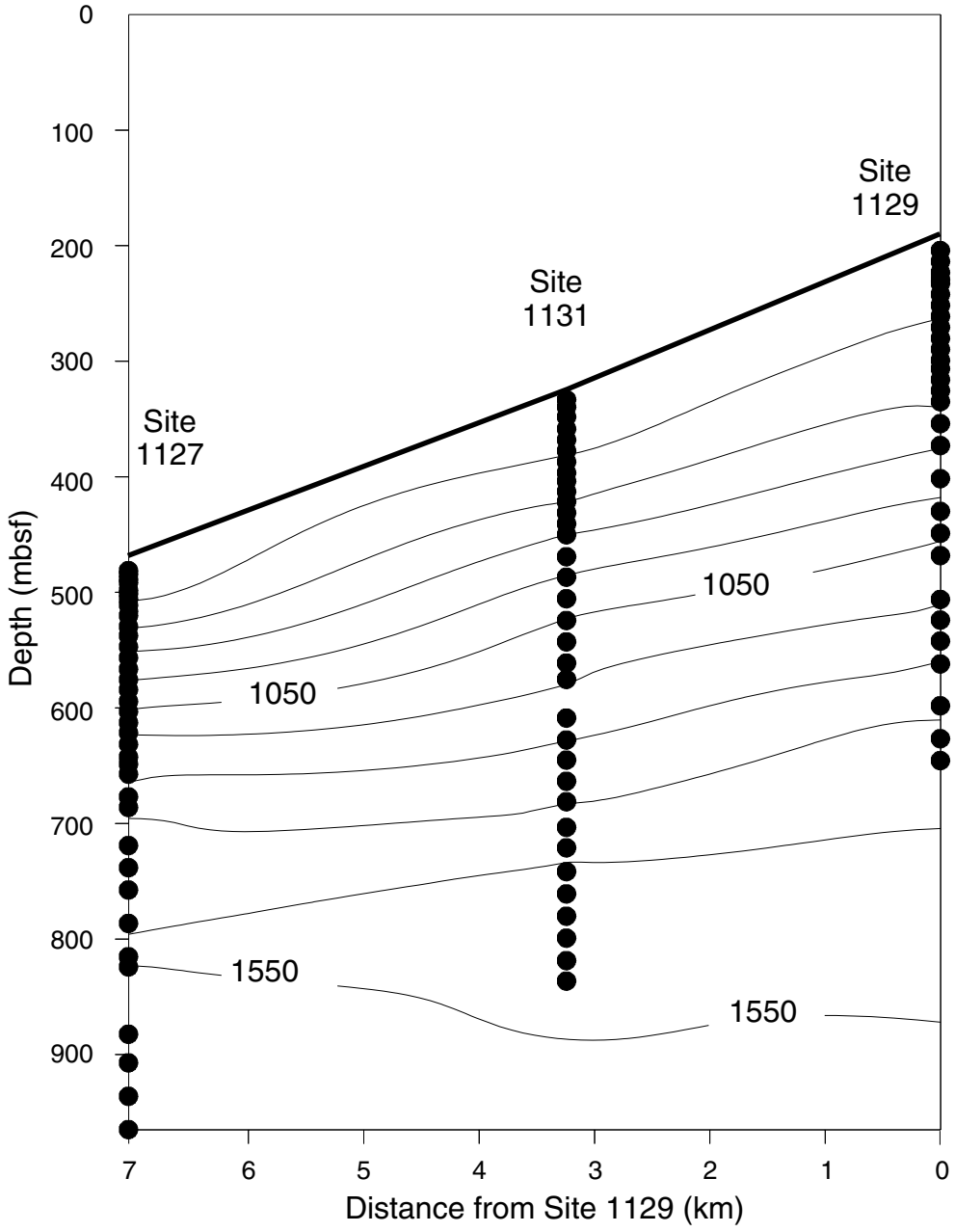

Figure F21. The Na^+/Cl^- ratio plotted vs. increasing depth for Sites 1129, 1131, and 1127. Note the well-defined increase in the Na^+/Cl^- ratio in the pore waters at Sites 1129 and 1131 compared to Site 1127. The more pronounced Na^+/Cl^- ratios at Sites 1129 and 1131 support a continental origin of the brine. The shaded interval indicates the range of Na^+/Cl^- ratios in seawater.

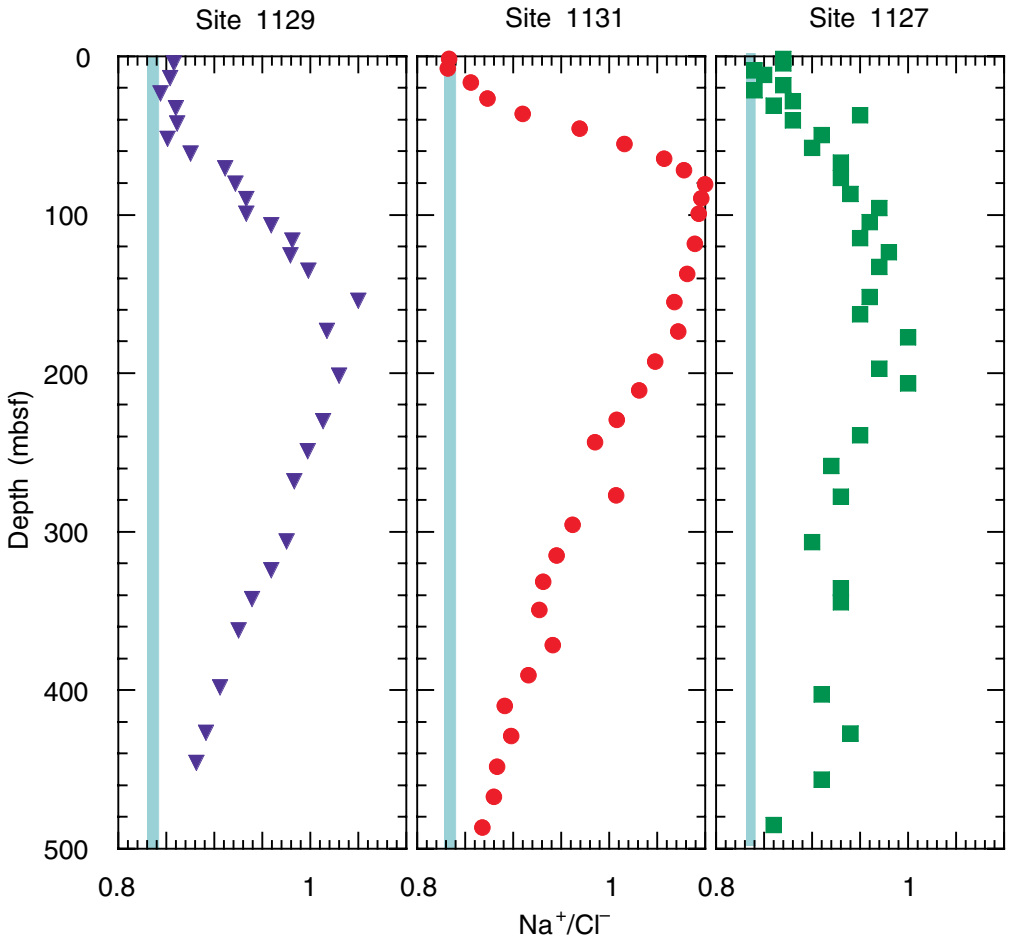

Figure F22. Excess SO_4^{2-} from Sites 1129, 1131, and 1127. Note the complete sulfate reduction at Site 1127, near the sediment/seawater interface, compared to Sites 1131 and 1129.

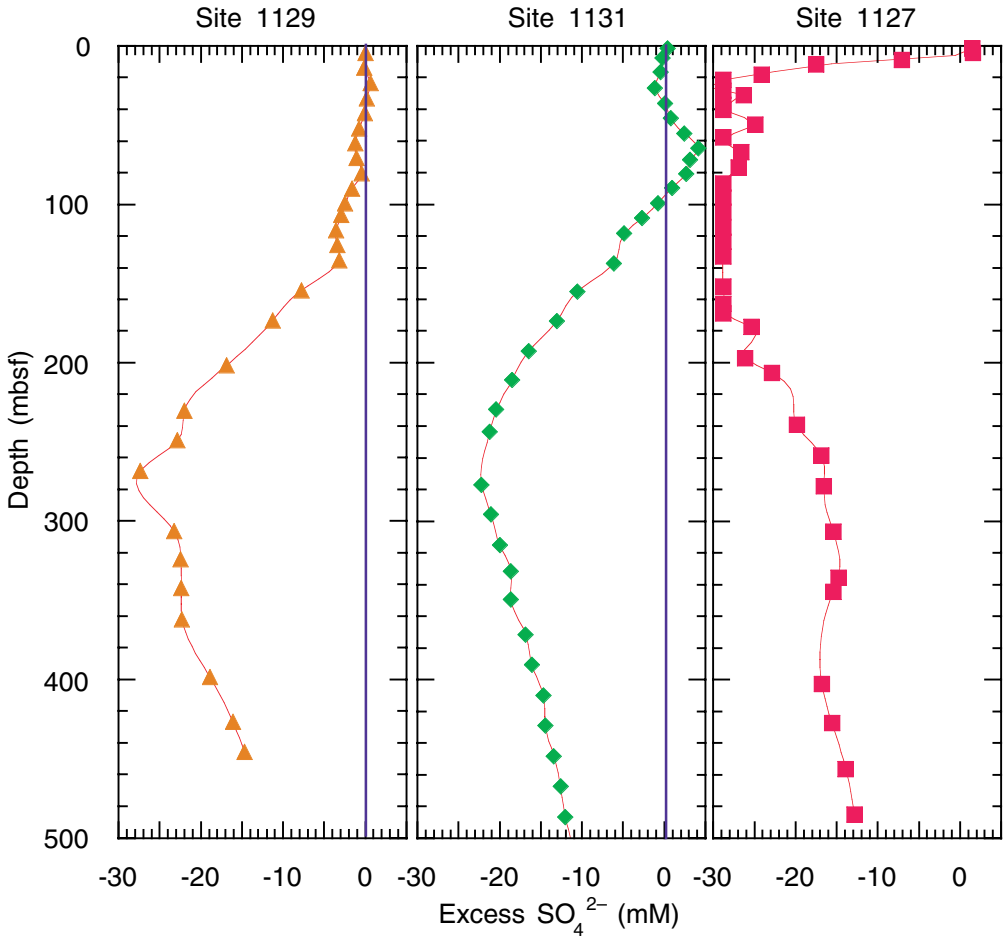

Figure F23. Contour map of alkalinity in the pore waters from Sites 1127, 1131, and 1129. The maximum alkalinity occurs at Site 1131. Note that the contouring program causes an artifact in the contours near the surface between Sites 1127 and 1131.

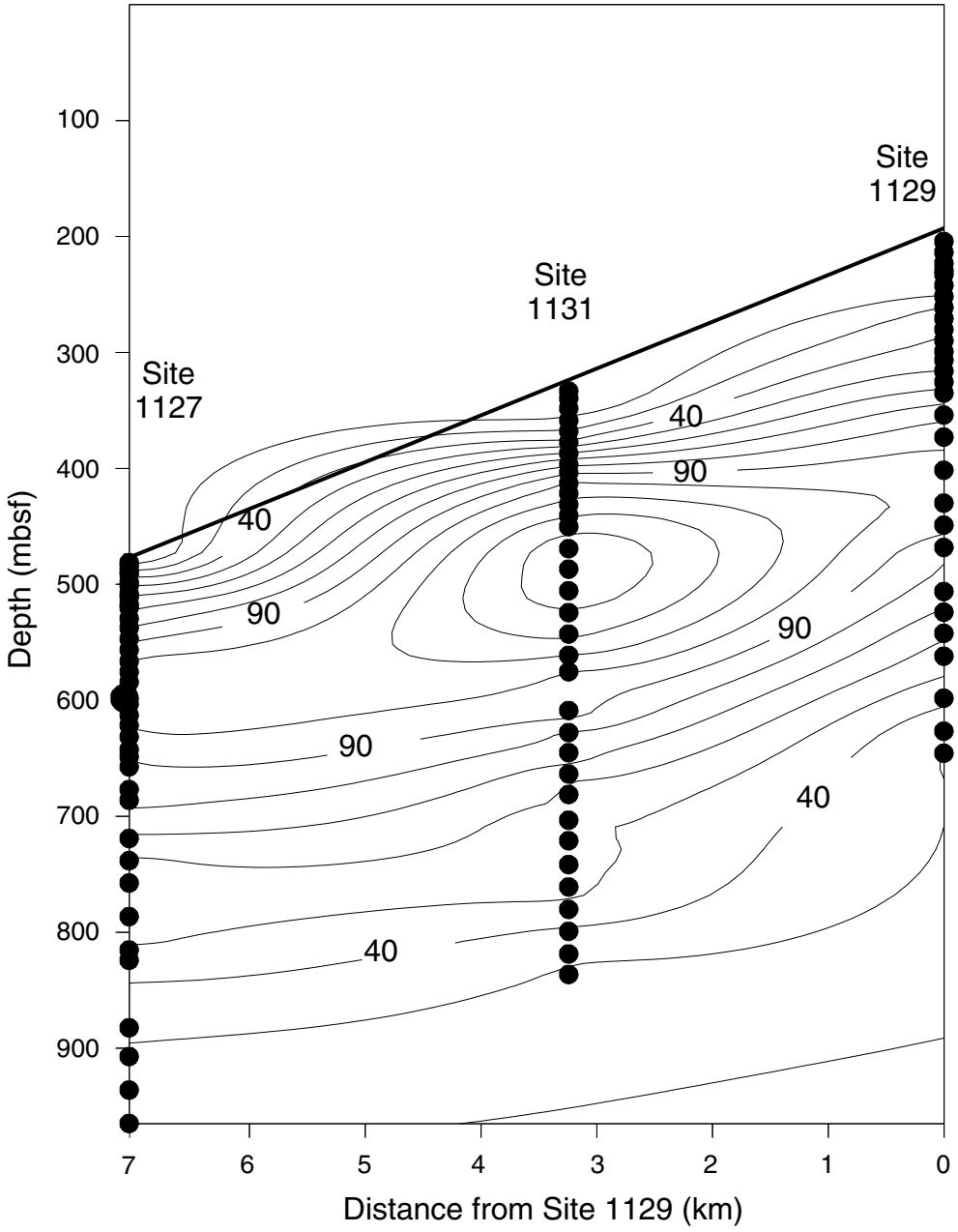

Figure F24. Combined plot of *P*-wave velocity, discrete moisture-and-density bulk density and porosity (red dots = Hole 1129C, green dots = Hole 1129D), corrected magnetic susceptibility, and NGR from Site 1129. Recovery column is shown on the left and physical properties units (PP units) are shown on the right. (**Figure shown on next page.**)

Figure F24. (Caption on previous page.)

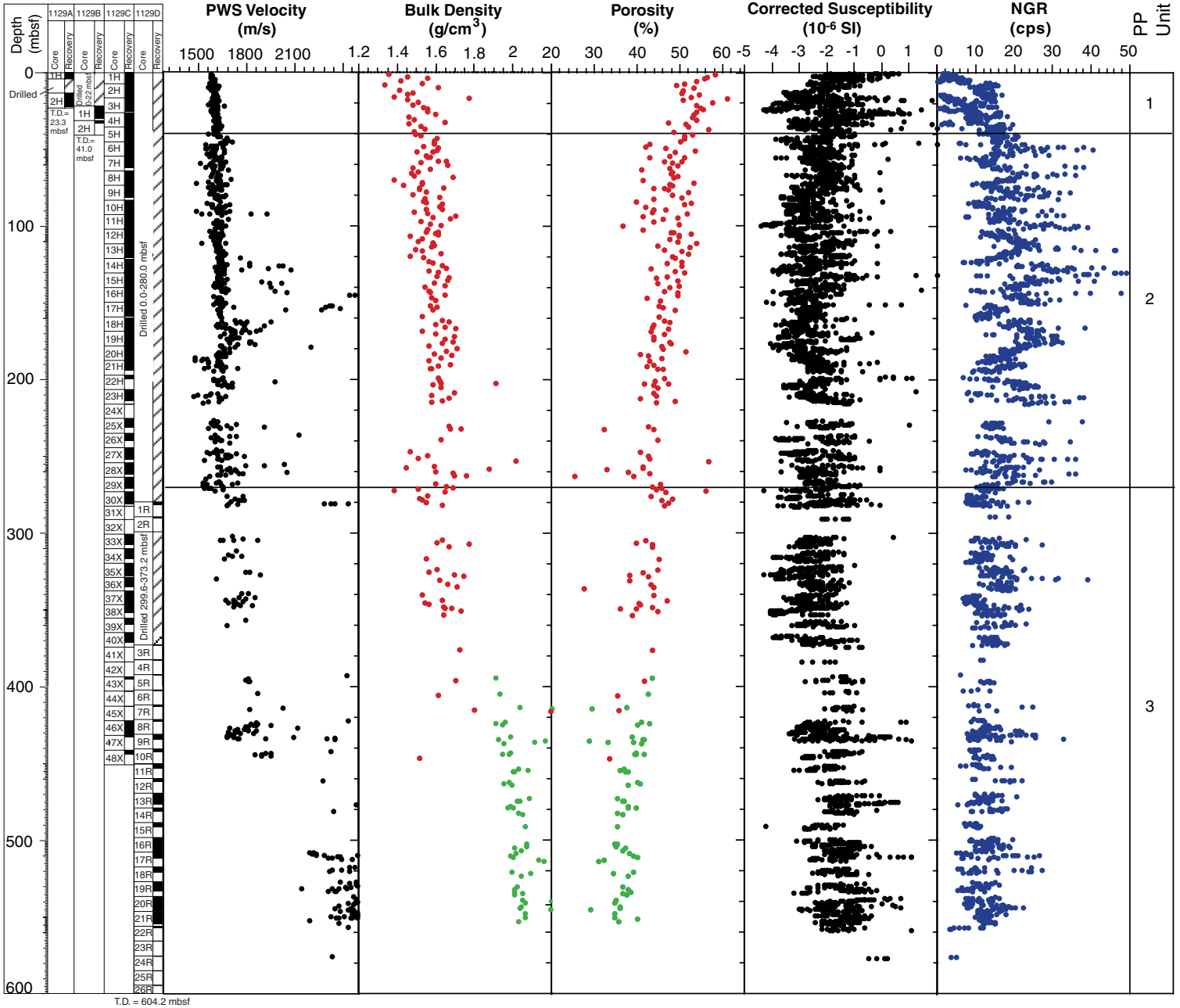

Figure F25. Maximum shear strength data with physical properties units (PP units) for the upper 250 m of Site 1129.

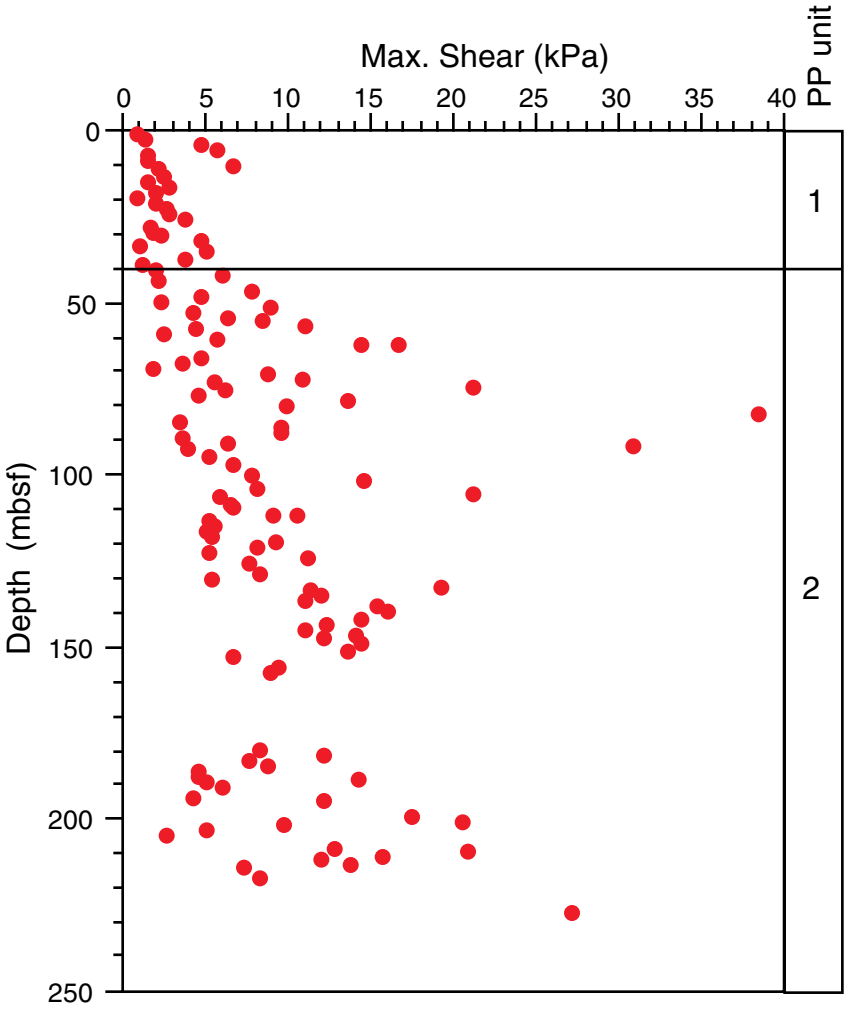

Figure F26. Thermal conductivity data (large dots) plotted with gamma-ray attenuation (GRA) bulk density (small dots) at Hole 1129D. Physical properties units (PP units) are shown on the right.

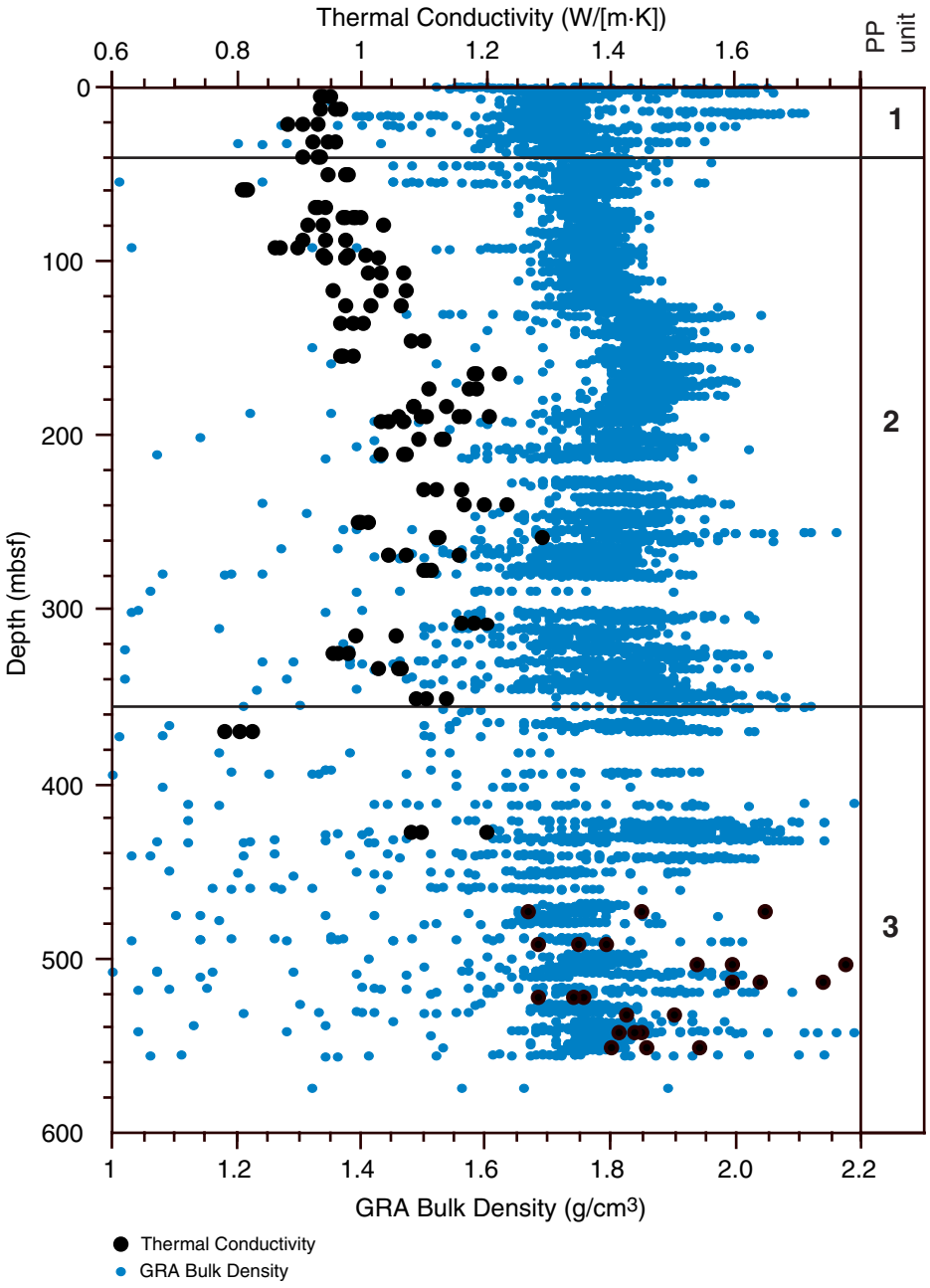

Figure F27. Variation of formation temperature with depth at Site 1129. XBT = expendable bathythermograph, DVTP = Davis-Villinger temperature probe.

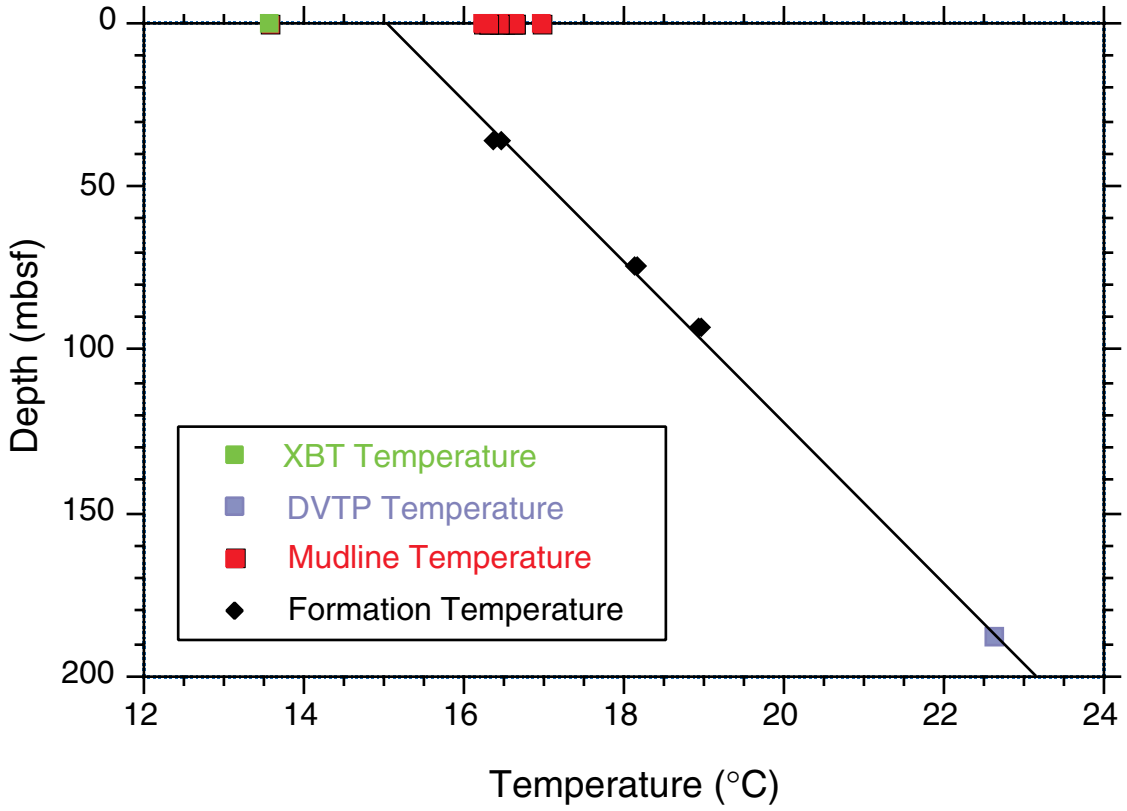

Figure F28. Summary of triple combination logging tool and sonic logs vs. depth for the open-hole logged interval. From left to right, columns are core recovery; total gamma radiation (HSGR) and caliper; porosity and density, plotted on compatible scales; photoelectric effect (PEF); shallow, medium and deep resistivity; sonic velocity; logging units; lithostratigraphic units, and biostratigraphic ages.

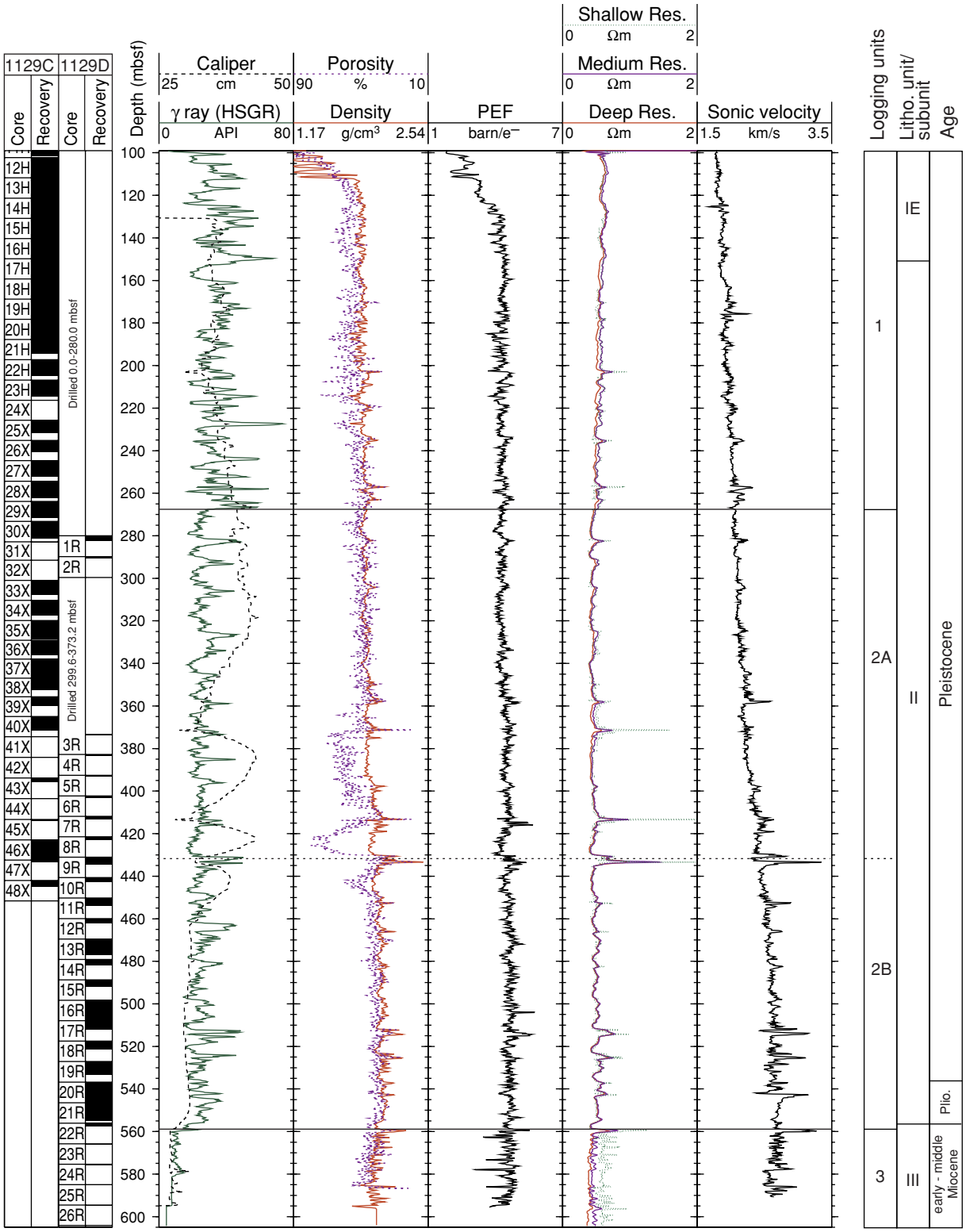

Figure F29. Summary of spectral gamma-ray logs from the hostile environment natural gamma-ray sonde, plotted on an expanded depth scale (mbsf) to highlight variations in the interval logged through pipe. From left to right, columns are core recovery, total gamma radiation (HSGR) and computed (uranium-free) gamma radiation (HCGR), uranium, thorium, potassium, logging units, lithostratigraphic units, and biostratigraphic ages.

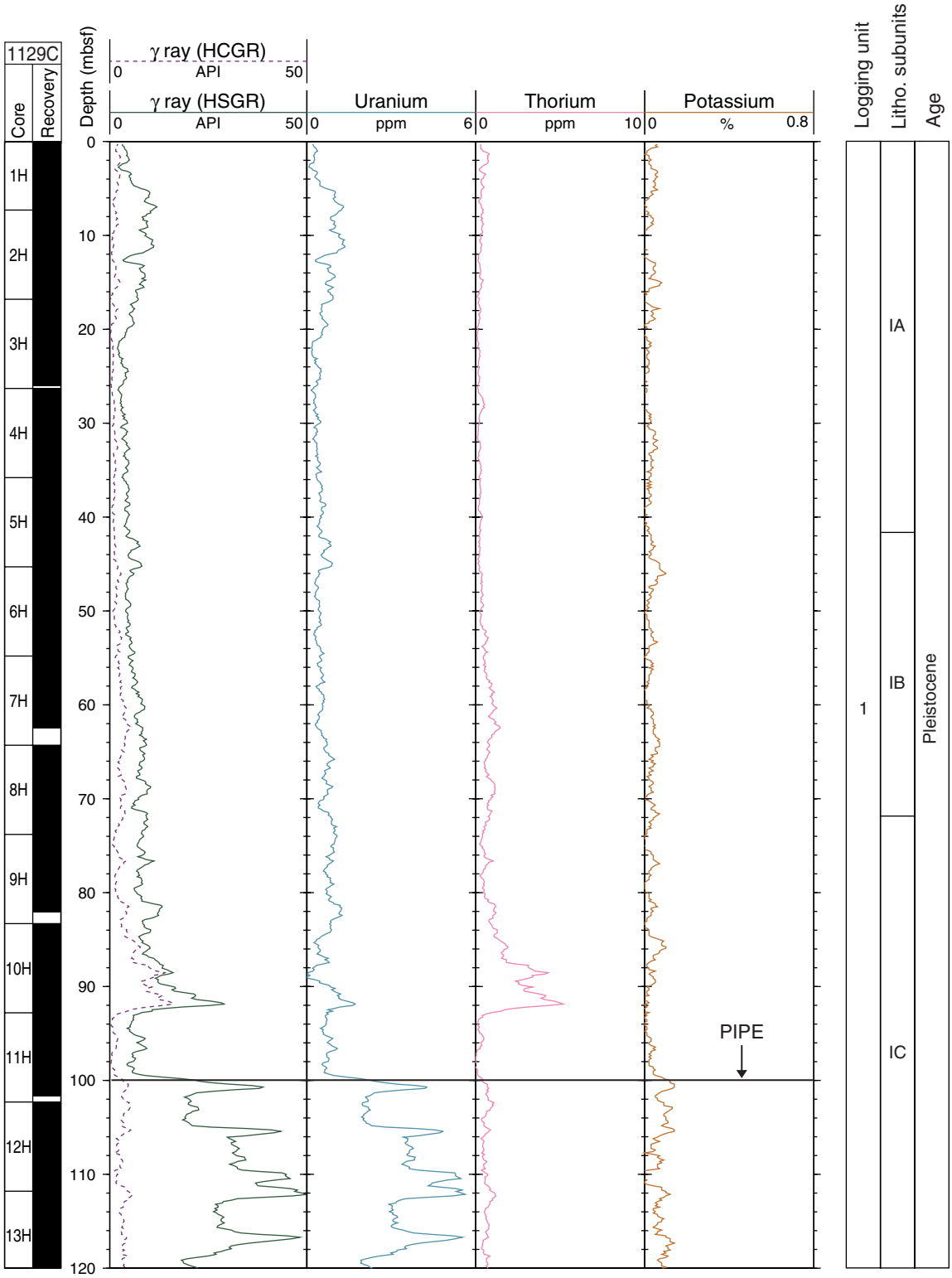

Figure F30. Summary of spectral gamma-ray logs from the hostile environment natural gamma-ray sonde, plotted vs. depth for the open-hole logged interval. From left to right, columns are core recovery, total gamma radiation (HSGR) and computed (uranium-free) gamma radiation (HCGR), uranium, thorium, potassium and caliper, logging units, lithostratigraphic units, and biostratigraphic ages.

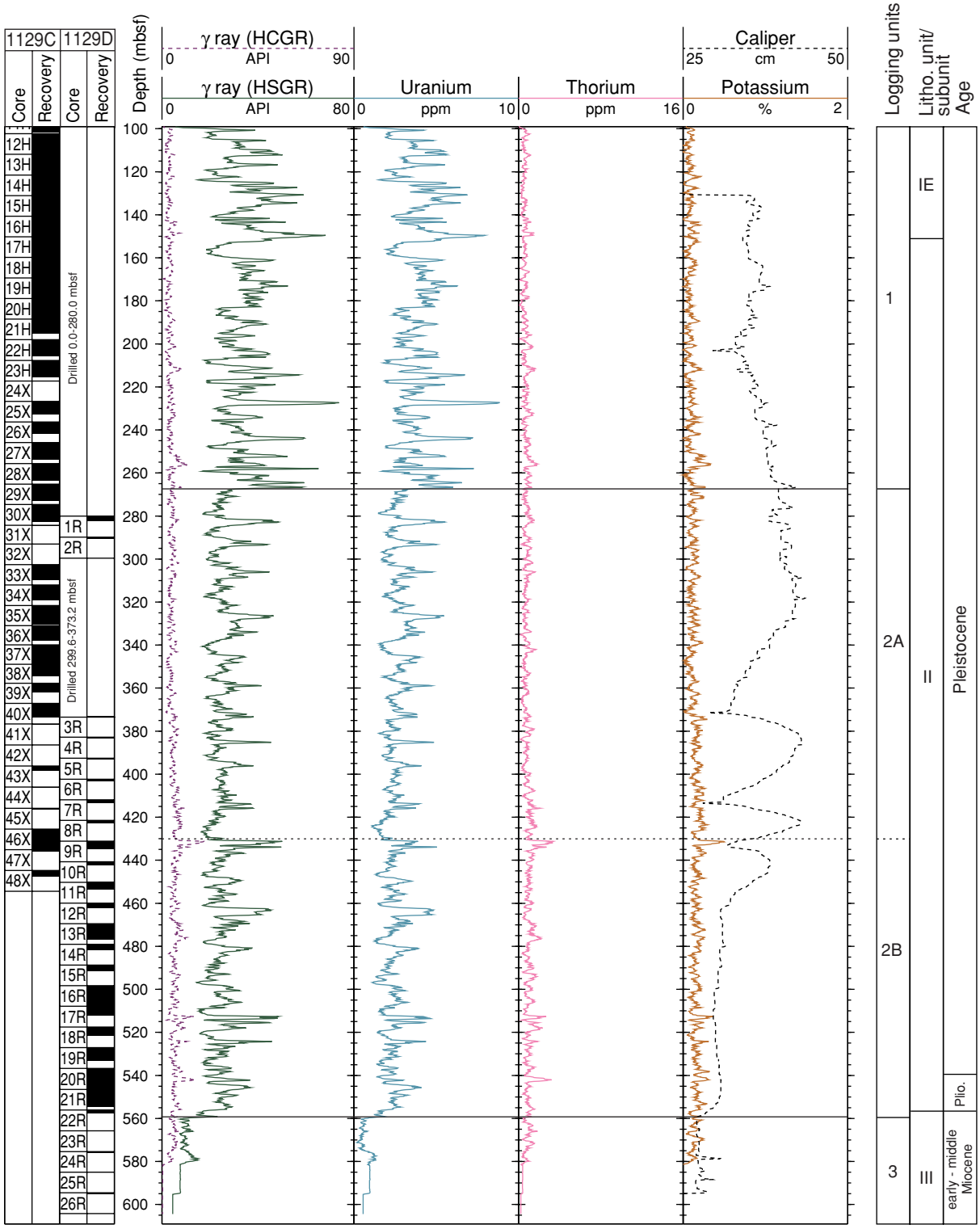

Figure F31. Formation MicroScanner (FMS) image showing the boundary between logging Units 2 and 3, coinciding with the boundary between lithostratigraphic Units II and III. Chert horizons in Unit 3 are imaged as resistive (bright) intervals, whereas the packstone/grainstone (Unit 3) and wackestone/packstone (Unit 2) intervals are shown as more conductive (dark) intervals. The boundary between Units 2 and 3 is defined by the inflection in the gamma-ray curve immediately above 560 mbsf.

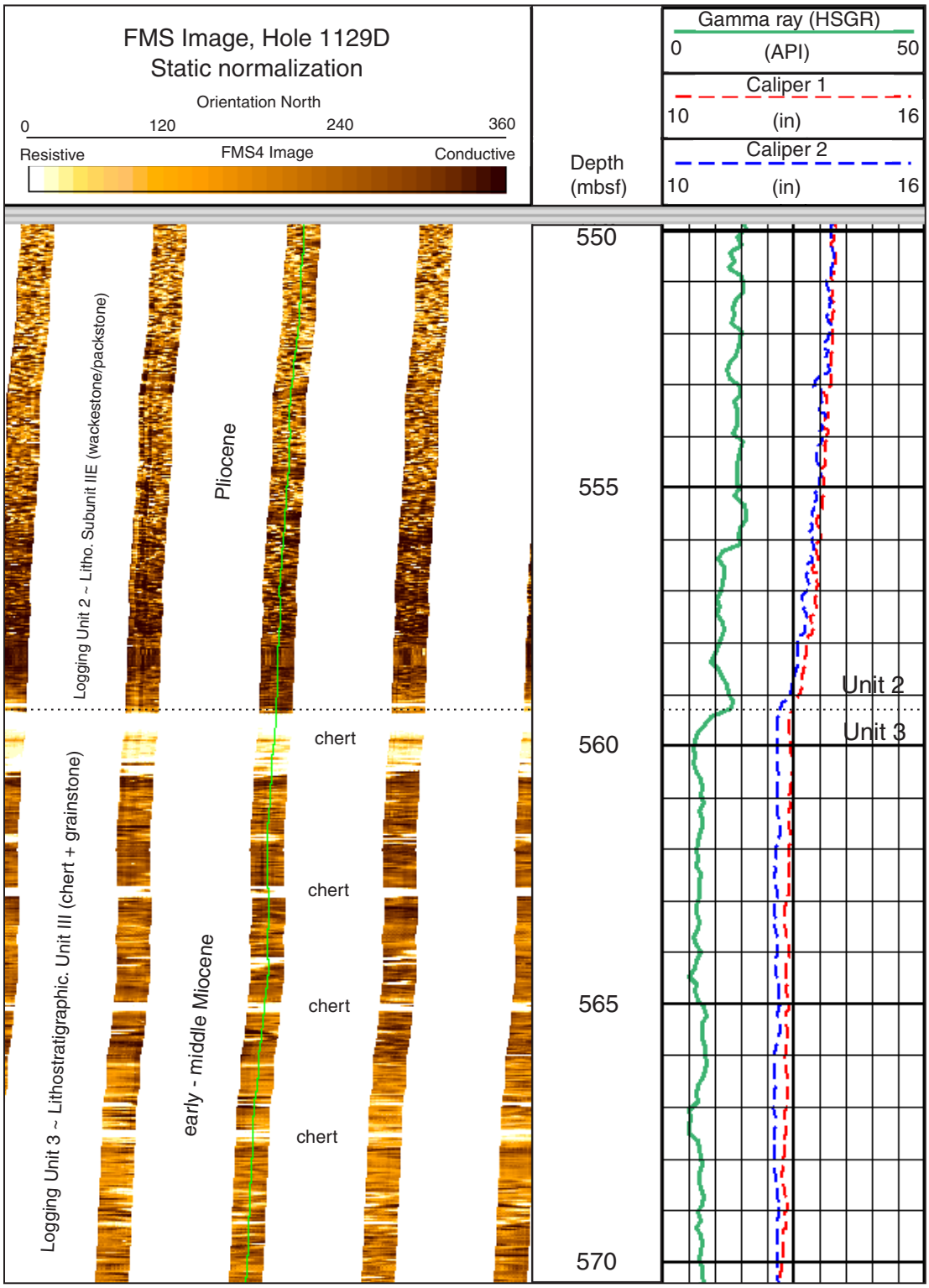

Table T1. Site 1129 coring summary. (See table note. Continued on next two pages.)

Hole 1129A

Latitude: –33.2897617° (33°17.3857′S)
Longitude: 128.481197° (128°28.8718′E)
Seafloor (drill-pipe measurement from rig floor, mbrf): 214.2
Distance between rig floor and sea level (m): 11.3
Water depth (drill-pipe measurement from sea level, m): 202.9
Total depth (from rig floor, mbrf): 237.5
Penetration (mbsf): 23.3
Total number of cores: 2
Total length of cored section (m): 13.8
Total number of drilled intervals: 1
Total length of drilled intervals (m): 9.5
Total core recovered (m): 13.27
Core recovery (%): 96.2

Hole 1129B

Latitude: –33.2896350° (33°17.3781′S)
Longitude: 128.481010° (128°28.8606′E)
Seafloor (drill-pipe measurement from rig floor, mbrf): 214.00
Distance between rig floor and sea level (m): 11.7
Water depth (drill-pipe measurement from sea level, m): 202.3
Total depth (from rig floor, mbrf): 255.0
Penetration (mbsf): 41.0
Total number of cores: 2
Total length of cored section (m): 19.0
Total number of drilled intervals: 1
Total length of drilled intervals (m): 22.0
Total core recovered (m): 10.24
Core recovery (%): 53.9

Hole 1129C

Latitude: –33.296570° (33°17.7942′S)
Longitude: 128.481310° (128°28.8786′E)
Seafloor (drill-pipe measurement from rig floor, mbrf): 214.2
Distance between rig floor and sea level (m): 11.8
Water depth (drill-pipe measurement from sea level, m): 202.4
Total depth (from rig floor, mbrf): 665.8
Penetration (mbsf): 451.6
Total number of cores: 48
Total length of cored section (m): 451.6
Total core recovered (m): 322.89
Core recovery (%): 71.5

Hole 1129D

Latitude: –33.296475° (33°17.7885′S)
Longitude: 128.481115° (128°28.8669′E)
Seafloor (drill-pipe measurement from rig floor, mbrf): 214.0
Distance between rig floor and sea level (m): 11.9
Water depth (drill-pipe measurement from sea level, m): 202.1
Total depth (from rig floor, mbrf): 818.2
Penetration (mbsf): 604.2
Total number of cores: 26
Total length of cored section (m): 250.6
Total number of drilled intervals: 2
Total length of drilled intervals (m): 353.6
Total core recovered (m): 76.72
Core recovery (%): 30.6

Core	Date (Nov 1998)	Time (UTC + 8 hr)	Depth (mbsf)	Length cored (m)	Length recovered (m)	Recovery (%)	Comment
182-1129A-							
1H	11	1345	0.00–4.30	4.3	4.35	101.2	
		*****Drilled from 4.30 to 13.80 mbsf*****					
2H	11	1515	13.80–23.30	9.5	8.92	93.9	
Coring totals:				13.8	13.27	96.2	
Drilled total:				9.5			
Total:				23.3			

Table T1 (continued).

Core	Date (Nov 1998)	Time (UTC + 8 hr)	Depth (mbsf)	Length cored (m)	Length recovered (m)	Recovery (%)	Comment
182-1129B-							
		*****Drilled from 0 to 22.00 mbsf*****					
1H	19	2250	22.00–31.50	9.5	8.41	88.5	
2H	20	0030	31.50–41.00	9.5	1.83	19.3	
Coring totals:				19.0	10.24	53.9	
Drilled total:				22.0			
Total:				41.0			
182-1129C-							
1H	25	0205	0.00–7.30	7.3	7.29	99.9	
2H	25	0230	7.30–16.80	9.5	9.82	103.4	
3H	25	0310	16.80–26.30	9.5	9.20	96.8	
4H	25	0425	26.30–35.80	9.5	10.01	105.4	
5H	25	0445	35.80–45.30	9.5	9.53	100.3	H_2S
6H	25	0535	45.30–54.80	9.5	9.80	103.2	H_2S
7H	25	0615	54.80–64.30	9.5	7.67	80.7	H_2S
8H	25	0730	64.30–73.80	9.5	10.11	106.4	H_2S
9H	25	0810	73.80–83.30	9.5	8.32	87.6	H_2S
10H	25	0910	83.30–92.80	9.5	9.80	103.2	H_2S
11H	25	0950	92.80–102.30	9.5	8.85	93.2	H_2S
12H	25	1030	102.30–111.80	9.5	9.54	100.4	H_2S
13H	25	1110	111.80–121.30	9.5	9.33	98.2	H_2S
14H	25	1210	121.30–130.80	9.5	9.71	102.2	H_2S
15H	25	1250	130.80–140.30	9.5	9.76	102.7	H_2S
16H	25	1330	140.30–149.80	9.5	9.64	101.5	H_2S
17H	25	1400	149.80–159.30	9.5	9.33	98.2	H_2S
18H	25	1440	159.30–168.80	9.5	9.59	101.0	H_2S
19H	25	1515	168.80–178.30	9.5	9.53	100.3	H_2S
20H	25	1615	178.30–187.80	9.5	9.77	102.8	H_2S
21H	25	1725	187.80–197.30	9.5	6.41	67.5	H_2S; crushed liner; sediment pushed into new liner; totally disturbed
22H	25	1840	197.30–206.80	9.5	7.47	78.6	H_2S
23H	25	1935	206.80–216.30	9.5	7.72	81.3	H_2S; crushed liner; contents transferred to new liner
24X	25	2040	216.30–225.70	9.4	0.19	2.0	H_2S
25X	25	2100	225.70–235.20	9.5	5.95	62.6	H_2S
26X	25	2135	235.20–244.70	9.5	5.33	56.1	H_2S
27X	25	2210	244.70–254.40	9.7	7.68	79.2	H_2S
28X	25	2240	254.40–263.90	9.5	7.81	82.2	H_2S
29X	25	2310	263.90–273.30	9.4	7.77	82.7	H_2S
30X	25	2355	273.30–282.80	9.5	7.87	82.8	H_2S
31X	26	0035	282.80–291.50	8.7	0.16	1.8	H_2S
32X	26	0115	291.50–301.00	9.5	0.00	0.0	No recovery
33X	26	0210	301.00–310.40	9.4	6.93	73.7	H_2S
34X	26	0250	310.40–319.80	9.4	6.96	74.0	H_2S
35X	26	0330	319.80–329.10	9.3	8.70	93.6	H_2S
36X	26	0500	329.10–338.00	8.9	6.76	76.0	H_2S
37X	26	0545	338.00–346.90	8.9	9.50	106.7	H_2S
38X	26	0630	346.90–355.70	8.8	5.49	62.4	H_2S
39X	26	0715	355.70–365.00	9.3	4.19	45.1	H_2S
40X	26	0810	365.00–374.50	9.5	6.50	68.4	H_2S
41X	26	0910	374.50–384.20	9.7	0.07	0.7	H_2S
42X	26	0950	384.20–393.90	9.7	0.00	0.0	No recovery
43X	26	1020	393.90–403.60	9.7	1.89	19.5	H_2S
44X	26	1100	403.60–413.30	9.7	0.16	1.7	H_2S
45X	26	1220	413.30–422.90	9.6	0.73	7.6	
46X	26	1300	422.90–432.40	9.5	10.06	105.9	
47X	26	1400	432.40–442.00	9.6	1.08	11.3	
48X	26	1445	442.00–451.60	9.6	2.91	30.3	
Totals:				451.6	322.89	71.5	
182-1129D-							
		*****Drilled from 0 to 280.00 mbsf*****					
1R	29	0335	280.00–289.80	9.8	2.36	24.1	H_2S
2R	29	0405	289.80–299.60	9.8	0.80	8.2	H_2S
		*****Drilled from 299.60 to 373.20 mbsf*****					
3R	29	0745	373.20–382.80	9.6	0.45	4.7	H_2S
4R	29	0820	382.80–392.60	9.8	0.43	4.4	H_2S
5R	29	0850	392.60–402.30	9.7	0.37	3.8	H_2S
6R	29	0940	402.30–411.90	9.6	0.85	8.9	H_2S

Table T1 (continued).

Core	Date (Nov 1998)	Time (UTC + 8 hr)	Depth (mbsf)	Length cored (m)	Length recovered (m)	Recovery (%)	Comment
7R	29	1040	411.90–421.50	9.6	1.47	15.3	H_2S
8R	29	1115	421.50–431.10	9.6	1.49	15.5	H_2S
9R	29	1205	431.10–440.70	9.6	3.65	38.0	H_2S
10R	29	1235	440.70–450.30	9.6	1.85	19.3	H_2S
11R	29	1310	450.30–459.90	9.6	3.37	35.1	H_2S
12R	29	1350	459.90–469.50	9.6	2.13	22.2	H_2S
13R	29	1420	469.50–479.10	9.6	7.46	77.7	H_2S
14R	29	1500	479.10–488.70	9.6	2.68	27.9	H_2S
15R	29	1535	488.70–498.30	9.6	3.03	31.6	H_2S
16R	29	1605	498.30–507.90	9.6	9.36	97.5	H_2S
17R	29	1645	507.90–517.50	9.6	4.27	44.5	H_2S
18R	29	1725	517.50–527.10	9.6	4.05	42.2	H_2S
19R	29	1805	527.10–536.80	9.7	6.12	63.1	H_2S
20R	29	1840	536.80–546.50	9.7	9.56	98.6	H_2S
21R	29	1915	546.50–556.10	9.6	8.23	85.7	H_2S
22R	29	2000	556.10–565.80	9.7	1.60	16.5	H_2S
23R	29	2100	565.80–575.40	9.6	0.14	1.5	
24R	29	2140	575.40–585.00	9.6	0.47	4.9	
25R	29	2225	585.00–594.60	9.6	0.20	2.1	
26R	29	2315	594.60–604.20	9.6	0.33	3.4	
Coring totals:				250.6	76.72	30.6	
Drilled total:				353.6			
Total:				604.2			

Note: UTC = Universal Time Coordinated.

Table T2. Datum levels used for the calculation of the Site 1129 sedimentation rate.

Datum type	Datum level	Age (Ma)	Midpoint (mbsf)	Stratigraphic error (m)	Fossil group	Upper sample		Lower sample	
						Core, section, interval (cm)	Depth (mbsf)	Core, section, interval (cm)	Depth (mbsf)
						182-1129C-		182-1129C-	
T	*P. lacunosa*	0.45	163.99	4.90	1	17H-CC, 13-16	159.05	18H-CC, 8-12	168.85
	Brunhes/Matuyama	0.78	343.00	4.20		37X-3			
T	*G. tosaensis*	0.65	341.68	5.82	4	36X-CC, 27-30	335.83	37X-CC, 24-27	347.47
B	*G. truncatulinoides*	2	423.47	9.47	4	45X-CC, 6-9	413.86	46X-CC, 53-56	432.93
						182-1129D-		182-1129D-	
	Top of Jaramillo	0.99	397.75	4.85		5R	392	6R	402
	Bottom of Jaramillo	1.07	440.80	8.90		9R	435	10R	445
	Top of Olduvai	1.77	540.38	0.67		20R-3			
B	*G. crassaformis*	4.5	556.19	1.49	4	21R-CC, 31-34	554.70	22R-CC, 16-18	557.68
B	*G. puncticulata*	4.5	556.19	1.49	4	21R-CC, 31-34	554.70	22R-CC, 16-18	557.68
T	*S. heteromorphus*	13.6	556.19	1.49	1	21R-CC, 31-34	554.70	22R-CC, 16-18	557.68

Notes: T = top of taxon stratigraphic range, B = bottom of taxon stratigraphic range. Midpoint = the middle depth between the sample where the taxon occurs and the adjacent sample where it does not occur. Stratigraphic error = one-half the distance between these two samples. Fossil groups = calcareous nannofossils (1) and planktonic foraminifers (4).

Table T3. Composition of vacutainer gases, Hole 1129C.

Core, section	Depth (mbsf)	CO_2 (ppmv)	H_2S (ppmv)	C_1 (ppmv)	C_2 (ppmv)	C_3 (ppmv)	*i*-C_4 (ppmv)	*n*-C_4 (ppmv)	*i*-C_5 (ppmv)	C_1/C_2
182-1129C-										
7H-6	62.25	9,095	927	313						
34X-3	313.90		134,852	147,503	369	66	25	11	21	400
35X-4	324.80		98,540	159,724	382	68	28	13	22	418
36X-3	332.60	326,737	77,666	159,991	389	67	28	16	24	411
37X-2	340.00		105,475	244,598	618	100	37	20	28	396
38X-1	347.97		127,480	140,016	331	65	26	16	25	423
39X-3	359.40	99,608	25,230	19,344	29	9				669
40X-1	366.31		136,577	173,591	404	75	30	19	28	430

Table T4. Composition of headspace gas in sediment, Site 1129.

Core, section	Depth (mbsf)	CO_2 (ppmv)	H_2S (ppmv)	C_1 (ppmv)	C_2 (ppmv)	C_3 (ppmv)	*i*-C_4 (ppmv)	*n*-C_4 (ppmv)	i-C_5 (ppmv)	*n*-C_5 (ppmv)	n-C_6 (ppmv)	*i*-C_6 (ppmv)	C_1/C_2
182-1129B-													
1H-6	29.50	NA	NA	2			NA	NA	NA	NA	NA	NA	
182-1129C-													
1H-4	4.50	NA	NA	3			NA	NA	NA	NA	NA	NA	
2H-4	11.80	NA	NA	2			NA	NA	NA	NA	NA	NA	
3H-4	21.30	NA	NA	2			NA	NA	NA	NA	NA	NA	
4H-4	30.80	NA	NA	2			NA	NA	NA	NA	NA	NA	
5H-4	40.30	NA	NA	6			NA	NA	NA	NA	NA	NA	
6H-4	49.80	8,350		65	2								40
7H-4	59.30	6,677		122	3								49
8H-4	68.80	19,888	1,863	208	4								55
9H-4	78.30	17,816	736	271	5								60
10H-4	87.80	22,027	1,839	314	5								67
11H-4	97.30	24,730	2,791	331	4	1							75
12H-4	106.80	34,238	5,039	637	8								85
13H-4	116.30	26,275	1,688	595	7								89
14H-4	125.80	39,351	4,924	662	7	2							91
15H-4	135.30	64,058	4,133	1,368	15	4							94
16H-4	144.80	45,101	3,346	845	9	2							94
17H-4	154.30	44,490	3,934	1,081	10	3							108
18H-4	163.80	82,676	6,682	2,643	26	8			6				102
19H-4	173.30	57,004	6,527	1,949	15	5							127
20H-4	182.80	11,610	524	1,927	14	4							136
22H-4	201.80	47,186	4,732	1,535	9	3							169
25X-3	228.70	149,812	17,355	6,196	20	6							316
26X-3	238.20	139,830	19,505	9,363	27	8							348
27X-4	249.20	192,587	27,019	9,088	25	8							368
28X-4	258.90	170,364	27,218	12,043	29	9							417
29X-4	268.40	181,259	29,801	6,093	14	5							429
30X-4	277.80	163,853	28,905	8,066	18	6							451
33X-4	305.50	176,658	24,972	6,070	13	5							474
34X-4	314.90	145,993	31,680	7,113	14	6							501
35X-4	324.30	163,143	40,445	8,922	20	10			6				440
36X-4	333.60	69,562	4,779	5,475	11	5							485
37X-4	342.50	125,862	12,322	8,928	17	6							519
38X-2	348.40	125,733	22,957	7,027	14	7			4				513
39X-2	357.20	NA	NA	7,889	17	9		NA	NA	NA			456
40X-3	368.00	104,853	20,525	6,576	14	7			5				484
41X-1	374.50	120,686	22,253	8,817	19	10			8				474
43X-2	394.90	7,741	257	11,267	21	9				5			534
44X-1	403.60			3,600	9	4			5				387
45X-1	413.30	2,328		8,256	17	9			5				500
46X-4	427.40	9,202		9,080	15	8							605
47X-1	432.40	2,837		2,291	6	5							402
48X-2	443.50	6,351		8,666	17	10			6				516
182-1129D-													
1R-1	280.00	91,583	1,317	11,167	24	8			5				458
2R-1	289.80	81,005	8,785	9,360	19	7							488
3R-1	373.61	4,987		4,249	8	5							506
10R-2	441.78	4,785		6,132	12	7			6				533
11R-2	451.80	6,112		8,400	17	10	17	14	12	6			506
12R-1	460.49	2,363		7,897	14	7	9	10	7	5	15	8	572
13R-4	474.00	2,675		6,638	13	8			9				523
14R-2	480.60	4,831		6,697	15	11	7		10				438
15R-2	490.20	28,512		6,098	12	6			6				526
16R-4	502.80	19,717		4,412	10	6			8				437
17R-3	510.90	7,149		2,790	6	3							465
18R-2	519.05	19,088	276	1,984	5	3							413
19R-2	528.60	24,920		1,875	5	3			4		46	5	354
20R-4	541.30	22,957		1,366	4	1							379
21R-4	550.83	27,470		1,318	6	3							235
22R-1	556.10	31,469		1,000	4	1							278
23R-CC	565.80	19,532		523	2								262
24R-1	575.40	9,355		235	2								157

Note: NA = not analyzed, blank = not detected.

Table T5. Calcium carbonate ($CaCO_3$), organic carbon (C_{org}), nitrogen (N), and sulfur (S) data, Holes 1129C and 1129D.

Core, section, interval (cm)	Depth (mbsf)	$CaCO_3$ (wt%)	C_{org} (wt%)	N (wt%)	S (wt%)
182-1129C-					
1H-1, 60-61	0.60	89.6	NA	NA	NA
1H-3, 60-61	3.60	90.5	0.53	0.05	
1H-5, 60-61	6.60	93.3	NA	NA	NA
2H-1, 60-61	7.90	92.1	NA	NA	NA
2H-3, 60-61	10.90	93.7	0.33		
2H-5, 60-61	13.90	93.3	NA	NA	NA
3H-1, 60-61	17.40	93.0	NA	NA	NA
3H-3, 60-61	20.40	92.7	0.50	0.04	
3H-5, 60-61	23.40	91.9	NA	NA	NA
4H-1, 60-61	26.90	92.7	NA	NA	NA
4H-3, 60-61	29.90	91.6	0.32		
4H-5, 60-61	32.90	90.6	NA	NA	NA
5H-1, 60-61	36.40	90.1	NA	NA	NA
5H-3, 60-61	39.40	90.5	0.42		
5H-5, 60-61	42.40	93.3	NA	NA	NA
6H-1, 94-95	46.24	92.9	NA	NA	NA
6H-3, 60-61	48.90	92.3	0.64	0.05	
6H-5, 60-61	51.90	93.2	NA	NA	NA
7H-2, 60-61	56.90	93.4	NA	NA	NA
7H-3, 60-61	58.40	93.4	0.51	0.04	
7H-5, 60-61	61.40	93.1	NA	NA	NA
8H-1, 60-61	64.90	91.0	NA	NA	NA
8H-3, 60-61	67.90	92.0	0.60	0.05	
8H-5, 60-61	70.90	92.6	NA	NA	NA
9H-1, 60-61	74.40	92.9	NA	NA	NA
9H-3, 60-61	77.40	93.2	0.60		
9H-5, 60-61	80.40	93.3	NA	NA	NA
10H-1, 60-61	83.90	93.7	NA	NA	NA
10H-3, 60-61	86.90	92.5	0.53	0.05	
10H-5, 60-61	89.90	91.3	NA	NA	NA
11H-3, 60-61	96.40	94.6	0.62	0.04	
11H-5, 60-61	99.40	93.5	NA	NA	NA
12H-1, 60-61	102.90	94.2	NA	NA	NA
12H-3, 60-61	105.90	92.5	0.58		
12H-5, 60-61	108.90	91.8	NA	NA	NA
13H-1, 60-61	112.40	93.4	NA	NA	NA
13H-3, 60-61	115.40	93.6	0.48	0.05	
13H-5, 60-61	118.40	94.0	NA	NA	NA
14H-1, 60-61	121.90	92.7	NA	NA	NA
14H-3, 60-61	124.90	94.7	0.45	0.05	
14H-5, 60-61	127.90	93.6	NA	NA	NA
15H-1, 60-61	131.40	93.9	NA	NA	NA
15H-3, 60-61	134.40	92.8	0.69	0.04	
15H-5, 60-61	137.40	92.6	NA	NA	NA
16H-1, 60-61	140.90	94.5	NA	NA	NA
16H-3, 60-61	143.90	93.1	0.71	0.06	
16H-5, 60-61	146.90	92.8	NA	NA	NA
17H-1, 60-61	150.40	95.2	NA	NA	NA
17H-3, 60-61	153.40	93.7	0.59		
17H-5, 60-61	156.40	93.7	NA	NA	NA
18H-1, 60-61	159.90	94.0	NA	NA	NA
18H-3, 60-61	162.90	93.7	0.76	0.08	
18H-5, 60-61	165.90	93.0	NA	NA	NA
19H-1, 60-61	169.40	94.1	NA	NA	NA
19H-3, 60-61	172.40	94.0	0.50		
19H-5, 60-61	175.40	93.3	NA	NA	NA
20H-1, 60-61	178.90	94.5	NA	NA	NA
20H-3, 60-61	181.90	93.0	0.46		
20H-5, 60-61	184.90	92.5	NA	NA	NA
21H-1, 58-59	188.38	93.4	NA	NA	NA
21H-3, 60-61	191.40	93.2	0.41		
22H-1, 60-61	197.90	91.3	NA	NA	NA
22H-3, 60-61	200.90	89.7	0.51		
22H-5, 60-61	203.90	94.0	NA	NA	NA
23H-1, 60-61	207.40	94.0	NA	NA	NA
23H-3, 60-61	210.10	93.8	0.41	0.04	
23H-5, 65-66	212.13	93.6	NA	NA	NA

Table T5 (continued).

Core, section, interval (cm)	Depth (mbsf)	$CaCO_3$ (wt%)	C_{org} (wt%)	N (wt%)	S (wt%)
25X-1, 60-61	226.30	92.8	NA	NA	NA
25X-3, 60-61	229.30	89.2	0.70	0.06	
26X-1, 60-61	235.80	93.1	NA	NA	NA
26X-3, 60-61	238.80	93.0	0.66	0.04	
27X-1, 60-61	245.30	91.0	NA	NA	NA
27X-3, 60-61	248.30	89.7	0.71	0.05	
27X-5, 60-61	251.30	87.7	NA	NA	NA
28X-1, 60-61	255.00	84.2	NA	NA	NA
28X-3, 60-61	258.00	91.8	0.49		
28X-5, 60-61	261.00	91.8	NA	NA	NA
29X-1, 60-61	264.50	94.6	NA	NA	NA
29X-3, 60-61	267.50	92.8	0.49	0.07	
29X-5, 60-61	270.50	91.5	NA	NA	NA
30X-1, 60-61	273.90	90.4	NA	NA	NA
30X-3, 60-61	276.90	88.7	0.38		
30X-5, 60-61	279.90	91.1	NA	NA	NA
33X-1, 60-61	301.60	92.1	NA	NA	NA
33X-3, 60-61	304.60	94.2	0.47	0.04	
33X-5, 60-61	307.60	90.1	NA	NA	NA
34X-1, 60-61	311.00	92.2	NA	NA	NA
34X-3, 60-61	314.00	91.4	0.55		
34X-5, 60-61	317.00	90.9	NA	NA	NA
35X-1, 60-61	320.40	90.5	NA	NA	NA
35X-3, 60-61	323.40	93.6	0.55	0.05	
35X-5, 60-61	326.40	94.7	NA	NA	NA
36X-1, 60-61	329.70	91.9	NA	NA	NA
36X-3, 60-61	332.70	91.8	0.62	0.05	
37X-1, 60-61	338.60	98.3	NA	NA	NA
37X-3, 60-61	341.60	87.7	0.27		
37X-5, 60-61	344.60	92.4	NA	NA	NA
38X-1, 60-61	347.50	92.9	NA	NA	NA
38X-3, 60-61	350.50	92.7	0.76	0.07	
39X-1, 60-61	356.30	93.1	NA	NA	NA
39X-3, 60-61	359.30	90.8	0.48	0.05	
40X-1, 60-61	365.60	91.5	NA	NA	NA
40X-3, 60-61	368.60	92.5	0.54	0.06	
43X-1, 60-61	394.50	93.8	0.29	0.06	
46X-1, 60-61	423.50	90.4	NA	NA	NA
46X-3, 60-61	426.50	86.3	0.61	0.04	
46X-5, 60-61	429.50	90.2	NA	NA	NA
47X-1, 60-61	433.00	74.5	1.46	0.12	
48X-1, 60-61	442.60	87.4	0.74	0.07	
182-1129D-					
13R-1, 60-61	470.10	90.3	0.44	0.05	
13R-3, 60-61	473.10	89.5	0.27	0.05	
13R-5, 60-61	476.10	82.9	0.40		0.10
16R-1, 60-61	498.90	88.0	0.57	0.13	
16R-3, 60-61	501.90	90.0	0.52	0.05	
16R-5, 60-61	504.90	86.7	0.26		
17R-1, 60-61	508.50	86.5	0.29		0.11
17R-3, 60-61	511.50	91.1	0.51	0.05	0.17
18R-1, 60-61	518.10	89.0	0.29		
18R-3, 60-61	521.10	91.3	0.53	0.15	
19R-1, 60-61	527.70	90.5	0.65	0.04	
19R-3, 60-61	530.70	85.7	0.83	0.05	
19R-5, 59-60	533.19	87.4	0.47	0.04	0.10
29R-1, 60-61	537.40	93.1	0.44		
20R-3, 66-67	540.46	92.5	0.19		
20R-5, 60-61	543.37	94.9	0.15		
21R-1, 35-36	546.85	91.0	0.39	0.04	0.08
21R-3, 60-63	549.96	89.8	0.45		
21R-5, 49-50	552.82	84.4	0.61	0.04	

Note: NA = not analyzed, blank = not detected.

Table T6. Rock-Eval pyrolysis data for selected samples, Sites 1127, 1129, 1131, and 1132.

Core, section, interval (cm)	T_{max} (°C)	S_1 (mg HC/g)	S_2 (mg HC/g)	S_3 (mg HC/g)	TOC (wt%)	HI (mg HC/g)	OI (mg CO_2/g TOC)
182-1127B-							
4H-5, 49-50	424	0.17	1.65	2.11	0.37	445	570
11H-5, 49-50	427	0.09	1.67	2.63	0.56	298	469
18X-3, 49-50	420	0.25	2.26	2.34	0.48	470	487
29X-1, 49-50	428	0.15	1.59	2.24	0.45	353	497
30X-3, 49-50	420	0.19	1.74	2.01	0.45	386	446
33X-1, 49-50	421	0.07	1.04	1.63	0.32	325	509
38X-3, 49-50	420	0.12	1.03	1.53	0.42	245	364
182-1129C-							
16H-3, 60-61	413	0.04	0.59	1.38	0.34	173	405
34X-3, 60-61	411	0.06	0.73	0.83	0.37	197	224
38X-3, 60-61	417	0.14	1.90	1.00	0.43	441	232
47X-1, 60-61	418	0.30	3.10	2.46	1.03	300	238
48X-1, 60-61	420	0.12	1.31	1.00	0.29	451	344
182-1131A-							
2H-3, 60-61	414	0.12	0.84	2.20	0.35	240	628
21X-3, 60-61	412	0.02	0.36	1.14	0.39	92	292
37X-3, 60-61	412	0.05	0.56	0.86	0.35	160	245
42X-3, 60-61	413	0.13	0.95	1.36	0.68	139	200
50X-3, 60-61	417	0.07	0.79	1.17	0.43	183	272
57X-1, 59-61	416	0.05	0.83	1.14	0.50	166	228
182-1132B-							
8H-1, 60-61	418	0.06	0.72	1.56	0.41	175	380

Table T7. Interstitial water geochemistry, Site 1129.

Core, section, interval (cm)	Depth (mbsf)	pH	ppH	Alkalinity (mM)	Salinity	Cl^- (mM)	SO_4^{2-} (mM)	Na^+ (mM)	K^+ (mM)	Mg^{2+} (mM)	Ca^{2+} (mM)	Sr^{2+} (μM)	Li^+ (μM)	$H_4SiO_4^0$ (μM)	NH_4^+ (mM)	Fe^{2+} (μM)
182-1129B-																
1H-5, 145-150	29.45	7.50	7.770		36.0	567.7	29.5	487.3	11.5	56.9	11.5	89.3	31	55.3	0.5	1.0
182-1129C-																
1H-3, 145-150	4.45	7.48	7.530	3.42	35.5	562.7	28.8	480.7	11.5	56.4	11.1	86	32	103.6	0.5	0.6
2H-3, 145-150	11.75	7.48	7.687	2.77	35.5	571.5	29.0	482.5	11.3	56.8	11.7	86	31	56.1	0.3	0.0
3H-3, 145-150	21.25	7.46	7.700	2.78	35.5	565.7	29.5	486.5	11.5	56.5	11.2	89	31	26.2	0.3	0.0
4H-3, 145-150	30.75	7.48	7.675	2.91	35.5	565.7	29.1	487.2	11.3	56.7	11.3	95	32	41.1	0.3	0.6
5H-3, 145-150	40.25	7.38	7.500	4.14	35.5	571.6	29.2	486.3	11.5	56.8	10.8	95	33	74.1	0.9	6.3
6H-3, 140-150	49.70	6.82	6.850	21.70	39.0	614.1	30.6	537.2	11.8	49.7	8.6	297	68	396.4	4.2	0.2
7H-3, 140-150	59.20	6.72	6.732	33.65	41.5	647.8	31.7	590.3	12.2	44.0	8.3	391	94	619.9	7.0	0.2
8H-3, 140-150	68.70	6.72	6.670	36.97	43.5	676.4	33.3	623.9	12.4	42.8	7.9	486	109	627.2	8.7	0.1
9H-3, 140-150	78.20	6.67	6.560	37.58	44.0	688.3	34.6	642.5	12.6	41.2	7.4	497	114	746.6	9.7	0.5
10H-3, 140-150	87.70	6.69	6.560	39.60	45.0	705.1	34.0	657.7	12.7	39.7	7.2	520	118	542.1	10.6	2.3
11H-3, 140-150	97.20	6.67	6.550	44.25	46.0	717.0	33.5	687.7	12.9	35.0	6.5	520	115	604.2	11.9	3.1
12H-3, 140-150	106.70	6.60	6.496	48.46	47.0	729.8	33.5	716.2	13.0	31.7	5.8	489	116	595.7	13.4	1.4
13H-3, 140-150	116.20	6.74	6.595	49.97	47.5	737.8	33.0	722.5	13.0	28.8	6.0	478	119	679.2	14.4	0.0
14H-3, 140-150	125.70	6.57	6.500	55.44	48.0	751.6	33.8	750.4	13.1	25.6	5.2	467	110	716.9	15.5	0.0
15H-3, 140-150	135.20	6.60	6.500	62.74	50.0	730.8	33.2	767.6	13.3	23.5	4.8	387	116	689.4	16.7	0.0
17H-3, 140-150	154.20	6.56	6.480	77.41	52.0	810.9	30.2	824.7	13.4	16.9	4.0	482	116	827.2	18.7	0.0
19H-3, 140-150	173.20	6.67	6.520	85.96	55.0	845.5	26.2	871.0	13.6	15.7	3.9	434	116	766.6	20.8	0.0
22H-3, 140-150	201.70	6.52	6.410	95.65	58.0	909.8	19.1	921.9	13.6	14.6	3.9	550	121	893.7	24.8	0.0
25X-2, 140-150	228.60	6.46	6.390	97.28	62.0	981.0	11.4	978.1	14.1	15.1	3.8	788	145	908.9	26.0	0.0
27X-3, 140-150	249.10	6.41	6.388	93.84	65.0	1039.4	10.6	1021.7	14.6	16.8	4.1	1062	168	920.7	26.4	0.0
29X-3, 140-150	268.30	6.41	6.320	82.61	65.0	1069.0	2.2	1042.5	14.8	19.9	4.9	1401	190	916.0	25.8	0.0
33X-3, 140-150	305.40	6.27	6.290	74.18	71.5	1151.1	10.9	1103.4	16.0	23.8	6.2	2003	211	970.6	26.7	0.0
35X-3, 140-150	324.20	6.14	6.260	69.30	70.0	1154.1	12.6	1083.5	16.3	29.1	8.4	1810	224	940.5	25.0	0.0
37X-3, 140-150	342.40	6.16	NM	60.75	72.0	1198.6	13.3	1108.6	17.1	34.1	9.5	1483	221	1005.4	25.3	0.0
39X-3, 140-150	358.60	6.10	NM	56.18	75.0	1265.8	14.2	1147.1	17.8	40.4	11.6	1237	227	1030.5	25.6	0.0
43X-3, 90-100	394.80	6.05	NM	42.07	77.0	1272.8	21.9	1133.7	18.3	54.4	18.1	818	216	1010.2	21.8	5.4
46X-3, 140-150	427.30	5.90	NM	32.27	88.0	1454.7	32.4	1281.8	24.8	78.6	35.1	636	233	1083.2	16.2	0.8
48X-3, 140-150	443.40	6.01	NM	29.51	85.0	1404.3	34.9	1202.6	21.4	78.5	37.2	554	213	1034.6	13.9	0.0
182-1129D-																
10R-1, 100-108	441.70	5.97	NM	24.55	86.0	1421.1	34.4	1200.8	21.9	80.4	37.3	510.0	233	1113.5	10.1	0.0
12R-1, 60-70	460.50	5.90	NM	23.36	86.0	1409.2	37.6	1195.5	21.9	82.4	41.0	435.0	209	1044.2	9.4	27.3
14R-1, 140-150	480.50	5.93	NM	20.74	88.0	1440.9	41.0	1221.9	22.2	85.8	45.7	413.0	207	1067.3	8.6	0.0
17R-2, 140-150	510.80	NM	NM	NM	88.0	1417.2	44.1	1207.5	23.2	88.8	48.7	345.0	174	943.5	6.8	0.0
20R-3, 140-150	541.20	6.06	NM	15.38	90.0	1467.6	49.0	1235.9	23.2	92.8	55.6	331.0	160	1012.8	5.3	2.4

Note: NM = not measured.

Table T8. Summary of X-ray diffraction analysis, Site 1129. (See table note. Continued on next page.)

Leg	Site	Hole	Core	Type	Section	Top (cm)	Bottom (cm)	Depth (mbsf)	Aragonite (wt%)	Quartz (%)	LMC (wt%)	HMC (wt%)	Dolomite (wt%)
182	1129	C	1	H	1	60	61	0.60	20	1	30	49	0
182	1129	C	1	H	3	60	61	3.60	13	1	20	66	0
182	1129	C	1	H	5	60	61	6.60	22	0	27	51	0
182	1129	C	2	H	1	60	61	7.90	17	0	31	51	0
182	1129	C	2	H	3	60	61	10.90	19	0	27	55	0
182	1129	C	2	H	5	60	61	13.90	9	0	12	79	0
182	1129	C	3	H	1	60	61	17.40	31	1	7	61	0
182	1129	C	3	H	3	60	61	20.40	20	2	28	50	0
182	1129	C	3	H	5	60	61	23.40	17	1	28	54	0
182	1129	C	4	H	1	60	61	26.90	18	1	23	59	0
182	1129	C	4	H	3	60	61	29.90	19	2	18	62	0
182	1129	C	4	H	5	60	61	32.90	15	1	30	54	0
182	1129	C	5	H	1	60	61	36.40	23	4	35	37	0
182	1129	C	5	H	3	60	61	39.40	20	3	45	32	0
182	1129	C	5	H	5	60	61	42.40	18	1	24	58	0
182	1129	C	6	H	1	94	95	46.24	14	0	24	62	0
182	1129	C	6	H	3	60	61	48.90	20	0	25	55	0
182	1129	C	6	H	5	60	61	51.90	15	0	34	51	0
182	1129	C	7	H	2	60	61	56.90	16	0	27	55	1
182	1129	C	7	H	3	60	61	58.40	17	1	27	54	2
182	1129	C	7	H	5	60	61	61.40	17	0	22	59	2
182	1129	C	8	H	1	60	61	64.90	22	1	16	57	4
182	1129	C	8	H	3	60	61	67.90	17	1	36	42	4
182	1129	C	8	H	5	60	61	70.90	14	3	38	39	5
182	1129	C	9	H	1	60	61	74.40	17	0	46	32	5
182	1129	C	9	H	3	60	61	77.40	19	0	42	36	3
182	1129	C	9	H	5	60	61	80.40	19	1	38	37	5
182	1129	C	10	H	1	60	61	83.90	11	1	41	44	3
182	1129	C	10	H	3	60	61	86.90	17	0	54	24	5
182	1129	C	10	H	5	60	61	89.90	17	1	24	54	5
182	1129	C	11	H	3	60	61	96.40	17	0	57	15	11
182	1129	C	11	H	5	60	61	99.40	19	1	60	17	3
182	1129	C	12	H	1	60	61	102.90	13	0	53	29	5
182	1129	C	12	H	3	60	61	105.90	12	1	53	30	5
182	1129	C	12	H	5	60	61	108.90	16	0	30	52	1
182	1129	C	13	H	1	60	61	112.40	18	1	47	31	4
182	1129	C	13	H	3	60	61	115.40	19	3	53	18	6
182	1129	C	13	H	5	60	61	118.40	16	1	70	0	13
182	1129	C	14	H	1	60	61	121.90	9	1	82	0	8
182	1129	C	14	H	3	60	61	124.90	15	0	55	20	10
182	1129	C	14	H	5	60	61	127.90	13	0	27	57	2
182	1129	C	15	H	1	60	61	131.40	10	0	49	37	4
182	1129	C	15	H	3	60	61	134.40	12	0	47	39	2
182	1129	C	15	H	5	60	61	137.40	15	0	57	21	7
182	1129	C	16	H	1	60	61	140.90	13	1	54	22	10
182	1129	C	16	H	3	60	61	143.90	15	0	63	15	6
182	1129	C	16	H	5	60	61	146.90	15	1	24	59	2
182	1129	C	17	H	1	60	61	150.40	7	1	74	0	18
182	1129	C	17	H	3	60	61	153.40	7	1	79	0	14
182	1129	C	17	H	5	60	61	156.40	5	1	77	0	17
182	1129	C	18	H	1	60	61	159.90	10	1	79	0	11
182	1129	C	18	H	3	60	61	162.90	18	2	69	0	11
182	1129	C	18	H	5	60	61	165.90	18	1	68	0	12
182	1129	C	19	H	1	60	61	169.40	11	1	69	0	19
182	1129	C	19	H	3	60	61	172.40	18	0	71	0	11
182	1129	C	19	H	5	60	61	175.40	15	1	76	0	9
182	1129	C	20	H	1	60	61	178.90	7	1	75	0	17
182	1129	C	20	H	3	60	61	181.90	6	3	77	0	14
182	1129	C	20	H	5	60	61	184.90	6	12	70	0	11
182	1129	C	21	H	1	58	59	188.38	6	1	77	0	17
182	1129	C	21	H	3	60	61	191.40	8	1	75	0	16
182	1129	C	22	H	1	60	61	197.90	7	4	78	0	11
182	1129	C	22	H	3	60	61	200.90	5	5	80	0	10
182	1129	C	22	H	5	60	61	203.90	7	1	68	0	24
182	1129	C	23	H	1	60	61	207.40	10	2	72	0	15
182	1129	C	23	H	3	60	61	210.10	5	4	75	0	16
182	1129	C	23	H	5	65	66	212.13	5	1	80	0	14
182	1129	C	25	X	1	60	61	226.30	4	1	81	0	15

Table T8 (continued).

Leg	Site	Hole	Core	Type	Section	Top (cm)	Bottom (cm)	Depth (mbsf)	Aragonite (wt%)	Quartz (%)	LMC (wt%)	HMC (wt%)	Dolomite (wt%)
182	1129	C	25	X	3	60	61	229.30	5	1	83	0	11
182	1129	C	26	X	1	60	61	235.80	7	0	76	0	16
182	1129	C	26	X	3	60	61	238.80	7	1	81	0	11
182	1129	C	27	X	1	60	61	245.30	5	0	78	0	16
182	1129	C	27	X	3	60	61	248.30	7	1	81	0	10
182	1129	C	27	X	5	60	61	251.30	5	2	79	0	14
182	1129	C	28	X	1	60	61	255.00	13	5	78	0	5
182	1129	C	28	X	3	60	61	258.00	8	1	78	0	12
182	1129	C	28	X	5	60	61	261.00	17	1	78	0	4
182	1129	C	29	X	3	60	61	267.50	7	0	83	0	10
182	1129	C	29	X	5	60	61	270.50	7	0	83	0	10
182	1129	C	30	X	1	60	61	273.90	6	1	84	0	9
182	1129	C	30	X	3	60	61	276.90	4	1	84	0	12
182	1129	C	30	X	5	60	61	279.90	7	1	82	0	10
182	1129	C	33	X	1	60	61	301.60	5	1	82	0	11
182	1129	C	33	X	3	60	61	304.60	5	1	80	0	14
182	1129	C	33	X	5	60	61	307.60	4	5	81	0	10
182	1129	C	34	X	1	60	61	311.00	4	1	84	0	11
182	1129	C	34	X	3	60	61	314.00	4	1	82	0	13
182	1129	C	34	X	5	60	61	317.00	3	4	81	0	13
182	1129	C	35	X	1	60	61	320.40	5	2	84	0	9
182	1129	C	35	X	3	60	61	323.40	3	0	83	0	13
182	1129	C	35	X	5	60	61	326.40	2	2	81	0	15
182	1129	C	36	X	1	60	61	329.70	5	2	81	0	11
182	1129	C	36	X	3	60	61	332.70	3	1	85	0	11
182	1129	C	37	X	1	60	61	338.60	2	1	86	0	11
182	1129	C	37	X	3	60	61	341.60	1	1	89	0	9
182	1129	C	37	X	5	60	61	344.60	1	1	81	0	18
182	1129	C	38	X	1	60	61	347.50	4	1	83	0	12
182	1129	C	38	X	3	60	61	350.50	4	0	77	0	19
182	1129	C	39	X	1	60	61	356.30	11	1	85	0	3
182	1129	C	39	X	3	60	61	359.30	0	3	81	0	15
182	1129	C	40	X	1	60	61	365.60	4	1	85	0	11
182	1129	C	40	X	3	60	61	368.60	2	1	92	0	5
182	1129	C	43	X	1	60	61	394.50	1	1	85	0	13
182	1129	C	46	X	1	60	61	423.50	1	2	91	0	6
182	1129	C	46	X	3	60	61	426.50	0	3	85	0	11
182	1129	C	46	X	5	60	61	429.50	0	2	83	0	15
182	1129	C	47	X	1	60	61	433.00	23	10	65	0	2
182	1129	C	48	X	1	60	61	442.60	0	1	84	0	15
182	1129	D	13	R	1	60	61	470.10	2	1	92	0	4
182	1129	D	13	R	3	60	61	473.10	1	1	92	0	6
182	1129	D	13	R	5	60	61	476.10	0	2	88	0	10
182	1129	D	16	R	1	60	61	498.90	3	1	86	0	9
182	1129	D	16	R	3	60	61	501.90	3	1	91	0	5
182	1129	D	16	R	5	60	61	504.90	0	1	77	0	23
182	1129	D	17	R	1	60	61	508.50	0	1	92	0	7
182	1129	D	17	R	3	60	61	511.50	1	2	92	0	5
182	1129	D	18	R	1	60	61	518.10	0	1	95	0	4
182	1129	D	18	R	3	60	61	521.10	4	1	87	0	8
182	1129	D	19	R	1	60	61	527.70	3	1	91	0	5
182	1129	D	19	R	3	60	61	530.70	3	1	81	0	15
182	1129	D	19	R	5	60	61	533.19	2	1	87	0	10
182	1129	D	20	R	1	60	61	537.40	1	0	95	0	4
182	1129	D	20	R	3	60	61	540.46	1	0	96	0	2
182	1129	D	20	R	5	60	61	543.37	0	0	65	0	35
182	1129	D	21	R	1	60	61	546.85	2	1	89	0	9
182	1129	D	21	R	3	60	61	549.96	2	1	89	0	7
182	1129	D	21	R	5	60	61	552.82	3	2	92	0	3

Note: This table is also available in **ASCII format.**

Table T9. *P*-wave velocity measurements from the multisensor track, Site 1129.

Leg	Site	Hole	Core	Type	Section	Interval (cm)	Depth (mbsf)	V_p (km/s)
182	1129	A	1	H	1	3.0	0.03	4.6141
182	1129	A	1	H	1	7.0	0.07	3.8628
182	1129	A	1	H	1	11.0	0.11	3.7893
182	1129	A	1	H	1	15.0	0.15	3.8445
182	1129	A	1	H	1	23.0	0.23	3.8166
182	1129	A	1	H	1	27.0	0.27	3.8433
182	1129	A	1	H	1	35.0	0.35	3.8443
182	1129	A	1	H	1	39.0	0.39	3.8198
182	1129	A	1	H	1	43.0	0.43	2.7994
182	1129	A	1	H	1	47.0	0.47	3.3136
182	1129	A	1	H	1	51.0	0.51	3.7921
182	1129	A	1	H	1	55.0	0.55	3.8358
182	1129	A	1	H	1	59.0	0.59	3.8213
182	1129	A	1	H	1	63.0	0.63	3.5429
182	1129	A	1	H	1	67.0	0.67	3.8018
182	1129	A	1	H	1	71.0	0.71	3.7864
182	1129	A	1	H	1	75.0	0.75	3.7821
182	1129	A	1	H	1	79.0	0.79	3.8195
182	1129	A	1	H	1	83.0	0.83	3.7886
182	1129	A	1	H	1	91.0	0.91	3.7965
182	1129	A	1	H	1	95.0	0.95	3.8119
182	1129	A	1	H	1	99.0	0.99	3.4805
182	1129	A	1	H	1	103.0	1.03	1.9521
182	1129	A	1	H	1	107.0	1.07	1.7811
182	1129	A	1	H	1	111.0	1.11	1.7608
182	1129	A	1	H	1	115.0	1.15	2.2614
182	1129	A	1	H	1	119.0	1.19	1.8184
182	1129	A	1	H	1	123.0	1.23	2.1443
182	1129	A	1	H	1	127.0	1.27	2.0256
182	1129	A	1	H	1	131.0	1.31	2.2186
182	1129	A	1	H	1	135.0	1.35	1.9510
182	1129	A	1	H	1	139.0	1.39	1.9876
182	1129	A	1	H	1	143.0	1.43	2.6245
182	1129	A	1	H	1	147.0	1.47	3.9140
182	1129	A	1	H	2	7.0	1.57	3.8752
182	1129	A	1	H	2	11.0	1.61	3.8456
182	1129	A	1	H	2	15.0	1.65	3.8321
182	1129	A	1	H	2	19.0	1.69	3.8692
182	1129	A	1	H	2	23.0	1.73	3.8198
182	1129	A	1	H	2	27.0	1.77	3.8264
182	1129	A	1	H	2	31.0	1.81	3.8386
182	1129	A	1	H	2	35.0	1.85	3.8297
182	1129	A	1	H	2	39.0	1.89	3.8252
182	1129	A	1	H	2	43.0	1.93	3.8173
182	1129	A	1	H	2	47.0	1.97	3.7874
182	1129	A	1	H	2	51.0	2.01	3.7739
182	1129	A	1	H	2	55.0	2.05	3.7788
182	1129	A	1	H	2	59.0	2.09	3.7478
182	1129	A	1	H	2	63.0	2.13	3.7366
182	1129	A	1	H	2	67.0	2.17	2.4635
182	1129	A	1	H	2	71.0	2.21	3.7652
182	1129	A	1	H	2	75.0	2.25	3.7804
182	1129	A	1	H	2	79.0	2.29	3.7905
182	1129	A	1	H	2	83.0	2.33	3.7721
182	1129	A	1	H	2	87.0	2.37	3.6871
182	1129	A	1	H	2	91.0	2.41	3.6272
182	1129	A	1	H	2	95.0	2.45	3.7381
182	1129	A	1	H	2	99.0	2.49	3.7755
182	1129	A	1	H	2	103.0	2.53	3.7669
182	1129	A	1	H	2	107.0	2.57	3.8084
182	1129	A	1	H	2	115.0	2.65	3.7799
182	1129	A	1	H	2	119.0	2.69	3.7917
182	1129	A	1	H	2	123.0	2.73	3.6025
182	1129	A	1	H	2	127.0	2.77	3.7730

Note: Only a portion of this table appears here. The complete table is available in **ASCII format.**

Table T10. Gamma-ray attenuation densiometry measurements from the multisensor track, Site 1129.

Leg	Site	Hole	Core	Type	Section	Interval (cm)	Depth (mbsf)	Density (g/cm^3)	Corrected density (g/cm^3)
182	1129	A	1	H	1	3.0	0.03	1.78	1.72
182	1129	A	1	H	1	7.0	0.07	1.83	1.77
182	1129	A	1	H	1	11.0	0.11	1.84	1.78
182	1129	A	1	H	1	15.0	0.15	1.82	1.76
182	1129	A	1	H	1	19.0	0.19	1.84	1.78
182	1129	A	1	H	1	23.0	0.23	1.82	1.76
182	1129	A	1	H	1	27.0	0.27	1.80	1.74
182	1129	A	1	H	1	31.0	0.31	1.81	1.75
182	1129	A	1	H	1	35.0	0.35	1.80	1.74
182	1129	A	1	H	1	39.0	0.39	1.80	1.74
182	1129	A	1	H	1	43.0	0.43	1.80	1.74
182	1129	A	1	H	1	47.0	0.47	1.78	1.72
182	1129	A	1	H	1	51.0	0.51	1.81	1.75
182	1129	A	1	H	1	55.0	0.55	1.81	1.76
182	1129	A	1	H	1	59.0	0.59	1.86	1.80
182	1129	A	1	H	1	63.0	0.63	1.88	1.83
182	1129	A	1	H	1	67.0	0.67	1.93	1.88
182	1129	A	1	H	1	71.0	0.71	1.94	1.89
182	1129	A	1	H	1	75.0	0.75	1.99	1.94
182	1129	A	1	H	1	79.0	0.79	2.06	2.02
182	1129	A	1	H	1	83.0	0.83	2.05	2.01
182	1129	A	1	H	1	87.0	0.87	2.06	2.02
182	1129	A	1	H	1	91.0	0.91	2.09	2.05
182	1129	A	1	H	1	95.0	0.95	2.07	2.03
182	1129	A	1	H	1	99.0	0.99	2.01	1.97
182	1129	A	1	H	1	103.0	1.03	1.72	1.66
182	1129	A	1	H	1	107.0	1.07	1.72	1.65
182	1129	A	1	H	1	111.0	1.11	1.74	1.68
182	1129	A	1	H	1	115.0	1.15	1.75	1.69
182	1129	A	1	H	1	119.0	1.19	1.77	1.71
182	1129	A	1	H	1	123.0	1.23	1.77	1.71
182	1129	A	1	H	1	127.0	1.27	1.81	1.75
182	1129	A	1	H	1	131.0	1.31	1.81	1.75
182	1129	A	1	H	1	135.0	1.35	1.80	1.74
182	1129	A	1	H	1	139.0	1.39	1.82	1.76
182	1129	A	1	H	1	143.0	1.43	1.83	1.77
182	1129	A	1	H	1	147.0	1.47	1.86	1.80
182	1129	A	1	H	2	3.0	1.53	1.90	1.85
182	1129	A	1	H	2	7.0	1.57	1.96	1.92
182	1129	A	1	H	2	11.0	1.61	1.90	1.85
182	1129	A	1	H	2	15.0	1.65	1.93	1.88
182	1129	A	1	H	2	19.0	1.69	2.00	1.95
182	1129	A	1	H	2	23.0	1.73	2.00	1.95
182	1129	A	1	H	2	27.0	1.77	1.89	1.84
182	1129	A	1	H	2	31.0	1.81	1.89	1.84
182	1129	A	1	H	2	35.0	1.85	1.91	1.86
182	1129	A	1	H	2	39.0	1.89	1.93	1.88
182	1129	A	1	H	2	43.0	1.93	1.87	1.81
182	1129	A	1	H	2	47.0	1.97	1.87	1.82
182	1129	A	1	H	2	51.0	2.01	1.86	1.80
182	1129	A	1	H	2	55.0	2.05	1.88	1.83
182	1129	A	1	H	2	59.0	2.09	1.97	1.93
182	1129	A	1	H	2	63.0	2.13	1.92	1.87
182	1129	A	1	H	2	67.0	2.17	1.86	1.80
182	1129	A	1	H	2	71.0	2.21	1.89	1.83
182	1129	A	1	H	2	75.0	2.25	1.91	1.86
182	1129	A	1	H	2	79.0	2.29	1.90	1.85
182	1129	A	1	H	2	83.0	2.33	1.93	1.88
182	1129	A	1	H	2	87.0	2.37	1.93	1.88
182	1129	A	1	H	2	91.0	2.41	1.95	1.90
182	1129	A	1	H	2	95.0	2.45	1.74	1.68
182	1129	A	1	H	2	99.0	2.49	1.79	1.73
182	1129	A	1	H	2	103.0	2.53	1.81	1.75

Note: Only a portion of this table appears here. The complete table is available in **ASCII format.**

Table T11. Magnetic susceptibility measurements from the multisensor track, Site 1129.

Leg	Site	Hole	Core	Type	Section	Interval (cm)	Depth (mbsf)	Magnetic susceptibility (10^{-6}; SI units)	Corrected susceptibility (10^{-6}; SI units)
182	1129	A	1	H	1	3.0	0.03	0.4	0.4
182	1129	A	1	H	1	11.0	0.11	0.3	0.3
182	1129	A	1	H	1	19.0	0.19	0.6	0.6
182	1129	A	1	H	1	27.0	0.27	–0.2	–0.2
182	1129	A	1	H	1	35.0	0.35	0.1	0.1
182	1129	A	1	H	1	43.0	0.43	–0.3	–0.3
182	1129	A	1	H	1	51.0	0.51	–0.1	–0.1
182	1129	A	1	H	1	59.0	0.59	–0.4	–0.4
182	1129	A	1	H	1	67.0	0.67	–0.7	–0.7
182	1129	A	1	H	1	75.0	0.75	–0.5	–0.5
182	1129	A	1	H	1	83.0	0.83	–0.8	–0.8
182	1129	A	1	H	1	91.0	0.91	0.2	0.2
182	1129	A	1	H	1	99.0	0.99	3.4	3.4
182	1129	A	1	H	1	107.0	1.07	–1.7	–1.7
182	1129	A	1	H	1	115.0	1.15	–1.6	–1.6
182	1129	A	1	H	1	123.0	1.23	–1.9	–1.9
182	1129	A	1	H	1	131.0	1.31	–2.5	–2.5
182	1129	A	1	H	1	139.0	1.39	–2.5	–2.5
182	1129	A	1	H	1	147.0	1.47	–2.2	–2.2
182	1129	A	1	H	2	3.0	1.53	–1.1	–1.1
182	1129	A	1	H	2	11.0	1.61	–1.0	–1.0
182	1129	A	1	H	2	19.0	1.69	0.2	0.2
182	1129	A	1	H	2	27.0	1.77	–1.8	–1.8
182	1129	A	1	H	2	35.0	1.85	–2.1	–2.1
182	1129	A	1	H	2	43.0	1.93	–2.4	–2.4
182	1129	A	1	H	2	51.0	2.01	–2.3	–2.3
182	1129	A	1	H	2	59.0	2.09	–2.4	–2.4
182	1129	A	1	H	2	67.0	2.17	–2.1	–2.1
182	1129	A	1	H	2	75.0	2.25	–1.9	–1.9
182	1129	A	1	H	2	83.0	2.33	–2.1	–2.1
182	1129	A	1	H	2	91.0	2.41	–2.0	–2.0
182	1129	A	1	H	2	99.0	2.49	–2.1	–2.1
182	1129	A	1	H	2	107.0	2.57	–2.2	–2.2
182	1129	A	1	H	2	115.0	2.65	–2.3	–2.3
182	1129	A	1	H	2	123.0	2.73	–2.3	–2.3
182	1129	A	1	H	2	131.0	2.81	–2.1	–2.1
182	1129	A	1	H	2	139.0	2.89	–2.1	–2.1
182	1129	A	1	H	2	147.0	2.97	–2.2	–2.2
182	1129	A	1	H	3	3.0	3.03	–0.5	–0.5
182	1129	A	1	H	3	11.0	3.11	–0.7	–0.7
182	1129	A	1	H	3	19.0	3.19	–0.2	–0.2
182	1129	A	1	H	3	27.0	3.27	–0.7	–0.7
182	1129	A	1	H	3	35.0	3.35	–0.9	–0.9
182	1129	A	1	H	3	43.0	3.43	–0.9	–0.9
182	1129	A	1	H	3	51.0	3.51	–1.2	–1.2
182	1129	A	1	H	3	59.0	3.59	–0.9	–0.9
182	1129	A	1	H	3	67.0	3.67	–0.9	–0.9
182	1129	A	1	H	3	75.0	3.75	–1.0	–1.0
182	1129	A	1	H	3	83.0	3.83	–1.0	–1.0
182	1129	A	1	H	3	91.0	3.91	–0.7	–0.7
182	1129	A	1	H	3	99.0	3.99	–0.9	–0.9
182	1129	A	1	H	3	107.0	4.07	–1.1	–1.1
182	1129	A	1	H	3	115.0	4.15	–0.4	–0.4
182	1129	A	1	H	3	123.0	4.23	–0.7	–0.7
182	1129	A	2	H	1	3.0	13.83	–1.0	–1.0
182	1129	A	2	H	1	11.0	13.91	–1.8	–1.8
182	1129	A	2	H	1	19.0	13.99	–1.3	–1.3
182	1129	A	2	H	1	27.0	14.07	–2.3	–2.3
182	1129	A	2	H	1	35.0	14.15	–2.0	–2.0
182	1129	A	2	H	1	43.0	14.23	–2.2	–2.2
182	1129	A	2	H	1	51.0	14.31	–2.0	–2.0
182	1129	A	2	H	1	59.0	14.39	–2.3	–2.3
182	1129	A	2	H	1	67.0	14.47	–2.4	–2.4

Note: Only a portion of this table appears here. The complete table is available in **ASCII format.**

Table T12. Natural gamma-ray measurements from the multisensor track, Site 1129.

Leg	Site	Hole	Core	Type	Section	Interval (cm)	Depth (mbsf)	NGR (cps)
182	1129	A	1	H	1	11.0	0.11	2.69
182	1129	A	1	H	1	27.0	0.27	1.89
182	1129	A	1	H	1	43.0	0.43	2.15
182	1129	A	1	H	1	59.0	0.59	2.35
182	1129	A	1	H	1	75.0	0.75	3.58
182	1129	A	1	H	1	91.0	0.91	3.73
182	1129	A	1	H	1	107.0	1.07	1.69
182	1129	A	1	H	1	123.0	1.23	2.23
182	1129	A	1	H	1	139.0	1.39	2.42
182	1129	A	1	H	2	11.0	1.61	4.23
182	1129	A	1	H	2	27.0	1.77	4.85
182	1129	A	1	H	2	43.0	1.93	3.85
182	1129	A	1	H	2	59.0	2.09	4.46
182	1129	A	1	H	2	75.0	2.25	3.00
182	1129	A	1	H	2	91.0	2.41	2.85
182	1129	A	1	H	2	107.0	2.57	1.12
182	1129	A	1	H	2	123.0	2.73	2.77
182	1129	A	1	H	2	139.0	2.89	1.77
182	1129	A	1	H	3	11.0	3.11	4.42
182	1129	A	1	H	3	27.0	3.27	3.69
182	1129	A	1	H	3	43.0	3.43	3.04
182	1129	A	1	H	3	59.0	3.59	2.50
182	1129	A	1	H	3	75.0	3.75	3.35
182	1129	A	1	H	3	91.0	3.91	3.15
182	1129	A	1	H	3	107.0	4.07	2.81
182	1129	A	1	H	CC	11.0	4.18	1.35
182	1129	A	1	H	CC	27.0	4.34	0.35
182	1129	A	1	H	CC	43.0	4.50	–1.15
182	1129	A	1	H	CC	59.0	4.66	–0.58
182	1129	A	1	H	CC	75.0	4.82	0.31
182	1129	A	1	H	CC	91.0	4.98	0.81
182	1129	A	1	H	CC	107.0	5.14	–0.85
182	1129	A	1	H	CC	123.0	5.30	0.04
182	1129	A	2	H	1	11.0	13.91	0.85
182	1129	A	2	H	1	27.0	14.07	1.54
182	1129	A	2	H	1	43.0	14.23	1.77
182	1129	A	2	H	1	59.0	14.39	2.08
182	1129	A	2	H	1	75.0	14.55	2.46
182	1129	A	2	H	1	91.0	14.71	0.96
182	1129	A	2	H	1	107.0	14.87	3.19
182	1129	A	2	H	1	123.0	15.03	1.69
182	1129	A	2	H	2	11.0	15.41	3.39
182	1129	A	2	H	2	27.0	15.57	2.85
182	1129	A	2	H	2	43.0	15.73	3.15
182	1129	A	2	H	2	59.0	15.89	1.73
182	1129	A	2	H	2	75.0	16.05	2.65
182	1129	A	2	H	2	91.0	16.21	1.69
182	1129	A	2	H	2	107.0	16.37	3.50
182	1129	A	2	H	2	123.0	16.53	5.08
182	1129	A	2	H	2	139.0	16.69	4.42
182	1129	A	2	H	3	11.0	16.91	6.89
182	1129	A	2	H	3	27.0	17.07	4.58
182	1129	A	2	H	3	43.0	17.23	3.62
182	1129	A	2	H	3	59.0	17.39	2.39
182	1129	A	2	H	3	75.0	17.55	4.81
182	1129	A	2	H	3	91.0	17.71	4.89
182	1129	A	2	H	3	107.0	17.87	5.39
182	1129	A	2	H	3	123.0	18.03	2.65
182	1129	A	2	H	3	139.0	18.19	6.46
182	1129	A	2	H	4	11.0	18.41	6.69
182	1129	A	2	H	4	27.0	18.57	5.00
182	1129	A	2	H	4	43.0	18.73	4.69
182	1129	A	2	H	4	59.0	18.89	5.73
182	1129	A	2	H	4	75.0	19.05	6.73

Notes: NGR = natural gamma radiation. Only a portion of this table appears here. The complete table is available in **ASCII format.**

Table T13. Thermal conductivity measurements, Site 1129.

Leg	Site	Hole	Core	Type	Section	Interval (cm)	Depth (mbsf)	Thermal conductivity (W/[m·K])
182	1129	C	1	H	3	75.0	3.75	0.937
182	1129	C	2	H	3	75.0	11.05	0.950
182	1129	C	3	H	3	75.0	20.55	0.902
182	1129	C	4	H	3	75.0	30.05	0.939
182	1129	C	5	H	3	40.0	39.20	0.920
182	1129	C	6	H	3	75.0	49.05	0.963
182	1129	C	7	H	3	75.0	58.55	0.809
182	1129	C	8	H	3	60.0	67.90	0.929
182	1129	C	9	H	3	80.0	77.60	0.960
182	1129	C	8	H	7	44.0	73.74	0.975
182	1129	C	9	H	1	66.0	74.46	0.991
182	1129	C	10	H	3	90.0	87.20	0.939
182	1129	C	10	H	6	89.0	91.69	0.872
182	1129	C	11	H	2	72.0	95.02	0.971
182	1129	C	11	H	3	77.0	96.57	0.991
182	1129	C	12	H	3	67.0	105.97	1.009
182	1129	C	13	H	3	75.0	115.55	1.022
182	1129	C	14	H	3	75.0	125.05	1.012
182	1129	C	15	H	3	72.0	134.52	1.019
182	1129	C	16	H	3	90.0	144.20	1.052
182	1129	C	17	H	3	75.0	153.55	1.049
182	1129	C	18	H	3	75.0	163.05	1.154
182	1129	C	19	H	3	75.0	172.55	1.143
182	1129	C	20	H	3	75.0	182.05	1.139
182	1129	C	20	H	7	45.0	187.75	1.137
182	1129	C	21	H	1	80.0	188.60	1.065
182	1129	C	21	H	3	80.0	191.60	1.072
182	1129	C	22	H	3	75.0	201.05	1.083
182	1129	C	23	H	3	73.0	210.23	1.077
182	1129	C	25	X	3	80.0	229.50	1.168
182	1129	C	26	X	3	80.0	239.00	1.115
182	1129	C	27	X	3	81.0	248.51	1.097
182	1129	C	28	X	3	75.0	258.15	1.129
182	1129	C	29	X	3	71.0	267.61	1.068
182	1129	C	30	X	3	63.0	276.93	1.086
182	1129	C	34	X	3	103.0	314.43	0.863
182	1129	C	33	X	3	71.0	304.71	0.819
182	1129	C	33	X	4	78.0	306.28	1.105
182	1129	C	35	X	3	75.0	323.55	0.984
182	1129	C	36	X	3	75.0	332.85	0.875
182	1129	C	37	X	3	75.0	341.75	0.519
182	1129	C	38	X	3	75.0	350.65	1.105
182	1129	C	40	X	3	65.0	368.65	0.801
182	1129	C	46	X	3	70.0	426.60	1.162
182	1129	C	46	X	3	75.0	426.65	1.327
182	1129	D	13	R	2	89.0	472.03	1.450
182	1129	D	15	R	1	88.0	489.66	1.315
182	1129	D	15	R	1	88.0	489.66	1.490
182	1129	D	16	R	3	40.0	501.80	1.976
182	1129	D	17	R	3	82.0	511.84	1.551
182	1129	D	18	R	3	55.0	521.14	1.369
182	1129	D	19	R	3	55.0	530.76	1.458
182	1129	D	20	R	3	60.0	540.63	1.447

Note: This table is also available in **ASCII format.**

Table T14. In situ formation temperature estimates, Site 1129.

Leg, core, section	Depth (mbsf)	Mudline temperature (°C)	Formation temperature (°C)	Fitting error (°C)
182-1129C-4	0	16.60		
	0	16.31		
	36.30		16.47	0.009
	36.30		16.38	0.007
182-1129C-8	0	16.65		
	0	16.49		
	0	16.43		
	74.40		18.14	0.032
	74.40		18.18	0.004
182-1129C-10	0	16.65		
	0	16.45		
	0	16.24		
	93.10		18.98	0.005
	93.10		18.94	0.004
182-1129C-20	0	16.30		
	0	16.97		
	188.00		22.70	0.005

Notes: Average mudline temperature = 1.92°C. Additional estimate of seafloor temperature using an expendable bathythermograph (XBT) = 13.15–13.56°C. This table is also available in **ASCII format.**

Table T15. Discrete *P*-wave velocity measurements using PWS1, PWS2, and PWS3, Site 1129.

Leg	Site	Hole	Core	Type	Section	Interval (cm)	Depth (mbsf)	PWS 1, 2, or 3	V_p (km/s)
182	1129	A	1	H	1	85.3	0.85	2	1.8016
182	1129	A	1	H	1	111.0	1.11	2	1.6297
182	1129	A	1	H	2	27.0	1.77	2	1.5990
182	1129	A	2	H	3	74.0	17.54	2	1.6146
182	1129	A	2	H	3	131.6	18.12	2	1.5939
182	1129	A	2	H	4	26.6	18.57	2	1.6146
182	1129	A	2	H	4	26.6	18.57	2	1.6101
182	1129	A	2	H	4	121.1	19.51	2	1.6252
182	1129	A	2	H	5	36.7	20.17	2	1.6116
182	1129	A	2	H	5	79.2	20.59	2	1.6312
182	1129	A	2	H	5	130.3	21.10	2	1.6328
182	1129	A	2	H	6	21.1	21.51	2	1.6576
182	1129	A	2	H	6	68.1	21.98	2	1.6343
182	1129	A	2	H	6	110.1	22.40	2	1.6116
182	1129	C	1	H	1	48.6	0.49	2	1.5818
182	1129	C	1	H	1	97.7	0.98	2	1.5770
182	1129	C	1	H	2	27.0	1.77	2	1.5740
182	1129	C	1	H	2	67.5	2.18	2	1.5783
182	1129	C	1	H	2	98.5	2.49	2	1.5840
182	1129	C	1	H	2	130.8	2.81	2	1.5740
182	1129	C	1	H	3	24.7	3.25	2	1.5927
182	1129	C	1	H	3	72.8	3.73	2	1.6015
182	1129	C	1	H	3	102.7	4.03	2	1.5898
182	1129	C	1	H	3	131.3	4.31	2	1.5898
182	1129	C	1	H	4	30.0	4.80	2	1.6030
182	1129	C	1	H	4	74.4	5.24	2	1.5913
182	1129	C	1	H	4	107.2	5.57	2	1.5709
182	1129	C	1	H	4	134.0	5.84	2	1.5685
182	1129	C	1	H	5	59.5	6.60	2	1.5971
182	1129	C	1	H	5	95.6	6.96	2	1.5712
182	1129	C	2	H	1	24.2	7.54	2	1.6269
182	1129	C	2	H	1	60.0	7.90	2	1.6015
182	1129	C	2	H	1	103.1	8.33	2	1.5927
182	1129	C	2	H	1	132.7	8.63	2	1.5669
182	1129	C	2	H	2	14.1	8.94	2	1.5585
182	1129	C	2	H	2	76.8	9.57	2	1.6198
182	1129	C	2	H	2	101.5	9.82	2	1.5884
182	1129	C	2	H	2	134.6	10.15	2	1.5754
182	1129	C	2	H	3	16.2	10.46	2	1.5965
182	1129	C	2	H	3	49.8	10.80	2	1.6015
182	1129	C	2	H	3	77.2	11.07	2	1.5990
182	1129	C	2	H	4	16.8	11.97	2	1.5990
182	1129	C	2	H	4	67.8	12.48	2	1.6030
182	1129	C	2	H	4	94.0	12.74	2	1.6119
182	1129	C	2	H	4	118.9	12.99	2	1.5884
182	1129	C	2	H	5	21.5	13.52	2	1.5986
182	1129	C	2	H	5	61.2	13.91	2	1.5927
182	1129	C	2	H	5	98.4	14.28	2	1.5913
182	1129	C	2	H	5	136.2	14.66	2	1.6044
182	1129	C	2	H	6	16.5	14.97	2	1.6193
182	1129	C	2	H	6	51.6	15.32	2	1.5986
182	1129	C	2	H	6	76.7	15.57	2	1.5869
182	1129	C	2	H	6	103.3	15.83	2	1.6096
182	1129	C	2	H	6	134.8	16.15	2	1.6030
182	1129	C	2	H	7	12.5	16.43	2	1.5929
182	1129	C	2	H	7	39.1	16.69	2	1.5913
182	1129	C	2	H	7	67.5	16.98	2	1.6209
182	1129	C	3	H	1	107.4	17.87	2	1.6134
182	1129	C	3	H	1	107.4	17.87	2	1.6134
182	1129	C	3	H	1	131.7	18.12	2	1.5885
182	1129	C	3	H	2	26.6	18.57	2	1.5754
182	1129	C	3	H	2	69.6	19.00	2	1.5884
182	1129	C	3	H	2	99.0	19.29	2	1.5826

Note: Only a portion of this table appears here. The complete table is available in **ASCII format.**

Table T16. Index properties measurements, Site 1129.

Leg	Site	Hole	Core	Type	Section	Top (cm)	Bottom (cm)	Depth (mbsf)	Bulk water content (%)	Dry water content (%)	Bulk density (g/cm^3)	Dry density (g/cm^3)	Grain density (g/cm^3)	Porosity (%)	Void ratio
182	1129	C	1	H	1	88.0	90.0	0.88	44.100	78.900	1.351	0.755	1.806	58.200	1.391
182	1129	C	1	H	2	88.0	90.0	2.38	39.800	66.100	1.451	0.873	2.003	56.400	1.293
182	1129	C	1	H	3	88.0	90.0	3.88	36.500	57.500	1.556	0.988	2.220	55.500	1.247
182	1129	C	1	H	4	88.0	90.0	5.38	38.700	63.300	1.418	0.869	1.875	53.700	1.158
182	1129	C	1	H	5	88.0	90.0	6.88	34.300	52.100	1.526	1.003	2.048	51.000	1.042
182	1129	C	2	H	1	89.0	91.0	8.19	37.800	60.900	1.332	0.828	1.630	49.200	0.969
182	1129	C	2	H	2	89.0	91.0	9.69	33.900	51.200	1.608	1.063	2.273	53.200	1.137
182	1129	C	2	H	3	89.0	91.0	11.19	36.800	58.200	1.408	0.890	1.801	50.600	1.024
182	1129	C	2	H	4	89.0	91.0	12.69	34.700	53.200	1.481	0.967	1.942	50.200	1.009
182	1129	C	2	H	5	89.0	91.0	14.19	38.300	62.200	1.450	0.894	1.956	54.300	1.188
182	1129	C	2	H	6	89.0	91.0	15.69	39.000	63.800	1.380	0.842	1.773	52.500	1.105
182	1129	C	2	H	7	59.0	61.0	16.89	35.200	54.300	1.772	1.149	2.936	60.900	1.556
182	1129	C	3	H	1	89.0	91.0	17.69	35.700	55.600	1.453	0.934	1.893	50.700	1.028
182	1129	C	3	H	2	89.0	91.0	19.19	39.100	64.100	1.508	0.919	2.163	57.500	1.355
182	1129	C	3	H	3	89.0	91.0	20.69	37.200	59.300	1.480	0.929	2.010	53.800	1.164
182	1129	C	3	H	4	89.0	91.0	22.19	36.600	57.800	1.533	0.971	2.150	54.800	1.215
182	1129	C	3	H	5	89.0	91.0	23.69	36.600	57.700	1.551	0.984	2.207	55.400	1.243
182	1129	C	3	H	6	88.0	90.0	25.18	35.300	54.600	1.555	1.006	2.169	53.600	1.156
182	1129	C	4	H	1	89.0	91.0	27.19	34.100	51.700	1.597	1.053	2.249	53.200	1.136
182	1129	C	4	H	2	89.0	91.0	28.69	37.100	59.000	1.460	0.919	1.950	52.900	1.123
182	1129	C	4	H	3	89.0	91.0	30.19	37.100	59.100	1.486	0.934	2.025	53.900	1.168
182	1129	C	4	H	4	89.0	91.0	31.69	29.400	41.600	1.644	1.161	2.197	47.200	0.892
182	1129	C	4	H	5	89.0	91.0	33.19	36.100	56.600	1.455	0.929	1.910	51.300	1.055
182	1129	C	4	H	6	89.0	91.0	34.69	35.000	53.700	1.520	0.988	2.054	51.900	1.078
182	1129	C	5	H	1	88.0	90.0	36.68	37.700	60.500	1.538	0.958	2.210	56.600	1.306
182	1129	C	5	H	2	88.0	90.0	38.18	33.300	49.900	1.488	0.993	1.924	48.400	0.937
182	1129	C	5	H	3	88.0	90.0	39.68	36.200	56.800	1.491	0.951	2.011	52.700	1.116
182	1129	C	5	H	4	88.0	90.0	41.18	34.300	52.200	1.522	1.000	2.041	51.000	1.041
182	1129	C	5	H	5	88.0	90.0	42.68	32.500	48.200	1.606	1.084	2.211	51.000	1.040
182	1129	C	5	H	6	88.0	90.0	44.18	32.300	47.600	1.588	1.075	2.153	50.000	1.002
182	1129	C	6	H	1	86.0	88.0	46.16	27.500	37.900	1.591	1.154	2.014	42.700	0.746
182	1129	C	6	H	2	86.0	88.0	47.66	28.000	38.800	1.532	1.104	1.898	41.900	0.720
182	1129	C	6	H	3	45.0	47.0	48.75	29.700	42.200	1.608	1.131	2.117	46.600	0.872
182	1129	C	6	H	4	58.0	60.0	50.38	34.100	51.700	1.606	1.058	2.273	53.400	1.148
182	1129	C	6	H	4	111.0	113.0	50.91	31.500	46.000	1.582	1.084	2.112	48.700	0.949
182	1129	C	6	H	5	27.0	29.0	51.57	33.100	49.500	1.501	1.004	1.951	48.600	0.944
182	1129	C	6	H	6	73.0	75.0	53.53	31.400	45.800	1.548	1.062	2.021	47.500	0.903
182	1129	C	6	H	7	34.0	36.0	54.64	33.600	50.700	1.552	1.030	2.101	51.000	1.039
182	1129	C	6	H	7	67.0	69.0	54.97	28.000	38.900	1.566	1.128	1.973	42.800	0.749
182	1129	C	7	H	2	71.0	73.0	57.01	28.500	40.000	1.654	1.181	2.192	46.100	0.855
182	1129	C	7	H	2	118.0	120.0	57.48	32.000	47.100	1.612	1.095	2.209	50.400	1.016
182	1129	C	7	H	3	55.0	57.0	58.35	32.400	48.000	1.516	1.025	1.971	48.000	0.924
182	1129	C	7	H	4	68.0	70.0	59.98	30.500	43.900	1.658	1.153	2.276	49.400	0.975
182	1129	C	7	H	5	68.0	70.0	61.48	32.900	49.000	1.476	0.990	1.883	47.400	0.901
182	1129	C	7	H	6	15.0	17.0	62.15	26.700	36.500	1.570	1.151	1.950	41.000	0.695
182	1129	C	8	H	1	32.0	34.0	64.62	32.700	48.700	1.503	1.011	1.946	48.100	0.925
182	1129	C	8	H	1	65.0	67.0	64.95	33.200	49.700	1.472	0.984	1.881	47.700	0.912
182	1129	C	8	H	2	62.0	64.0	66.42	34.100	51.800	1.487	0.980	1.940	49.500	0.981
182	1129	C	8	H	3	68.0	70.0	67.98	29.400	41.700	1.683	1.188	2.301	48.400	0.936
182	1129	C	8	H	4	79.0	81.0	69.59	30.600	44.100	1.384	0.961	1.639	41.400	0.706
182	1129	C	8	H	5	80.0	82.0	71.10	35.700	55.400	1.525	0.981	2.093	53.100	1.133
182	1129	C	8	H	6	39.0	41.0	72.19	31.800	46.700	1.525	1.039	1.976	47.400	0.902
182	1129	C	8	H	6	96.0	98.0	72.76	34.400	52.500	1.427	0.936	1.798	48.000	0.922
182	1129	C	9	H	1	65.0	67.0	74.45	29.700	42.300	1.513	1.063	1.897	43.900	0.784
182	1129	C	9	H	1	102.0	104.0	74.82	29.000	40.900	1.635	1.160	2.164	46.400	0.865
182	1129	C	9	H	2	51.0	53.0	75.81	32.100	47.200	1.511	1.026	1.948	47.300	0.898
182	1129	C	9	H	3	70.0	72.0	77.50	34.200	52.000	1.550	1.020	2.115	51.800	1.073
182	1129	C	9	H	4	63.0	65.0	78.93	33.400	50.100	1.480	0.986	1.905	48.200	0.932
182	1129	C	9	H	5	68.0	70.0	80.48	32.000	47.000	1.616	1.099	2.217	50.400	1.017
182	1129	C	9	H	6	38.0	40.0	81.68	29.200	41.200	1.542	1.093	1.948	43.900	0.783
182	1129	C	10	H	1	5.0	7.0	83.35	26.500	36.100	1.535	1.128	1.872	39.700	0.660
182	1129	C	10	H	1	66.0	68.0	83.96	34.700	53.200	1.549	1.011	2.129	52.500	1.107
182	1129	C	10	H	2	65.0	67.0	85.45	31.900	46.900	1.629	1.109	2.252	50.800	1.031
182	1129	C	10	H	3	71.0	73.0	87.01	26.600	36.200	1.619	1.188	2.050	42.000	0.726
182	1129	C	10	H	4	63.0	65.0	88.43	30.900	44.800	1.546	1.068	2.003	46.700	0.876

Note: Only a portion of this table appears here. The complete table is available in **ASCII format.**

Table T17. Undrained shear strength measurements, Site 1129.

Leg	Site	Hole	Core	Type	Section	Interval (cm)	Depth (mbsf)	Maximum shear strength (kPa)	Peak (kPa)
182	1129	A	1	H	2	100.0	2.50	2.61	3.18
182	1129	A	1	H	3	93.2	3.93	2.88	3.51
182	1129	A	2	H	3	123.0	18.03	0.72	0.88
182	1129	A	2	H	4	104.4	19.34	1.53	1.87
182	1129	A	2	H	5	109.9	20.90	1.62	1.98
182	1129	A	2	H	6	103.8	22.34	3.96	4.83
182	1129	C	1	H	1	114.6	1.15	0.81	0.99
182	1129	C	1	H	2	110.9	2.61	1.35	1.65
182	1129	C	1	H	3	108.6	4.09	4.68	5.71
182	1129	C	1	H	4	122.2	5.72	5.67	6.92
182	1129	C	1	H	5	99.3	6.99	1.44	1.76
182	1129	C	2	H	1	122.8	8.53	1.44	1.76
182	1129	C	2	H	2	98.1	9.78	6.66	8.12
182	1129	C	2	H	3	62.9	10.93	2.07	2.53
182	1129	C	2	H	4	102.9	12.83	2.43	2.96
182	1129	C	2	H	5	105.4	14.35	1.44	1.76
182	1129	C	2	H	6	121.6	16.02	2.70	3.29
182	1129	C	3	H	1	133.2	18.13	1.98	2.42
182	1129	C	3	H	2	110.6	19.41	0.81	0.99
182	1129	C	3	H	3	108.3	20.88	1.89	2.31
182	1129	C	3	H	4	108.7	22.39	2.52	3.07
182	1129	C	3	H	5	111.9	23.92	2.79	3.40
182	1129	C	3	H	6	89.0	25.19	3.69	4.50
182	1129	C	4	H	1	120.0	27.50	1.62	1.98
182	1129	C	4	H	2	139.0	29.19	1.80	2.20
182	1129	C	4	H	3	124.4	30.54	2.25	2.74
182	1129	C	4	H	4	123.7	32.04	4.68	5.71
182	1129	C	4	H	5	127.7	33.58	0.99	1.21
182	1129	C	4	H	6	124.3	35.04	5.04	6.15
182	1129	C	5	H	1	149.6	37.30	3.69	4.50
182	1129	C	5	H	2	119.0	38.49	1.17	1.43
182	1129	C	5	H	3	116.6	39.97	1.89	2.31
182	1129	C	5	H	4	116.4	41.46	5.94	7.25
182	1129	C	5	H	5	130.7	43.11	2.16	2.63
182	1129	C	6	H	1	132.8	46.63	7.74	9.44
182	1129	C	6	H	2	140.5	48.21	4.68	5.71
182	1129	C	6	H	3	139.6	49.70	2.25	2.74
182	1129	C	6	H	4	138.1	51.18	8.91	10.87
182	1129	C	6	H	5	133.7	52.64	4.14	5.05
182	1129	C	6	H	6	149.7	54.30	6.21	7.57
182	1129	C	6	H	7	42.5	54.72	8.37	10.21
182	1129	C	7	H	1	142.6	56.23	10.98	13.39
182	1129	C	7	H	2	119.5	57.49	4.32	5.27
182	1129	C	7	H	3	134.7	59.15	2.34	2.85
182	1129	C	7	H	4	126.7	60.57	5.58	6.81
182	1129	C	7	H	5	119.0	61.99	14.40	17.56
182	1129	C	7	H	6	25.4	62.25	16.65	20.31
182	1129	C	8	H	1	149.9	65.80	4.68	5.71
182	1129	C	8	H	2	129.5	67.10	3.51	4.28
182	1129	C	8	H	3	135.6	68.66	1.80	2.20
182	1129	C	8	H	3	135.6	68.66	1.80	2.20
182	1129	C	8	H	4	126.8	70.07	8.64	10.54
182	1129	C	8	H	5	135.1	71.65	10.80	13.17
182	1129	C	8	H	6	118.8	72.99	5.49	6.70
182	1129	C	8	H	7	63.0	73.93	21.15	25.80
182	1129	C	9	H	1	106.8	74.87	6.12	7.46
182	1129	C	9	H	2	129.4	76.59	4.59	5.60
182	1129	C	9	H	3	104.8	77.85	13.50	16.47
182	1129	C	9	H	4	132.9	79.63	9.90	12.07
182	1129	C	9	H	6	63.0	81.93	38.34	46.76
182	1129	C	10	H	1	116.7	84.47	3.42	4.17
182	1129	C	10	H	2	134.6	86.15	9.45	11.53
182	1129	C	10	H	3	110.1	87.40	9.45	11.53

Note: Only a portion of this table appears here. The complete table is available in **ASCII format.**

Table T18. Summary of tool strings, intervals logged, and logging speeds, Hole 1129D.

	Tool strings	
First pass:	Triple combo	FMS/sonic
Logging speed (m/hr)	275.00	275.00
Total interval (mbsf)	550-604	0-604
Open hole interval (mbsf)	550-604	100-604
Calipers closed (mbsf)	550	140
Second pass:	Triple combo	
Logging speed (m/hr)	275	
Total interval (mbsf)	0-604	
Open hole interval (mbsf)	100-604	
Calipers closed (mbsf)	131	

Note: Triple combo = triple combination logging tool, FMS = Formation MicroScanner.